

Examining Relationships Between Nitric Oxide, Iron and Ecdysone Biosynthesis

By

Pendleton James Macklem Cox

A thesis submitted in partial fulfillment of the requirements for the degree of

Masters of Science

in

Molecular Biology and Genetics

Department of Biological Sciences

University of Alberta

©Pendleton James Macklem Cox, 2016

Abstract

Pulses of ecdysone, a steroid hormone, play an integral role during insect development however, how these ecdysone pulses are regulated has been relatively unexplored. I have shown that the presence of nitric oxide (NO) within the larval prothoracic gland (PG), the principal source of larval ecdysone, may correlate with the major hormone pulse that triggers metamorphosis. *Nitric Oxide Synthase* (NOS^{IR-X})-RNAi in the larval PG causes third instar larvae to arrest in development. In addition, NOS^{IR-X} -RNAi PGs are overgrown and exhibit a red-brownish color. Under UV light, NOS^{IR-X} -RNAi PGs autofluoresce in a bright red, and this autofluorescence largely originates from mitochondria. The King-Jones lab has shown that this phenotype is caused by a buildup of heme precursors, suggesting the impairment of heme biosynthesis. Heme is required for the production of ecdysone, and by extension iron, a key component of heme, is also needed in large quantities. Therefore, I predicted that nitric oxide (NO), which is synthesized by NOS, was as a cellular signal to ramp up iron availability and heme production to enable a major increase in ecdysone production. Previous work has established that NO can directly modulate the activity of the iron regulatory protein (IRP), and I proposed that NO-dependent IRP activation was required for an ecdysone peak to occur. I tested whether the predicted requirement for NO can be bypassed, by activating IRP to reduce dietary iron levels, or by providing active IRPs ectopically. My data revealed that ectopic expression of a mutant IRP that is constitutively active rescues NOS^{IR-X} -RNAi animals with respect to both the overgrown fluorescent ring glands and developmental arrest. However, my data also demonstrated that the NOS^{IR-X} -RNAi had an off-target, complicating the predicted relationship between NO, IRP, heme and ecdysone.

To Neelam Jamal,

I love you forever,

Thank you for putting up with the countless hours,
and providing your aid whenever possible.

Acknowledgements

I would like to begin by acknowledging Dr. Kirst King-Jones for accepting me in his lab and allowing me to pursue my graduate degree. His support, and resources allowed me to perform the research embodied in this thesis and find new, exciting ways to interpret all the data collected. I would also like to thank Dr. Andrew Simmonds from my committee for his additional mentorship and down-to-earth support as well as providing his lab as a resource to pursue my studies. Furthermore, I would like to thank Dr. Ted Allison in my committee for a great amount of help in providing broad pictured yet detailed suggestions for my project and for always being so kind and thoughtful and always providing a very hearty handshake. Additionally, I greatly appreciated Dr. Andrew Waskiewicz's input as a stand-in committee member and Dr. Frank Nargang's assessment during my examination.

A big thanks to my parents for all their support. Thanks Dad for always ensuring I had functional transportation and thanks Mom for the absurd amounts of cookies to keep me energized to count flies. And thank you Neelam Jamal, for always being there for me with all the exciting results and all the not-so-exciting ones.

Table of Contents

1.0	Introduction.....	1
1.1	The importance of studying steroid hormones.....	3
1.2	Using <i>Drosophila melanogaster</i> to study steroid hormone regulation.....	4
1.3	Steroid hormone production and signaling in <i>Drosophila melanogaster</i>	10
1.4	Heme biosynthesis in mammals and <i>Drosophila</i>	12
1.5	Iron regulation in mammals.....	15
1.6	Comparing iron regulation in mammals to <i>Drosophila</i>	21
1.7	Iron sulfur cluster biosynthesis.....	23
1.8	Nitric oxide signaling and regulation.....	24
1.9	Previous research.....	26
2.0	Materials and Methods.....	31
2.1	<i>Drosophila</i> stocks and care.....	31
2.2	Computational IRE search.....	31
2.3	Cloning IRP-1A and IRP-1B for injections.....	31
2.4	Site-directed mutagenesis of <i>IRP-1A</i> to create a form of IRP-1A that is always RNA-binding.....	33
2.5	Competent Cells.....	33
2.6	Sequencing Reaction.....	34
2.7	RNA extraction from dissected tissue.....	34
2.8	RNA extraction of whole body samples.....	35
2.9	RNA quality verification.....	36
2.10	cDNA synthesis.....	36
2.11	qPCR primer validation.....	36
2.12	qPCR analysis.....	37
2.13	pIRES reactions/Gibson.....	37
2.14	<i>Drosophila</i> embryo injections.....	37
2.15	Immunoprecipitation of GFP-tagged ribosomes.....	39
2.16	NO detection.....	40
2.17	Holidic medium and BPS iron food.....	41
2.18	Vial analysis for iron-feeding, IRP rescue experiments.....	41
2.19	DNA extractions.....	41
2.20	PCR purifications.....	42
2.21	GRAPE plates.....	42
3.0	Results.....	51
3.1	Comparing transcriptional regulation of <i>IRP-1A</i> and <i>IRP-1B</i> in the ring gland and brain ring gland complex before and during the major L3 ecdysone pulse.....	51
3.2	NO pulses coordinate with ecdysone signaling and has three distinct staining patterns in the ring gland.....	55
3.3	Variable iron concentrations in the diet and the associated phenotypes.....	60
3.3.1	Decreasing iron concentrations through the diet does not rescue <i>phm22>NOS^{IR-X}-RNAi</i> animals.....	60
3.3.2	<i>NOS</i> mutants fed BPS have increased viability.....	66
3.4	Constitutively active IRP-1A in the prothoracic gland rescues <i>phm22>NOS^{IR-X}-RNAi</i> animals to adulthood.....	69

3.5 <i>NOS^{IR-X}</i> -RNAi phenotype is the result of an off-target effect.....	73
4.0 Discussion.....	76
4.1 The importance of IRP in the mammalian brain and the <i>Drosophila</i> ring gland	76
4.2 IRP-1A RNA-binding activity activated through transgene manipulation as opposed to dietary iron manipulation rescues <i>phm22>NOS^{IR-X}</i> -RNAi animals to adulthood.....	78
4.3 Exploring the role of NOS and NO in ecdysone production	84
4.4 A novel patterning of NO signaling in the RG	88
4.4 Future directions	91
4.4.1 Searching for novel IREs in <i>Drosophila</i>	91
4.4.2 Elucidating IRP-1A activity prior to the major L3 ecdysone pulse using the Translating Ribosome Affinity Purification assay.....	95
4.4.3 Using an Internal Ribosomal Entry Site to elucidate the timing of IRP-1A RNA-binding activity	98
4.4.4 Looking at ferritin degradation in relation to ecdysone production	101
4.4.5 RNA-Seq to identify genes that are affected from IRP-1A overexpression.....	102
4.5 Conclusions.....	103

List of Figures

Introduction

Figure 1.1. Ecdysteroid concentration as a function of <i>Drosophila melanogaster</i> developmental stages.....	7
Figure 1.2. Ecdysone biosynthesis occurs in the prothoracic gland of the ring gland.....	8
Figure 1.3. Illustrations of GAL4/UAS and Φ C31 transgenic techniques in <i>Drosophila melanogaster</i>	9
Figure 1.4. The heme biosynthetic pathway.....	14
Figure 1.5. Iron absorption and delivery in vertebrates.....	18
Figure 1.6. Activation modes for Iron Regulatory Proteins (IRPs).....	19
Figure 1.7. Comparing the consensus IRE motif to human, <i>Mus musculus</i> , and <i>Drosophila</i> H-ferritin IREs.....	20
Figure 1.8. Giant red ring glands from third instar larvae of <i>phm22>spz5-RNAi</i> and <i>phm22>NOS^{IR-X}-RNAi</i> are phenotypically similar to heme biosynthesis disruptions.....	29
Figure 1.9. The proposed <i>Drosophila</i> NOS/IRP-1A/ecdyson pathway.....	30

Materials and Methods

Figure. 2. 1. Illustration of the IRP-1A transgenic lines used in this thesis.....	43
Figure. 2. 2. Illustration of the IRP-1A ^{C450S} transgenic lines used in this thesis.....	44
Figure. 2. 3. Illustration of the IRP-1B transgenic lines used in this thesis.....	45
Figure. 2. 4. The three key cysteine residues required for iron-sulfur cluster binding of IRP1 in humans are conserved in <i>Drosophila melanogaster</i> IRP-1A.....	46

Results

Figure 3. 1. IRP-1A and IRP-1B expression within the RG and BRGC at 30 and 44 hr post L2/L3 molt.....	54
Figure 3. 2. NO was present in the RG during and prior to ecdysone pulses in three distinct patterns within the L3 larval stage.....	59
Figure 3. 3. <i>Drosophila</i> reared on a defined holidic diet had similar adult survival rates compared to controls reared on standard fly medium, but with a four to five-day delay to pupal formation.....	64
Figure 3. 4. <i>phm22>NOS^{IR-X}-RNAi</i> animals were not phenotypically rescued when fed an iron manipulated holidic diet.....	68
Figure 3. 6. Overexpressed constitutively active IRP-1A in the RG rescued <i>phm22>NOS^{IR-X}-RNAi</i> giant red RG phenotype and L3 arrest.....	72
Figure 3. 7. <i>NOS^{IR-X}-RNAi</i> had an off-target effect instead of or in addition to NOS.....	75

Discussion

Figure 4. 1. Illustration of the translating ribosome affinity purification (TRAP) technique to identify whether IRP-1A is RNA-binding or not.....	97
Figure 4. 2. An Internal Ribosomal Entry Site used as a tool for Iron Response Protein's RNA-binding ability.	100
Figure 4. 3. An updated illustration of the predicted model for IRP-1A, iron regulation and heme production in the biosynthesis of ecdysone.	106

List of Tables

Materials and Methods

Table 2. 1. Drosophila melanogaster lines used to obtain the results embodied in this thesis	47
Table 2. 2. Primers for qRT-PCR, cloning and sequencing.....	48
Table 2. 3. Solutions used for Chemically Competent Cells	49
Table 2. 4. Solutions used for the Translating Ribosome Affinity Purification experiment.	50

Discussion

Table 4. 1. Computational analysis of genes related to NO, iron, heme and ecdysone regulation.	94
---	----

Abbreviations

ALA	aminolevulinic acid
ALAS1/2	5'-aminolevulinate synthase $\frac{1}{2}$
PBG	(pyrrole) porphobilinogen
PBGD	PBG deaminase
BIP	2,2 -bipyridyl
BPS	bathophenanthroline disulfonic acid
CA	corpus allatum
CcO	cytochrome c oxidase
cDNA	complementary DNA
cGMP	cyclic GMP
CRISPR	clustered regularly interspaced short palindromic repeats
DAF2-DA	DAF-2 diacetate
DCYTB	ferrireductase duodenal cytochrome b561
DFO	desferrioxamine
DMT1	divalent metal transporter 1
DNA	deoxyribonucleic acid
ferritin HCH1	ferritin heavy chain homolog 1
Ferrozine	3-(2-pyridyl)-5,6-bis(4-phenylsulfonic acid)-1,2,4-triazine
FPN	ferroportin
GFP	green fluorescent protein
gRNA	guideRNA
HIF-2 α	hypoxia inducible factor-2alpha
hr	hour
JH	juvenile hormone
IRE	iron response element
IRES	internal ribosomal entry site
IRP	iron response protein
ISC	iron-sulfur cluster
L-NAME	N-nitro-L-Arginine Methyl Ester
MFRN	mitoferrin

min	minute
mRNA	messenger RNA
ms	milisecond
Naa60	N(alpha)-acetyltransferase 60
NADPHd	NADPH diapharose
NO	nitric oxide
NOS	nitric oxide synthase
P450	cytochrome P450
PBS	phosphate-buffered saline
PBT	phosphate-buffered saline with 0.1% Triton X
PG	prothoracic gland
PGC-1 α	peroxisome proliferator-activated receptor γ coactivator 1 α
phm22	phantom22
ppox	protoporphyrinogen oxidase
PTTH	prothoracicotropic hormone
RFP	red fluorescent protein
RG	ring gland
RNA	ribonucleic acid
RNS	reactive nitrogen species
ROS	reactive oxygen species
s/sec	second
Sdhb	succinate dehydrogenase b
SNAP	S-nitroso-N-acetylpenicillamine
TB	trituration buffer
TfR	transferrin receptor
Tsf1/2	transferrin 1/2
TRAP	translating ribosome affinity purification
UTR	untranslated region

1.0 Introduction

Overview

Developmental processes in animals are often coordinated through timed pulses of steroid hormones. Testosterone and estrogen in humans regulate the onset of puberty and sexual characteristics while ecdysone, the principal steroid hormone in *Drosophila*, regulates insect development. Ecdysone is responsible for triggering developmental transitions such as larval molts and initiating pupariation. The downstream actions of ecdysone have been well studied and are widely understood, however, less is known about how ecdysone itself is regulated. To study how ecdysone biosynthesis is controlled, the King-Jones lab began looking for genes that when disrupted, caused ecdysone deficient phenotypes. Typical characteristics of these phenotypes included the failure to proceed to the next developmental stage, such as failure to molt or initiate the larval-prepupal transition. Therefore, the King-Jones lab conducted a screen knocking down genes specifically in the prothoracic gland (PG), the principal tissue of ecdysone biosynthesis, to look for ecdysone deficient phenotypes. Ultimately, as a result of this screen, the lab came across a phenotype in which not only were larvae halted in development and arrested at the third instar stage, they also had enlarged red fluorescent ring glands (a three-part tissue that contains the prothoracic gland). This phenotype was the result of knocking down *nitric oxide synthase (NOS)*, encoding the protein responsible for synthesizing nitric oxide (NO), thus implicating NO in ecdysone biosynthesis. While pursuing this connection between NO and ecdysone, the King-Jones lab determined that the red fluorescence was a direct result of heme precursor buildup, indicating that heme biosynthesis was impaired. Therefore, heme, NO and ecdysone appeared to be connected. One potential link between ecdysone and heme are the cytochrome P450 enzymes (P450), which synthesize ecdysone and require heme as a cofactor. During ecdysone biosynthesis, P450 transcripts are upregulated¹, suggesting that increased quantities of heme would be required for each individual P450 protein. Furthermore, heme requires iron at its core, implicating that iron levels should be regulated during times of heme demand. Finally, the Iron Response Protein (IRP) regulates free cellular iron and NO has been implicated *in vitro* to control the activity of IRPs. Therefore, I suspected that NO was used to trigger IRP-1A (the *D.*

melanogaster IRP) activity to increase cellular iron levels for heme production needed for ecdysone biosynthesis by cytochrome P450 enzymes. The King-Jones lab discovered that an NO pulse occurred just prior to ecdysone production, leading to my prediction for the requirement of NO in ecdysone synthesis. Previous reports have shown that the *NOS^{IR-X}*-RNAi construct, when expressed in the PG, results in no detectable NOS proteins and a lack of NO in the ring gland², which suggests the L3 arrest and giant red ring glands were a result of a lack of NO. Therefore, I proposed that without NO, IRP-1A would not be activated in the PG to increase cellular iron levels for heme production, thereby resulting in a buildup of fluorescent heme precursors. My work, embodied in this thesis, suggested that NO was present in the PG prior to at least three of the four ecdysone pulses in the third instar larval stage, expanding on the previous King-Jones lab prediction that NO was correlated with ecdysone production. Furthermore, I demonstrated that the *NOS^{IR-X}*-RNAi construct has an off-target effect, likely causing the aforementioned phenotype of giant red RGs and L3 arrest. However, I was still able to demonstrate that IRP-1A can rescue *NOS* knock-down in the PG. Specifically, both the third instar arrest and the red fluorescent ring gland phenotypes were rescued by they approach. Because IRP-1A is responsible for increasing cellular iron levels, this further suggests that cellular iron levels were made available for heme production. I speculated that heme precursors no longer accumulate, and were likely used as cofactors for cytochrome P450 enzymes to produce ecdysone and trigger the larval-prepupal transition. Ultimately I was able to show that IRP and iron regulation are capable of rescuing the heme precursor build up and L3 arrest phenotypes in the *NOS^{IR-X}*-RNAi animals, linking IRP, iron, heme and ecdysone biosynthesis.

1.1 The importance of studying steroid hormones

Many organisms synthesize steroid hormones, a class of signaling molecules with important roles in development³. Humans require the steroid hormones testosterone and estrogen in controlled pulses^{4,5} to initiate the onset of puberty and development of sexual characteristics and behaviors⁶. Hormones are not only involved in sexual maturation, but also in stress response and immunity. For example, steroid hormones have been shown to mediate stress-related effects of cocaine dependence⁷ and high concentrations can even result in decreased antibody production and thereby decreased lifespan of *Junco hyemalis* (sparrows)⁸. Together, we see that steroid hormones are connected to multiple cellular responses covering development, stress and immunity. Therefore, steroids have been intensely studied with respect to how they are produced and how they mediate downstream signaling events. However, less is known on how they themselves are regulated. In *Drosophila*, we know that steroid hormone signals correlate with nutrition and critical weight, the point at which the animal has stored enough nutrients to successfully undergo metamorphosis⁹. How hormone production is initiated and what regulatory components must be present to produce a steroid hormone pulse is not well understood. The topic of this thesis is to determine NO and iron's involvement in how steroid hormones are produced and regulated in order to control developmental transitions.

1.2 Using *Drosophila melanogaster* to study steroid hormone regulation

To study steroid hormone regulation, I used the model organism *Drosophila melanogaster*. Like all known insects, *Drosophila* requires steroid hormones to trigger developmental transitions. Many of these steroids can be collectively referred to as ecdysteroids, with often multiple active compounds in any given insect species. I will refer to ecdysteroids as “ecdysone” from here on. *Drosophila* is the only model organism where its principal steroid of development, ecdysone, has been fully mapped starting from embryogenesis to adulthood, with large peaks of ecdysone occurring at key developmental transitions such as larval molts, pupariation and eclosion^{10,11} (Fig. 1.1). Extensive research has gone into elucidating how ecdysone is synthesized via the Halloween enzymes (Ch. 1.3), and together both the mapping and understanding of its synthesis lays a foundation for steroid hormone studies^{1,12-17} (Fig. 1.2). Furthermore, similarities exist between *Drosophila* and human steroid regulation. For example, prothoracicotropic hormone (PTTH) in *Drosophila* and adrenocorticotrophic hormone (ACTH) in humans both regulate their respective steroids ecdysone and glucocorticoids in hourly pulses, known as an ultradian rhythm^{5,18}, demonstrating a similarity between species in regulatory signaling. Additionally, the vertebrate nuclear receptor steroidogenic factor 1 (SF-1) regulates multiple steroidogenic genes and its orthologue in *Drosophila*, FTZ-F1, transcriptionally regulates expression of at least two steroidogenic enzymes¹⁹⁻²¹. Nuclear receptors have been a recurring theme in steroid hormone production. For example, *Drosophila* hormone receptor 4 (DHR4) acts through PTTH to regulate ecdysone and appears to work alongside DHR3²². As well, DHR51, a gene studied in the King-Jones lab, is thought to have importance in ecdysone biosynthesis in relation to heme sensing and regulation. The similarities between human and *Drosophila* steroidogenic regulation and the knowledge accompanying ecdysone biosynthesis makes *Drosophila* an ideal model organism to study steroid hormone regulation.

The vast array of genetic tools for use in *Drosophila* is another fundamental reason I chose this model organism to study steroid hormones. Firstly, *Drosophila* is an ideal organism for research because of its short 10-day lifecycle, its ability to exponentially generate offspring and financial feasibility in large quantities. *Drosophila* is simpler to study than mice, which have many repetitive and redundant genes and are generally more complex biologically²³. In mice studies, when knocking down a particular gene, homologous genes in the genome are often

capable of fulfilling the lost genes role in the animal, thus making knock-down studies more complex. In *Drosophila*, the smaller genome has less homologues. For example, in mice there are three NOS genes, whereas in *Drosophila* there is only one^{2,24}. Although mice are more related to humans than flies, a large body of work has been able to demonstrate the conservation between *Drosophila* and humans. Nearly 60% of human disease genes have homologous genes in *Drosophila*, and a number of studies have shown that certain vertebrate genes can replace their *Drosophila* counterparts and produce viable flies^{23,25}.

Many tools have been designed for use in *Drosophila* that have proven very effective in genomic studies. P-element insertion provided researchers the ability to insert or disrupt genes within the genome²⁶. This led to an increased level of genetic manipulation when *GAL4/UAS* was introduced in *Drosophila* using a P-element insertion technique. In this method, tissue-specific promoters drive *GAL4* expression and the GAL4 protein recognizes *UAS* enhancer regions to drive tissue-specific expression of a transgene²⁷ (Fig. 1.3A). *Drosophila* researchers also have access to the FLT-FRT recombinase system allowing for deletion, inversion and insertions in a controlled manner^{28,29}. Furthermore, RNAi control through *GAL4/UAS* allows for precisely controlled knockdown analysis in a time- and/or tissue-specific manner^{30,31}. Together, these techniques provided the foundations to create a database of *Drosophila* RNAi lines for nearly every gene^{32,33}. With all these tools available to the *Drosophila* researcher, a myriad of screening techniques have been developed to identify genes related to any particular pathway^{34,35}. Recently, two new tools have been created for use in *Drosophila* allowing for highly specific gene manipulation never before seen. Φ C31 integrase recombines an *attB* sequence associated with a transgene with an *attP* sequence previously inserted and mapped in the *Drosophila* genome (Fig. 1.3B). This resolved issues caused by position effects (insertions at different chromosomal locations), because each transgene can be expressed in the same chromosomal context, since the same *attP* site would be used for all experimental lines^{36,37}. Finally, the emergence of clustered regularly interspaced short palindromic repeats (CRISPR) technology has allowed for precise gene deletions, or other alterations of the endogenous gene. This eliminates issues of transgenes being expressed in conjunction with an endogenous gene, and limits the off-target effects associated with RNAi³⁸. Taking this technology further, researchers have combined the targeted gene removal of CRISPR with *GAL4/UAS* expression, allowing for genomic alterations of an endogenous gene in a tissue specific manner³⁹. CRISPR

mutational analysis provides a great tool to fully understand what happens when a gene is mutated or deleted, however this takes time, whereas we currently have a database of RNAi constructs for nearly every gene in *Drosophila*. Therefore, while CRISPR mutational analysis is preferred, RNAi analysis is still a great screening tool as it is already widely available and provides a starting foundation for subsequent CRISPR analysis. Additionally, when comparing a CRISPR mutant to an RNAi knock-down, RNAi has the added benefit, that while specific, can decrease transcript expression, as opposed to abolish it. This could be beneficial in regards to essential genes that when knocked down provide a phenotype, but are still viable whereas a CRISPR deletion of an essential gene could be embryonic lethal and not able to provide much information on the function of the gene in later stages of development. Altogether, the techniques, tools, and screening ability presented in *Drosophila* has made it an optimal model organism and this thesis has taken advantage of GAL4/UAS, RNAi, Φ C31, and CRISPR technologies to advance our understanding of steroid hormone regulation.

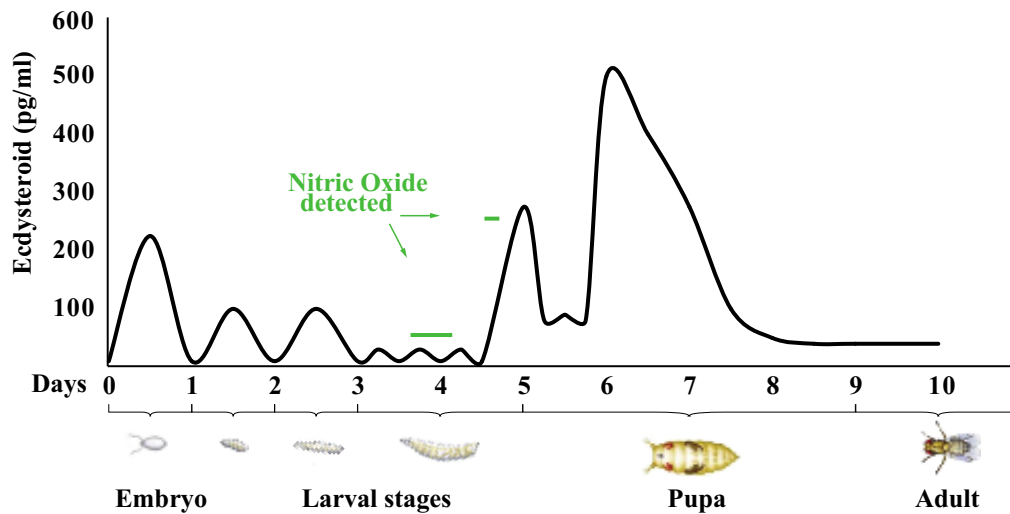


Figure 1.1. Ecdysteroid concentration as a function of *Drosophila melanogaster* developmental stages. *Drosophila melanogaster* larvae hatch after 24 hours of embryogenesis following an ecdysteroid pulse. Pulses occur as the larvae advance from 1st instar to 2nd (L2) to 3rd (L3) instar. Near the end of the L3 stage, approximately 44 hours after the L2/L3 molt, a major ecdysteroid pulse occurs, triggering pupariation. Finally, once pupariation occurs on day five, four days pass and an adult ecloses. The nitric oxide (NO) indicated in green represents the presence of NO prior and during minor ecdysone pulses, NO is present again prior and during the major L3 ecdysone pulse. *Drosophila* images were adapted from: <https://biotech-ntua.wikispaces.com>

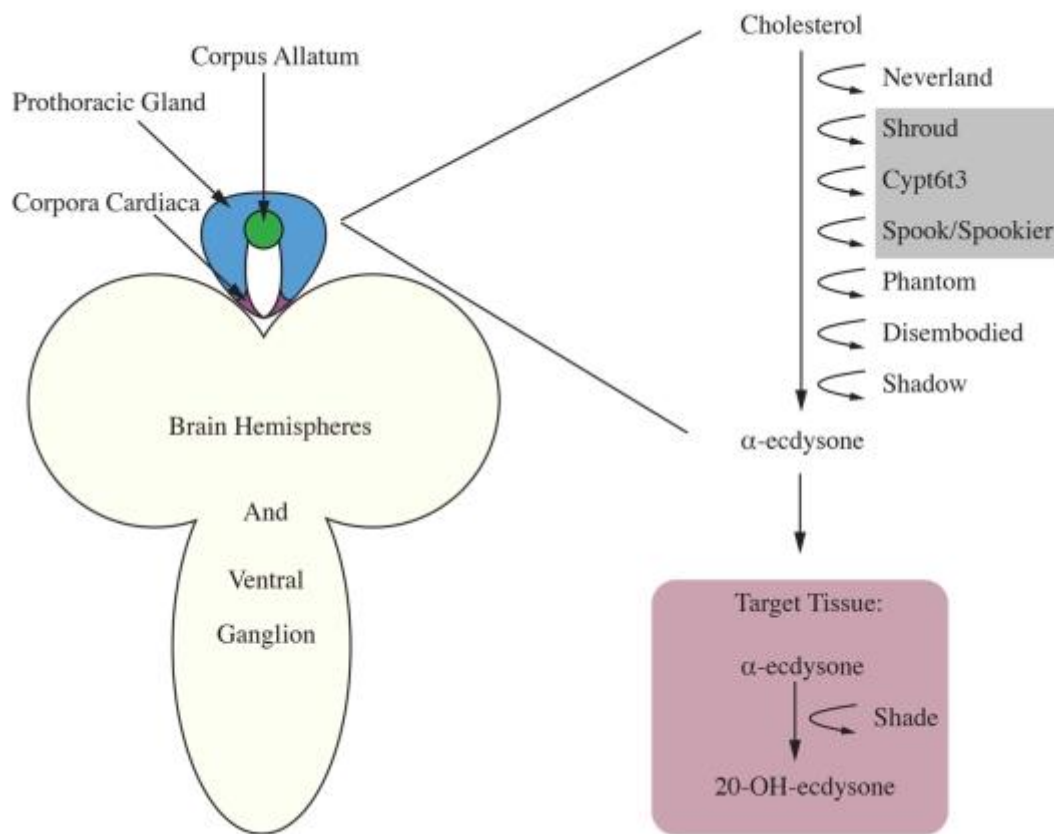


Figure 1.2. Ecdysone biosynthesis occurs in the prothoracic gland of the ring gland. The ring gland is composed of three tissues: The prothoracic gland (shown in blue), the corpus allatum (green) and the corpora cardiaca (purple). The ring gland is attached to two brain hemispheres and the ventral ganglion, together these tissues encompass the larval central nervous system. Ecdysone synthesis occurs in the prothoracic gland (PG) and α -ecdysone is synthesized by the Halloween enzymes. The black box represents the stage of ecdysone biosynthesis where we currently do not know what compounds are formed, however, we know that Shroud, Cyp6t3 and Spook/Spookier are involved. α -ecdysone is released from the PG to target tissues. At α -ecdysone's destination, Shade converts α -ecdysone to 20-Hydroxyecdysone, the biologically active form of ecdysone. In ecdysone biosynthesis, all enzymes shown except Neverland and Shroud are cytochrome P450 enzymes and this thesis will refer to these ecdysteroids as "ecdysone". PG: prothoracic gland.

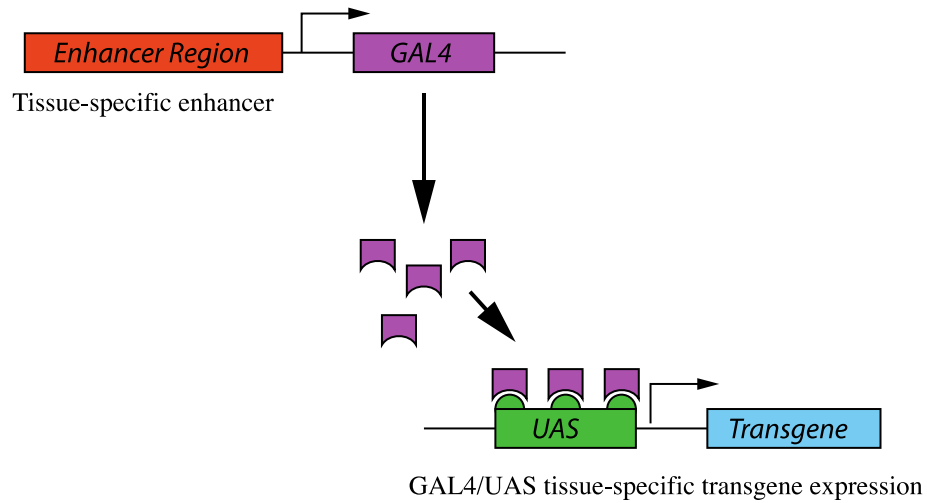
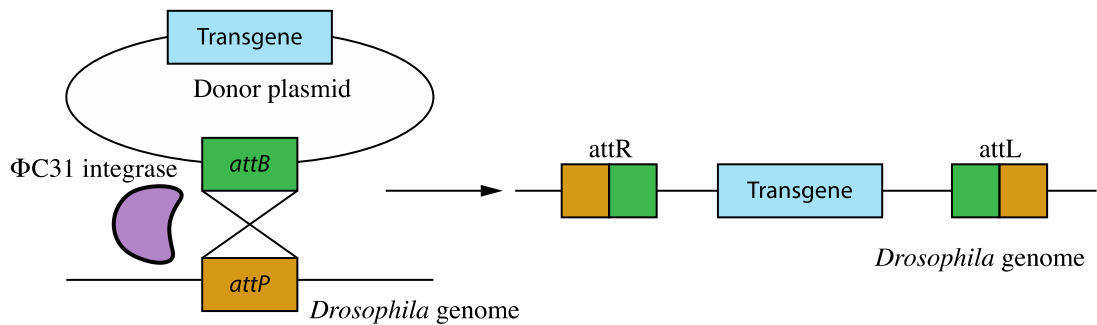
A**B**

Figure 1.3. Illustrations of *GAL4/UAS* and Φ C31 transgenic techniques in *Drosophila melanogaster*. **A)** *GAL4* is expressed in a tissue specific manner with respect to the upstream enhancer region. The *GAL4* protein binds to the *UAS* enhancer region, resulting in expression of the downstream gene. This technique allows for tissue-specific expression of a transgene in *Drosophila*. **B)** A donor plasmid containing the *attB* attachment site is incorporated into the phage *attP* landing site located in the *Drosophila* genome via the activity of Φ C31 integrase. This results in a transgene being incorporated into the *Drosophila* genome in a site-specific and directional manner creating the recombination sites of *attR* and *attL* flanking the transgene.

1.3 Steroid hormone production and signaling in *Drosophila melanogaster*

Ecdysone is synthesized in the prothoracic gland (PG) within the ring gland (RG), a three part tissue in which the PG is fused to the corpus allatum (CA) and the corpus cardiacum (CC)⁴⁰ (Fig. 1.2A). Ecdysone is released from the PG in controlled pulses (Fig. 1.1) to regulate developmental transitions. The neuropeptide PTH is synthesized in PTH-producing neurons and is sent to the PG where it binds to Torso, triggering a signaling cascade that results in Halloween gene upregulation, the principal genes of ecdysone synthesis⁴¹. Ultimately, *Drosophila* is incapable of synthesizing its own source of cholesterol and produces ecdysone from dietary sterols (e.g. cholesterol if present)⁴². The ecdysteroid pathway has been characterized for cholesterol as a starting sterol, but *Drosophila* is able to utilize other dietary sterols, which explains why several biologically active forms of ecdysone have been identified in *Drosophila*⁴³.

When demand for ecdysone production ramps up, cholesterol is converted to 7-dehydrocholesterol by Neverland (a Rieske electron oxygenase)¹⁴. Following this conversion, our current understanding is limited until 5 β -ketodiol is synthesized, this stage is known as the black box and all we know is that Shroud (a single short-chain dehydrogenase/reductase), Spook/Spookier and Cyp6t3 (both cytochrome P450 enzymes) are required^{16,22,44}. The black box is hard to elucidate because of the predicted short-lived nature of the intermediate products. Afterwards, Phantom, Disembodied and Shadow (all of which are cytochrome P450 enzymes) convert 5 β -ketodiol into α -ecdysone^{17,45-47} which is then released into the hemolymph and taken up by its target tissues. Shade (a cytochrome P450 enzyme) then converts α -ecdysone to its biologically active form: 20-Hydroxyecdysone (20E)⁴⁸ (Fig. 1.2B). Together, the collection of enzymes that convert cholesterol to 20E are known as the Halloween enzymes and from now on I will refer to α -ecdysone and 20E interchangeably as ecdysone and cytochrome P450 enzymes as “P450”.

P450s are a superfamily of heme oxygenases with a wide range of chemical and substrate specificity. In the context of this thesis I am focusing on their ability to convert ecdysone intermediates into the final form, however, they are also used for detoxification of xenobiotics and the degradation of carbon and vitamins. P450s require oxygen to deliver electrons from NADPH to the bound heme cofactor in order to perform oxygenation reactions⁴⁹. An important

aspect of P450 enzymes is that they require heme as a cofactor, which relates to why this thesis is focusing on iron and NO in ecdysone biosynthesis. At the center of every heme molecule lies iron, and so iron metabolism is important for the activity of P450s and ecdysone biosynthesis.

1.4 Heme biosynthesis in mammals and *Drosophila*

Heme is a valuable prosthetic group required in many of the living organisms studied to date. It is critical for the proper function of hemoglobin to transport oxygen throughout the body and for myoglobin to store oxygen in muscle cells. Furthermore, heme is required for catalases, peroxidases, P450s, nitric oxide synthase (NOS) and numerous other proteins involved with electron transfer to function. It is even required for the proper detection of the diatomic gases O₂ and NO.

To synthesize heme (Fig. 1.4A), glycine and succinyl-CoA are recruited to mitochondria and converted to aminolevulinic acid (ALA) by vertebrate ALAS1. This is considered the rate limiting step in heme biosynthesis and comes in two forms in mammals: ALAS1 and ALAS2 (or erythroid ALAS). ALAS2 is only expressed in erythroid cells, almost always in high amounts and is responsible for heme production for red blood cells whereas ALAS governs all other heme production.

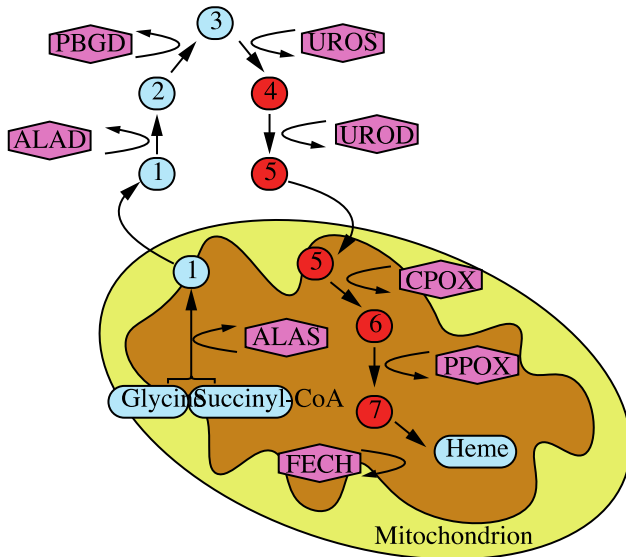
ALA is the sole source of carbon and nitrogen for heme production and is transferred out of the mitochondria where ALA dehydratase (ALAD) converts two ALA molecules into the porphobilinogen (PBG). Four PBG molecules are combined to form the tetrapyrrole hydroxymethylbilane intermediate by PBG Deaminase (PBGD). Afterwards, the first tetrapyrrole ring structure is formed when UROIII synthase (UROS) converts hydroxymethylbilane to Uroporphyrinogen III (UROIII). From this intermediate, until heme is produced, the ring structure can be spontaneously oxidized and is very sensitive to UV light, which alters these heme precursors from a colorless compound to a fluorescent red molecule (Fig. 1.4B). It is important to note that the red fluorescence is not generally noticeable when heme biosynthesis is unperturbed. However, when protoporphyrinogens (heme precursors with a ring structure) begin to build up, fluorescence becomes apparent upon UV excitation. The next conversion step involves UROIII decarboxylase (UROD) to create coproporphyrinogen III which is then transported back to the mitochondria and metabolized into protoporphyrinogen IX by coproporphyrinogen II oxidase (CPOX). This intermediate is aromatized into protoporphyrin IX by protoporphyrinogen IX oxidase (PPOX). Finally, iron is added to the core of the ring structure to form heme via ferrochelatase (FECH), preventing any further spontaneous oxidization of the

porphoryinogen ring structures, thereby preventing red autofluorescence to occur and desensitizing the compound from light.

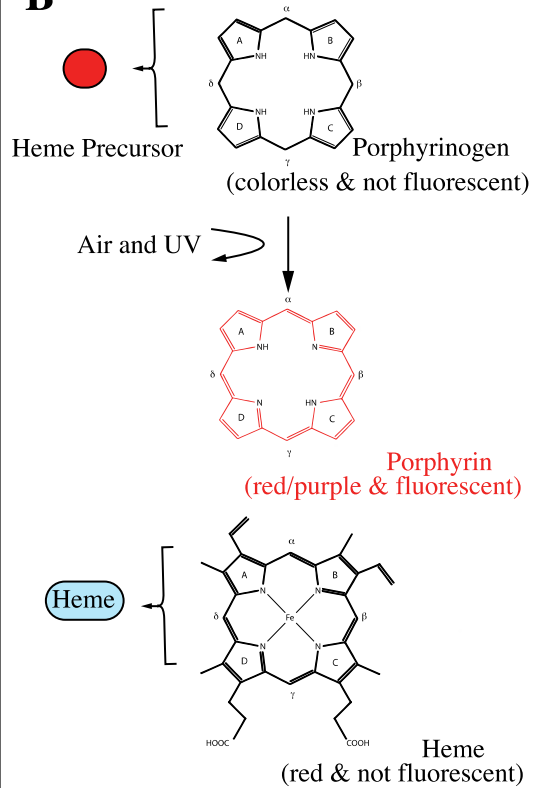
In mammals, Peroxisome Proliferator-Activated Receptor γ Coactivator 1 α (PGC-1 α) regulates and promotes the translation of ALAS1^{50,51}. PGC-1 α is turned on in low glucose conditions and is repressed by the heme sensor Rev-ER β . The *Drosophila* ortholog of Rev-ER β is E75 which also binds heme, but is thought to bind very tightly and instead is utilized as an NO sensor⁵².

When heme biosynthesis is impaired, precursors build up, resulting in a human disease called porphyria which is a severe metabolic disorder⁵³. After the production of ALA, any deficiency in the heme biosynthetic genes can result in a specific porphyria attuned to the particular porphyrin that is building up. Generally, individuals with this disease suffer from acute attacks triggered by fasting, drugs, stress, steroid hormones and more. During the attack, the nervous system can be greatly affected, proving fatal in 1% of cases⁵³. Furthermore, increased sensitivity to light results in skin lesions, inflammation and scarring. Porphyria can be treated with hemin and glucose transfusions to decrease protoporphyrin generation and buildup⁵⁴.

A



B



C

Abbreviation	Vertebrate Name	Fly Ortholog	Fly ID	Enzyme Product
ALAS	ALA Synthase	Alas	CG3017	1.Aminolevulinic acid (ALA)
ALAD	ALA Dehydratase	Pbgs	CG10335	2.Porphobilinogen (PBG)
PBGD	PBG Deaminase	l(3)02640	CG9165	3.Hydroxymethylbilane
UROS	UROIII Synthase	CG1885	CG1885	4.Uroporphyrinogen III (UROIII)
UROD	UROIII Decarboxylase	Updo	CG1818	5.Coproporphyrinogen III
CPOX	Coproporphyrinogen III oxidase	Coprox	CG3433	6.Protoporphyrinogen IX
PPOX	Protoporphyrinogen IX oxidase	Ppox	CG5796	7.Protoporphyrin IX
FECH	Ferrochelatase	FeCH	CG2098	8.Heme

Figure 1.4. The heme biosynthetic pathway. A) Starting with succinyl-CoA and glycine, eight enzymatic steps occur either within or outside of the mitochondria. The heme precursor protoporphyrin molecule is produced after the UROS conversion and is autofluorescent, indicated by a red circle. Each following step is autofluorescent until the incorporation of iron from FECH. **B)** The heme precursor porphyrinogen rings autofluoresce red when exposed to UV light, whereas heme does not. These structures are composed of four pyrrole rings connected with methyl groups (for porphyrinogens) or methane bridges (porphyrins and heme) and a porphyrinogen ring. The heme intermediates can convert to porphyrins upon exposure to air and light, resulting in fluorescence. Fluorescence is lost when iron is incorporated, producing the final heme structure. **C)** A table representing the *Drosophila* orthologs of the mammalian heme biosynthetic genes.

1.5 Iron regulation in mammals

Iron is a biologically critical element required to sustain life for the majority of organisms we are currently aware of. A fundamental characteristic of iron is its ability to switch between an oxidized or reduced state for chemical reactions. Iron is primarily utilized in heme as a cofactor but also for iron sulfur clusters (ISCs). Proteins that require heme or ISCs are important for many cellular actions such as oxygen transport, transcriptional regulation and DNA repair. The mitochondrial respiratory chain contains twelve enzymes that either require heme or ISCs^{55,56}. When not properly regulated, iron can have damaging effects on the cell. Byproducts of cellular respiration such as hydrogen peroxide and superoxide can react with excess free iron to produce reactive oxygen species (ROS) through a process known as Fenton Chemistry, which can result in the damaging of lipids, proteins and DNA⁵⁷. Anemia can arise via a lack of iron, preventing optimal circulation of oxygen, and other effects such as chronic inflammation and heart complications⁵⁸. Therefore, a very tightly controlled system of iron regulation is required due to both the critical role of iron in cell function and the severe health effects of misregulation.

A number of proteins regulate iron uptake, transport and storage (Fig 1.5). Once ingested, iron is absorbed in two different forms, heme-bound and non-heme-bound. Heme-bound iron is endocytosed into enterocytes via the Heme Carrier Protein-1 (HCP1). Heme is then degraded by a heme oxygenase, releasing ferrous iron as an end product where iron metabolism continues in line with non-heme iron. In the diet, non-heme iron in the ferric form is reduced to its ferrous state via the ferrireductase Duodenal Chytochrome B561 (DCYTB); ferrous iron then binds to the Divalent Metal Transporter 1 (DMT1) which carries iron across the apical membrane and into the cytosol of duodenal epithelial cells^{59,60}. Iron is then exported into the blood via Ferroportin (FPN), and then Hephaestin converts the ferrous iron back to its ferric state so that iron can bind Transferrin in the blood⁶¹⁻⁶³. All cells except epithelial intestinal cells then receive iron via holo-Transferrin: a Transferrin molecule bound to two ferric atoms. Cells import iron through binding of holo-Transferrin with the Transferrin Receptor (TfR) and internalize iron into endosomes, where the acidification process releases ferric iron for STEAP3 to convert it back to ferrous iron. Finally, DMT1 transports iron across the endosomal membrane to import iron into the cell^{64,65}. Once imported, iron is stored away into ferritin. Ferritin is an iron storage molecule capable of storing 4500 iron atoms, and is thought to release the iron upon cellular demand via

lysosomal degradation, however this method of iron release has been debated^{66,67}. Alternatively, Mitoferrin (MFRN) can transport iron into the mitochondria where it is used to complete the synthesis of heme and ISCs^{68,69}.

To achieve intracellular iron homeostasis, iron storage and iron import must be regulated as demand fluctuates. The Iron Response Protein/iron regulatory element (IRP/IRE) is an intricate regulatory system controlling iron availability within the cell (Fig. 1.6A). In humans and other vertebrates, transcripts from a number of genes important for iron availability form an RNA stem loop structure in their 5' or 3' untranslated regions (UTR), termed IRE⁷⁰ (Fig. 1.7). The consensus sequence for an IRE is a six base loop composed of the sequence CAGUGH (H being A, C or T) at the top followed by a four to five base pair helix that is just above an unpaired cytosine bulge, which is followed by a variable helix sequence⁷¹⁻⁷³. IRP will bind to this sequence, to either stabilize the mRNA or inhibit its translation depending on whether binding occurs in the 3' UTR or 5' UTR respectively.

Human *TfR* mRNA is an example of a 3' UTR IRE-containing transcript in humans. Under low iron conditions, IRP binds the IRE and stabilizes the transcript allowing for an increase in translation of the *TfR* mRNA, thereby increasing iron uptake. A second classic example is *ferritin*, which contains a 5' UTR IRE. Again, when iron levels are low, IRP binds the 5' UTR of *ferritin* mRNA and blocks the ribosome from binding and subsequently blocks translation of the *ferritin* transcript. This process decreases the amount of newly stored iron; ensuring iron is available in sufficient amounts for vital cellular processes. When iron levels are high or normal, IRP no longer inhibits ferritin or promotes TfR upregulation, and iron is stored away within ferritin cages.

Other examples of genes that are regulated by IRP in mammals to affect cellular iron levels include *FPN*, *DMT1*, *hypoxia inducible factor-2alpha (HIF-2α)* and *5'-aminolevulinate synthase 2 (ALAS2)*^{61-63,74-76}. *FPN* and *DMT1*, as previously mentioned, are involved in iron transport (Fig. 1.5), and so IRP acts to regulate cellular iron mobilization. *HIF-2α* contains a regulatory IRE as well as the ability to transcriptionally regulate *DMT1* and *FPN*, providing an extra layer of regulatory feedback^{77,78}. Finally, ALAS-2 is the first enzyme and rate limiting step required for heme synthesis in red blood cells, and so IRP regulates the rate of ALAS-2 production based on the availability of iron in the cell as heme requires iron at its core⁷⁵.

The IRP/IRE system has evolved as a cellular switch, sensing the concentration of iron to determine whether the promotion of iron uptake or storage is needed. This switch-like behavior is a result of the dual nature of IRP1 (one of two mammalian IRP proteins). Apo-IRP1 is the active RNA/IRE-binding form and holo-IRP1 is an active cytoplasmic aconitase that isomerizes citrate to isocitrate in the tricarboxylic acid cycle and is unable to bind RNA⁷⁹. This ability comes from the fact that holo-IRP1 aconitase must contain an ISC to function⁸⁰⁻⁸². If cellular iron is low, ISC formation becomes a limiting factor and dissociates from holo-IRP1. This is followed by a conformational change in IRP1 and enables the newly formed apo-IRP1 to bind RNA⁸⁰⁻⁸². Once iron levels have reached a sufficient concentration, ISCs are produced and are no longer limiting, allowing IRP1 to bind ISCs and resume IRP1 aconitase activity⁸⁰⁻⁸² (Fig. 1.6A).

Cells exert further control over IRP1 activity through phosphorylation, but how phosphorylation affects IRP1 RNA-binding activity is not very well understood. What is known, is that serine 138 of IRP1, when phosphorylated by protein kinase C, is highly sensitized to ISC levels. This causes a shift in RNA-binding activity to occur at a lower threshold of cellular iron concentrations⁸³. Furthermore, this regulation of protein kinase C is also capable of affecting serine 711, thereby reducing both aconitase and RNA-binding capabilities of IRP1⁸⁴⁻⁸⁶.

Another mechanism triggering the switch from holo-IRP1 to RNA-binding IRP1 is contact with NO, which results in the loss of IRP1's ISC, a process that has been studied *in vitro* but is poorly understood *in vivo*^{87,88} (Fig. 1.6B). NO is a well-studied secondary messenger molecule found in many developmental pathways, most commonly known for initiating the cGMP signaling pathway for the vasodilation of blood vessels⁸⁹. It is synthesized by NOS⁹⁰ and may play an important role in iron regulation.

The other IRP, IRP2, is 56% identical to IRP1 and has a 73 cysteine rich amino acid insert that currently has no known purpose⁵⁷. Unlike IRP1, IRP2 is only an RNA-binding protein and rather than losing its RNA-binding ability in high iron environments, it is instead rapidly degraded⁹¹. This regulation is under the control of an F-Box protein, FBXL5, which targets an E3-ubiquitin ligase complex to degrade IRP2^{92,93}. FBXL5 reversibly binds both iron and oxygen, allowing IRP2 to respond to cellular iron levels as well as hypoxic conditions⁹⁴⁻⁹⁷. Ultimately, both IRP1 and IRP2 regulate cellular iron levels through binding IREs.

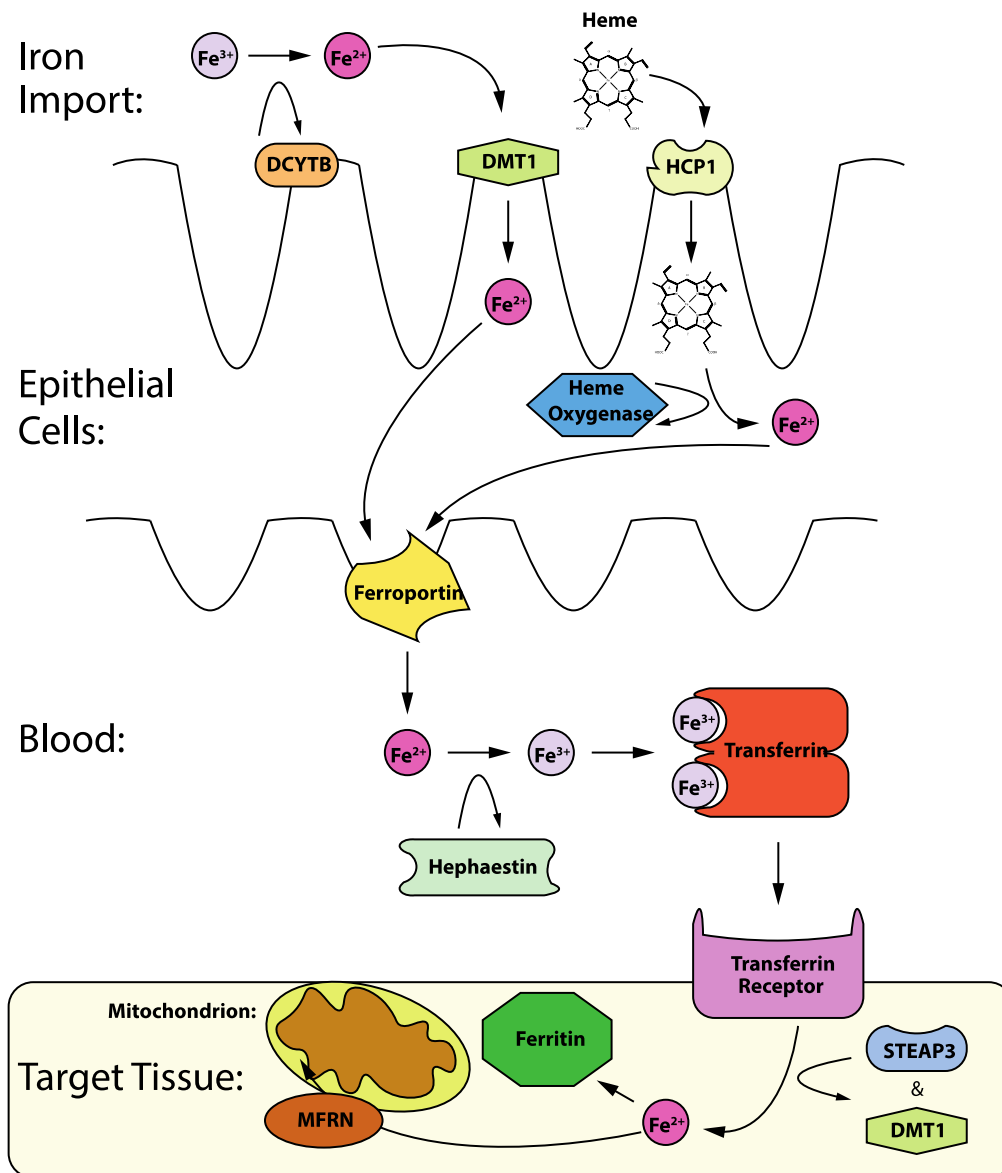


Figure 1.5. Iron absorption and delivery in vertebrates. Ferric iron (Fe^{3+}) in the diet is converted to ferrous iron (Fe^{2+}) by ferrireductase Duodenal Cytochrome b561 (DCYTB) and then imported into endothelial cells by Divalent Metal Transporter 1 (DMT1). Additionally, heme-bound iron is imported into endothelial cells by the Heme Carrier Protein-1 (HCP1) and then it is degraded by Heme Oxygenase with an end product of ferrous iron. Ferrous iron is then exported out of the cell and into the blood for transport via Ferroportin. In order to be transported to target tissues by Transferrin, ferrous iron is converted to ferric iron by Hephaestin. Once Transferrin reaches its target tissues, it is imported by the Transferrin Receptor where STEAP3 and DMT1 alter iron to its ferrous state and export it from the endosome, respectively. Ferrous iron can then be stored within ferritin or imported into the mitochondria via Mitoferrin (MFRN) for cellular activities such as iron sulfur biogenesis or heme biosynthesis.

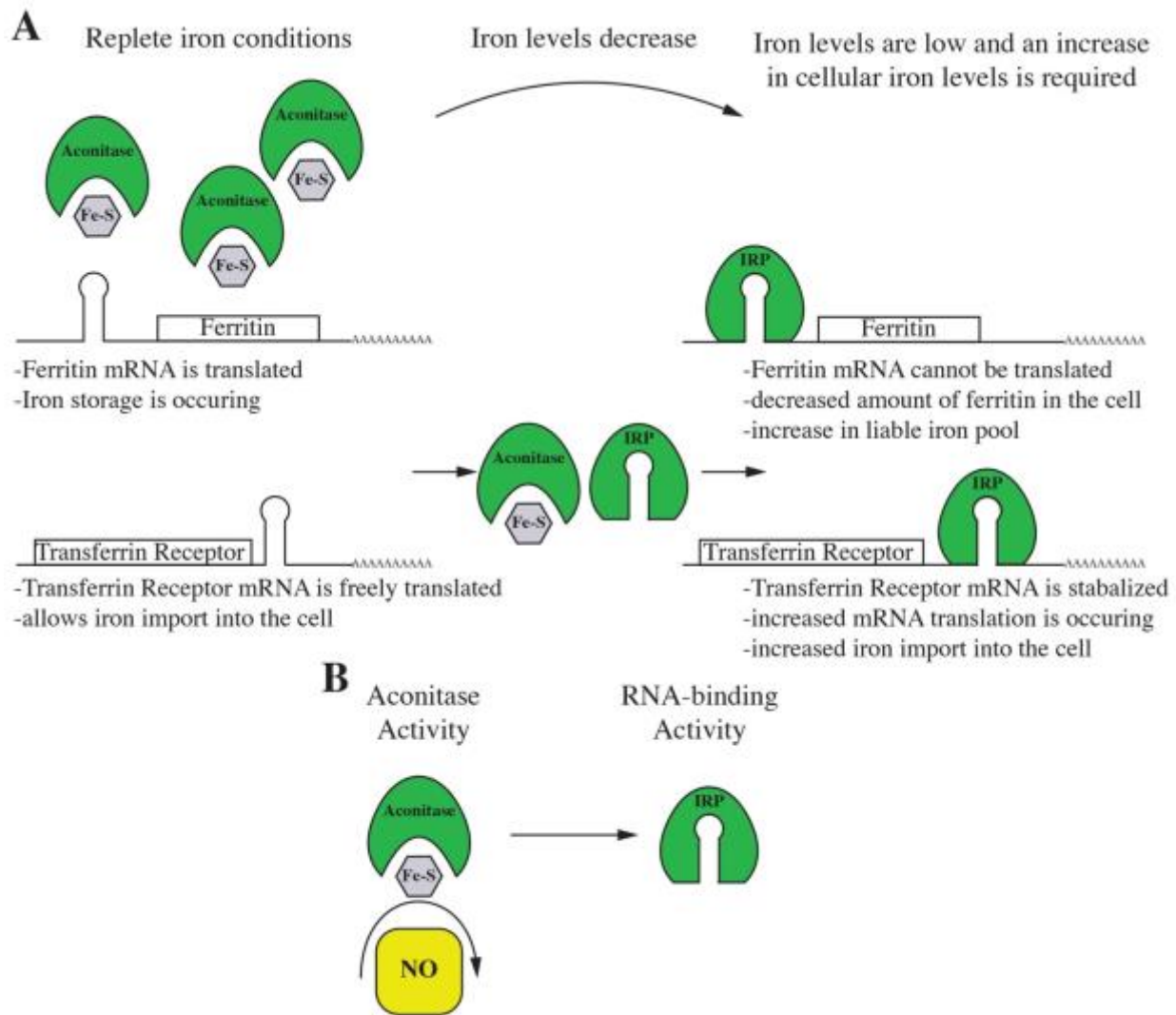


Figure 1.6. Activation modes for Iron Regulatory Proteins (IRPs). Shown here is how IRPs in both mammals and insects function under variable cellular iron concentrations and how they behave in the presence of nitric oxide (NO). This is a representation of the IRPs that switch between their aconitase form and RNA-binding form: IRP1 in mammals and IRP-1A in *Drosophila*. IRP2 in mammals is purely RNA binding, has no aconitase activity and is degraded in low iron conditions. IRP-1B in *Drosophila* has no RNA-binding activity, and acts as an aconitase. **A**) Under low iron conditions, the Iron-sulfur (Fe-S) cluster is destabilized and is unbound to holo-IRP, resulting in a conformational change to the apo/RNA-binding form. IRP then binds IREs in either the 5' or 3' UTR of its mRNA targets, thereby blocking ribosome binding and preventing translation of the transcript (5' UTR IRE) or stabilizing the transcript and increasing translation (3' UTR IRE), ultimately increasing cellular iron levels. *ferritin* and *transferrin receptor* are both used as examples of iron regulatory genes containing an IRE either in the 5' UTR or 3' UTR of their transcripts, respectively. **B**) NO attacks the Fe-S cluster contained in holo-IRP and removes it from IRP, triggering the switch from holo- to apo/RNA-binding IRP. In replete iron conditions, IRP would normally be in its holo form, however, regardless of iron levels, NO will cause the switch to the RNA-binding form. It is important to note that this function of NO has only been shown in vitro. IRP: Iron Regulatory Protein NO: nitric oxide.

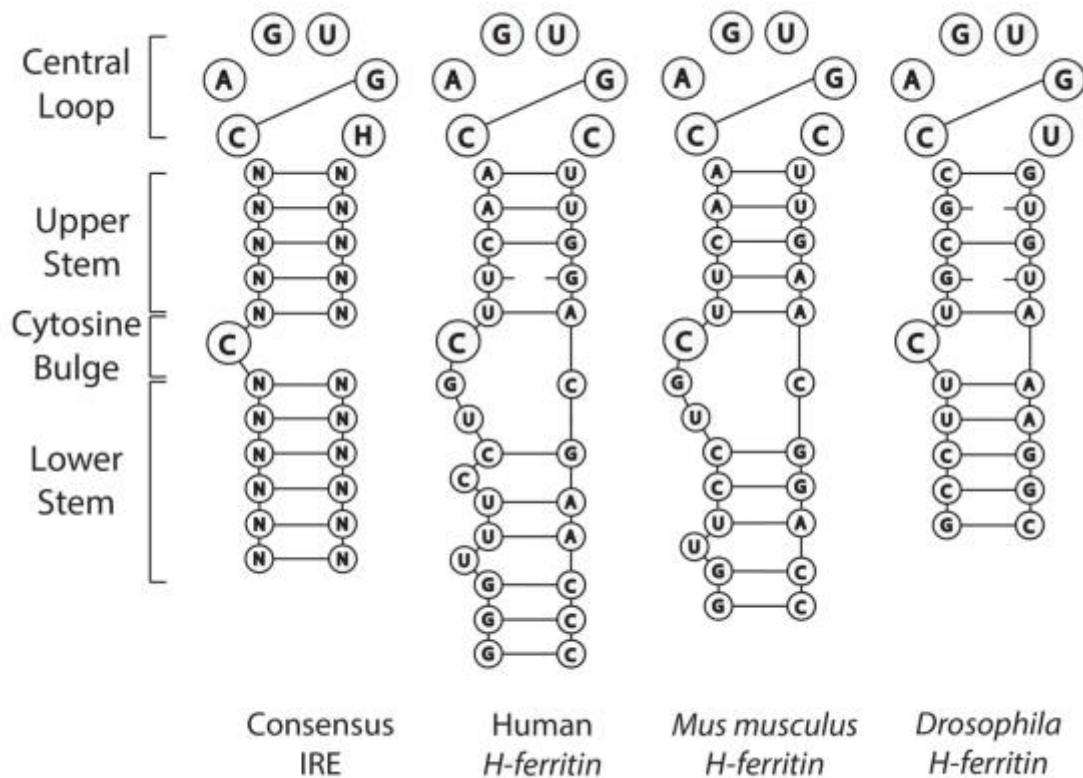


Figure 1.7. Comparing the consensus IRE motif to human, *Mus musculus*, and *Drosophila H-ferritin* IREs. The hexanucleotide loop CAGUGN/H atop a five base pair stem followed by an unpaired cytosine bulge and six base pair lower stem. N indicates any possible base and H in the hexanucleotide loop cannot represent guanine. This is because the first cytosine interacts with the second guanine in the loop to form the proper IRE structure; if N was guanine, this interaction would be impaired. The cytosine bulge can either consist of two base pairs and a cytosine or simply just cytosine, interestingly the three base pair bulge is seen mostly in *H-ferritin transcripts*, although not in *Drosophila*. The stem structure can consist of both standard base pairing and wobble base pairing (broken line).

1.6 Comparing iron regulation in mammals to *Drosophila*

The majority of studies in iron regulation have been in mammals, perhaps because mammals undergo erythropoiesis, a process connected to iron regulation, whereas all known insects do not. This highlights why it is important to know where the differences lie between *Drosophila* and mammalian iron regulation because our understanding of iron regulation in the two systems will inherently have differences and similarities. The mammalian proteins DMT1, ferritin, Transferrin, Melanotransferrin, Hephastin and IRP1/2 have direct *Drosophila* homologs named Malvolio (Mvl), ferritin, Tsf1, Tsf2, MCO1/3 and IRP-1A/B, respectively. Malvolio, like vertebrate DMT1, is an iron import protein^{98,99}, and both ferritin proteins perform the same purpose although it is predicted in *Drosophila* that ferritin is for iron transport as well as iron storage^{100,101}. Transferrins are abundant in the *Drosophila* hemolymph, known to bind iron and are implicated in the immune response. However, it is currently unknown if transferrins are involved in iron transport¹⁰². The MCOs are known ferroxidases required to oxidize iron from its ferrous to ferric state in order to be used by cell machinery¹⁰³. Lastly, and most relevant to this thesis, *Drosophila* has two genes similar to *IRP1* and no genes similar to *IRP2*. The two IRP1 like proteins are IRP-1A and IRP-1B and have 87% sequence similarity¹⁰⁴. *Drosophila* was the first insect shown to have IRP/IRE binding activity, specifically regulating *succinate dehydrogenase b (sdhb)* mRNA^{105,106}. Since the discovery of an IRE in *sdhb*, researchers have only been able to find one additional *Drosophila* gene harboring an IRE, located in the 5' UTR of *ferritin* mRNA, which is utilized only within one of its nine predicted isoforms: *ferritin heavy chain homolog 1 (ferritin HCH1) RA*¹⁰⁷⁻¹⁰⁹. Unlike mammals, which have two proteins capable of binding IREs, *Drosophila* only has one. *Drosophila* IRP-1A has the switch-like behavior of IRP1, acting as an aconitase when bound to an ISC or an RNA-binding protein when the ISC is lost. *Drosophila* IRP-1B on the other hand, is only an aconitase¹¹⁰.

There are also some iron protein homologs conserved between mammals and *Drosophila*, in which their role in iron metabolism is not understood. DCYTB in mammals, as previously mentioned, is required to reduce ferric iron for subsequent iron import, but the *Drosophila* homologs *CG1275* and *no extended memory (nemy)* are not currently associated with iron metabolism. *CG1275* has yet to be studied and *nemy* is only studied in the context of memory¹¹¹.

Also, the HIF α/β mammalian proteins are homologous to Sima and Tango, but are only studied in their relation to hypoxia, with no direct studies on iron regulation¹¹².

The main differences in mammalian and *Drosophila* iron metabolism are the functions of ferroportin and the TfR. Mammalian Ferroportin is the exporter of ferrous iron, and with no known homologue in *Drosophila*, researchers are unclear as to how iron is released from *Drosophila* cells¹¹³. This could be where the aforementioned ferritin cages of *Drosophila* play a major role, because in ticks, it is shown that ferritin is exported, likely for transport¹⁰¹. The other difference is that there is no known TfR in *Drosophila*, despite Tsf1 being highly abundant¹¹³. It is possible that Tsf1 has an evolutionarily diverged TfR, explaining why researchers have not yet identified it, however, it is also possible that ferritin has its own receptor in *Drosophila* and that a *Drosophila* TfR does not exist¹¹⁴.

Overall, much of our knowledge about iron metabolism stems from the mammalian system, but a major disadvantage to studying iron in mammals is the high priority for iron in erythropoiesis¹¹⁵. And so, with *Drosophila* dedicating less iron demand into erythropoiesis, it is an easier task to analyze iron metabolism in other tissues and for the extent of this thesis, studying iron metabolism in the PG of *Drosophila* and its relation to ecdysone biosynthesis.

1.7 Iron sulfur cluster biosynthesis

Iron sulfur clusters are vital to many life processes as inorganic cofactors for many proteins and are a major expenditure of cellular iron. ISCs come in two main forms, 2Fe-2S or the more common 4Fe-2S (found in IRP1 and IRP-1A). Assembly occurs in the mitochondria and involves a surprisingly complex set of over 20 genes and proteins that fall into three main categories of ISC biosynthesis¹¹⁶. The first category is the ISC assembly machinery. Cysteine Desulfurase provides sulfur and the ferredoxin electron transfer chain provides ferrous iron to the scaffold protein Isa1, where ISCs are constructed^{117,118}. The proper formation of ISCs on the scaffold protein also require the HSP70 chaperone system to maintain proper connections¹¹⁹. The second category is the ISC export system, which is involved with transporting the ISCs out of the mitochondria towards the third category: the cytosolic iron-sulfur protein assembly (CIA) machinery. This is where ISCs are incorporated into their respective proteins and concludes ISC biosynthesis¹²⁰.

Researchers found the first link between ISC biosynthesis and heme regulation in 2005, within zebrafish. When ISC biosynthesis was disrupted by a knockdown of the gene *glutaredoxin 5 (grx5)*, they found that IRP1 was activated and bound to *ALAS* mRNA causing a decrease in heme production¹²¹. Furthermore, *grx5* yeast mutants were rescued with the corresponding zebrafish homologue, further demonstrating a high level of conservation in ISC biosynthesis between species.

1.8 Nitric oxide signaling and regulation

The role of nitric oxide as a signaling molecule was originally found to be involved in the inflammatory/immune response and blood vessel vasodilation. It has a very short half-life ranging from 2 ms to 2 s, therefore, the site of synthesis needs to remain close to the site of action¹²². NO is produced by NOS; it is a homodimeric enzyme with heme cofactors that reduce oxygen to convert L-arginine to L-citrulline and NO^{123,124}. NOS has an N-terminus oxygenase domain that binds to a heme cofactor and a C-terminus reductase domain that binds FAD, FMN and NADPH for electron transfer¹²⁵. To activate NOS, acetylcholine activates the phospholipase C signaling pathway to increase cellular levels of Ca²⁺, activating calmodulin. Calmodulin binds NOS and causes an electron flow from its NADPH cofactor to the heme cofactor to reduce oxygen and synthesize NO¹²⁶.

Mammalian genomes harbor three *NOS* genes: *neuronal NOS*, *endothelial NOS* and *inducible NOS*. *Drosophila* however, has only one *NOS* gene, which encodes ten transcripts, one of which is the functional enzyme¹²⁷. It is proposed that *Drosophila NOS* is also regulated by its alternative transcripts through dominant negative binding. The idea is that since NOS is a homodimeric enzyme, a dominant negative isoform could bind and inhibit the active form of NOS¹²⁸. Furthermore, it has been proposed that a fourth mitochondrial *NOS* gene exists, however this proposal is heavily debated¹²⁹.

NO is utilized in many different forms via auto-oxidation and catalysis into nitrite (NO₂⁻), nitrate (NO₃⁻), peroxynitrite (ONOO⁻), iron-nitrosyl (FeNO), s-nitroso (SNO) and N-nitroso (NNO), which are all capable of acting on their downstream effectors^{130,131}. NO can be stored as either nitrate or nitrite in a cellular NO pool. NO can be released when needed by Xanthine Oxidoreductase and hemoglobin during times of stress when NOS has limited activity due to minimal O₂ levels in the cell¹³².

NO acts in a multitude of signaling pathways, either through direct action, or through its various forms. NO can directly regulate potassium ion channels to initiate hyperpolarization of the vascular smooth muscle, resulting in vasodilation. NO also plays a role in cellular signaling through protein modifications, similar in nature to phosphorylation: s-nitrosylation, s-glutathionylation, and tyrosine nitration. S-nitrosylation involves a nitro group being added to a cysteine thiol to form a nitrosothiol, which is a reversible protein modification implicated in NO

signal transduction¹³³. S-glutathionalation occurs when a low molecular mass thiol is added to a protein that is connected to a cysteine through a mixed disulfide bridge and is primarily indicated in redox signaling. Finally, tyrosine nitration refers to a nitro-group (NO₂) being added to a phenolic ring of tyrosine to form a 3-nitrotyrosine residue and results in a signal to the cell informing the presence of nitro-oxidative stress¹²⁹.

NO also plays a role in the mitochondria by affecting cytochrome c oxidase (CcO). NO competes with oxygen to increase the k_m for O₂ in respiration, thereby regulating the oxygen sensitivity of CcO. As a result of NO's ability to inhibit CcO, it can block oxidative phosphorylation, control the degree by which CcO-related apoptosis is initiated and regulate ROS generation^{134,135}. Furthermore, NO can also regulate the oxygen-dependent transcription factor HIF. HIF is destabilized when oxygen levels are plentiful, and unable to activate hypoxic response genes. However, NO is capable of stabilizing HIF, causing the cell to act as if it was in a hypoxic state¹³⁶. As previously mentioned, HIF regulates FPN and DMT1 in iron metabolism and constitutes a second mechanism in addition to IRP1 RNA-binding activation, in which NO can influence iron biology. Finally, the most commonly known action of NO is that it triggers the cyclic GMP (cGMP) signaling pathway by activating guanylyl cyclases for vasodilaion¹³⁷ and that NO is used in response to bacterial invasion for its damaging oxidative capabilities in high concentrations¹³⁸.

The most pertinent mechanism of NO to my work was its ability to affect the stability of ISCs. It was first noted that when exposed to nitrite (which produces NO), the electron spin resonance signal of ISCs in laboratory samples was lost, and the signal indicating iron-nitrosyl compounds became detectable. This signified to researchers that NO was to some degree affecting the stability of ISCs¹³⁹. Next, it was discovered that ISC containing enzymes lost their function when exposed to NO, and again that iron-nitrosyl complexes were formed¹⁴⁰. Around this time, the study of the IRP/IRE system was being elucidated and researches wondered if the ability of NO to disrupt ISCs and ISC containing enzymes could translate to the iron metabolic system. Indeed, it was found that NO could activate IRP by disrupting its ISC and cause an increase in cellular iron through its RNA-binding capabilities (Fig. 1.6B). NO was implicated in the regulation of both *ferritin* and *TfR*, with the other IRE associated genes to be elucidated in the future^{141,142}.

1.9 Previous research

The original research interest in the King-Jones lab focused on how the formation of steroid hormone pulses were regulated. This led to the surprising connections between NO, iron regulation and ecdysone. A microarray identified genes that had tenfold increased expression in the RG compared to the whole body. The rationale was that genes related to the synthesis of ecdysone would have higher expression in ecdysone-producing tissues. The top 100 hits with the highest specificity to the RG were then subjected to phenotypic analysis by knocking down the gene expression using RNAi-targeted to the PG¹. This was performed using the *GAL4/UAS* system where the *GAL4* driver *phantom22* (*phm22*) promoted expression of the *UAS*-associated RNAi in the PG. The goal was to identify any delay in development or larval lethality, which would be indicative of a defect in ecdysone production. A commonly observed phenotype when ecdysone production is disrupted is the failure to proceed to the next developmental stage, such as the larval-prepupal transition. Ultimately, our lab came across a phenotype associated with a subset of genes related to ecdysone regulation: third instar arrest and giant red fluorescent ring glands (Fig. 1.8).

The first gene discovered using this RNAi knockdown screen in the PG that resulted in arrested larval development and the giant red ring gland phenotype was *spatzle5*. Literature searches revealed that *NOS^{IR-X}-RNAi* driven by *phantom22-GAL4* (*phm22>NOS^{IR-X}-RNAi*) have a similar phenotype². The King-Jones lab then performed a spectrophotometer analysis of the fluorescent peaks from the red ring glands and determined that the red fluorescence was a result of heme precursor buildup. The protoporphyrin ring structure of a heme precursor fluoresces red under UV light until an iron molecule is incorporated into the center, producing heme (Fig. 1.4). Additionally, *phm22>NOS^{IR-X}-RNAi* L3 larvae can be rescued to adulthood when fed ecdysone, signifying the connection between NOS and steroid hormones. As well, when PPOX, an enzyme required for heme biosynthesis, is knocked down in the PG using RNAi, the same phenotype of L3 arrest and giant red fluorescent ring glands occurs, further supporting that the fluorescence is attributed to heme precursor build up (Ch. 1.8). Unfortunately, the phenotype resulting from the *spatzle5*-RNAi knockdown was later found to be caused by an off-target effect, and so myself and the King-Jones lab chose to focus on the connections between NOS, heme, and ecdysone.

Since IRP's conformational state is influenced by NO *in vitro*, I wanted to examine whether NOS produces NO to activate the RNA-binding form of IRP-1A in *Drosophila* PGs prior to the major L3 ecdysone pulse. The resulting influx of iron from IRP-1A's RNA-binding activity is predicted to be used in times of heme demand, such as when P450 enzymes are required to synthesize ecdysone pulses (heme is a cofactor), particularly in the late L3. P450 transcripts are increasingly abundant in the late L3 larvae ranging in increases from 5-100-fold¹. This would likely result in a high demand for heme generation by the presence of P450s in the PG. Qiuxiang Ou, a postdoc in the lab, discovered that a NO signal is present in the PG just prior to the late L3 pulse of ecdysone, and removing NOS via RNAi ablates the NO signal. The King-Jones lab has also been able to show that ectopic expression of *IRP-1A* in *Drosophila* rescues *phm22>NOS^{IR-X}-RNAi* from larvae to adults as well as the large fluorescent RG phenotype. This suggests NOS and NO do indeed play a role in ecdysone synthesis, perhaps through iron regulation. It is important to note that iron levels are sufficient for larval growth at this time and an NO signal may be required to increase cellular iron levels, specifically in the PG, for ecdysone synthesis.

How the two genes harboring IREs in *Drosophila* play a role in iron regulation and metabolism is not fully understood. The 5' UTR IRE of *ferritin* should result in decreased translation when IRP-1A is present and RNA-binding, thereby decreasing cellular iron storage capabilities of the cell, making iron more available for heme. *sdhb* has a role in the citric acid cycle and when active, prevents the production of the heme precursor molecule succinyl-CoA. Therefore, downregulation of *sdhb* through its 5' UTR IRE should allow for increased heme production.

I explored the role of IRP-1A in the PG in relation to ecdysone production. I hypothesized that NO was required to increase available cellular iron concentrations within the PG by triggering IRP-1A to become RNA-binding. The increased abundance of iron could be utilized for incorporation into heme for subsequent use as a P450 cofactor, which is required for ecdysone production (Fig. 1.9). Do NO pulses occur at specific times in the PG, are they correlated to IRP-1A RNA-binding activity or ecdysone signaling? To answer these questions, I wanted to know if the lack of NO in *phm22>NOS^{IR-X}-RNAi* animals and the associated phenotype of giant red ring glands and L3 arrest could be rescued with IRP-1A RNA-binding activity. The idea being that the NO signal was required to shift IRP-1A to its RNA-binding form

to promote increases in cellular iron, these increases would supply iron for heme, allowing P450s to synthesize ecdysone. If IRP-1A could be biologically or artificially induced to become RNA-binding in the PG, then a lack of NO signal in *phm22>NOS^{IR-X}-RNAi* animals should not be lethal. I manipulated dietary iron in an attempt to trigger IRP-1A to switch to its RNA-binding form, however that approach was unable to rescue the *NOS^{IR-X}-RNAi* animal. Expressing a constitutively active form of *IRP-1A* in the PG however, did rescue the *NOS^{IR-X}-RNAi* animal to adulthood. However, I also determined that the *NOS^{IR}-RNAi* phenotype is likely due to an off-target effect, suggesting that IRP-1A is rescuing the animal with respect to iron regulation and heme production, as opposed to bypassing a lack of NO. Finally, I showed that NO signaling occurred prior to and during ecdysone signaling in the L3 stage, suggesting that NO had a role correlated to ecdysone biosynthesis, but leaving to question how NO signaling was connected with the off-target effect of the *NOS^{IR}-RNAi* phenotype.

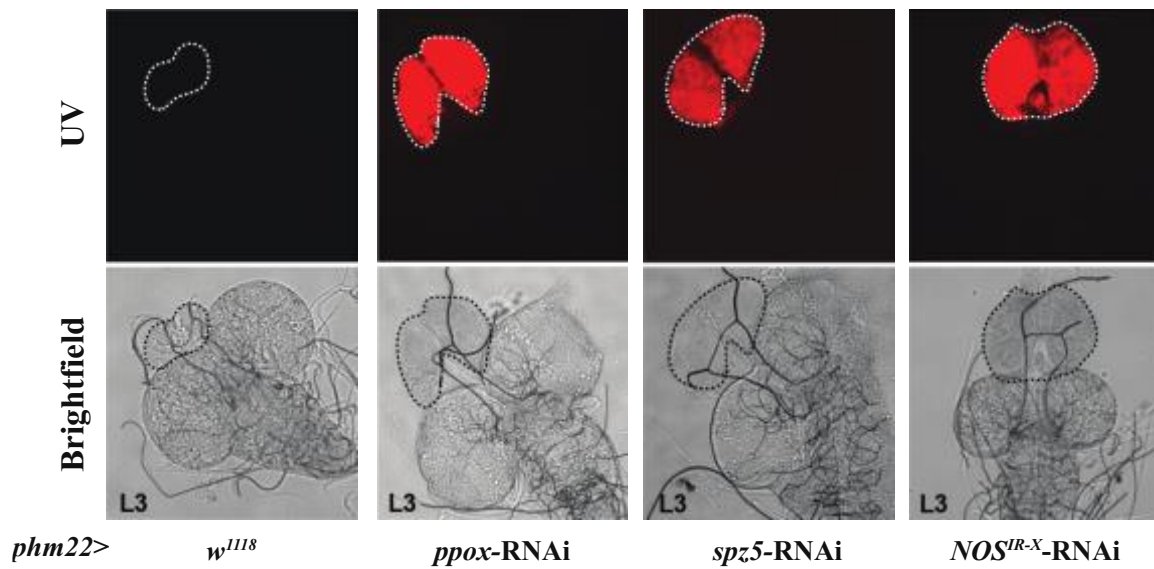


Image credits: Qiuxiang Ou, Kirst King-jones

Figure 1.8. Giant red ring glands from third instar larvae of *phm22>spz5-RNAi* and *phm22>NOS^{IR-X}-RNAi* are phenotypically similar to heme biosynthesis disruptions. Control ring glands were dissected approximately 4 hours prior to pupariation (~116 hours after egg laying) and were compared to *PpoX*-, *spz5*-, and *NOS^{IR-X}*-RNAi ring glands of developmentally delayed third instar larvae (~168 hours after egg laying). *PpoX*: porphyrinogens oxidase (required for heme biosynthesis). *Spz5*: spätzle5. *NOS*: Nitric Oxide Synthase. L2: second instar. L3: third instar.

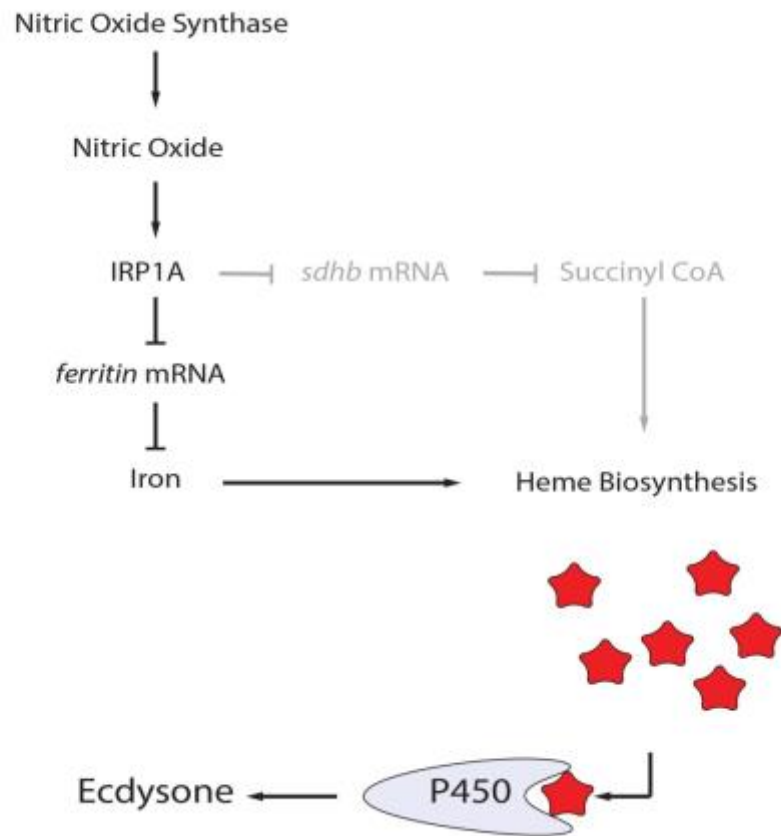


Figure 1.9. The proposed *Drosophila* NOS/IRP-1A/ecdysones pathway. In the model, Nitric Oxide Synthase (NOS) produces Nitric Oxide (NO) prior to the major third instar ecdysone pulse. NO attacks the ISC cluster of IRP-1A, triggering a switch from the holo/aconitase- to apo/RNA-binding form. IRP-1A then binds the 5' untranslated region (UTR) Iron Response Element (IRE) of *ferritin 1 heavy chain homolog* mRNA ("*ferritin*") and decreases the amount of translation of *ferritin* mRNA by blocking ribosomal binding. A decrease in *ferritin* levels should increase iron availability for incorporation into heme, thus providing ample heme supply for the large amounts of Cytochrome P450 enzymes (P450) required for the late third instar ecdysone peak. Additionally, IRP-1A binds the 5' UTR IRE of *succinate dehydrogenase b* (*sdhb*), decreasing its translation, making succinyl CoA increasingly available for heme production. The connection with *sdhb* to the NOS/IRP-1A/ecdysones pathway is faded to represent the main focus of this thesis being IRP-1A binding to *ferritin* mRNA.

2.0 Materials and Methods

2.1 *Drosophila* stocks and care

Drosophila melanogaster lines were maintained on a cornmeal/agar-based diet produced in our facilities at the University of Alberta, Nutrifly Bloomington formulation or a holidic diet (Ch. 2.17 and 3.4.1) using propanoic acid as a fungicide. All stocks are created in our lab, donated by colleagues (as indicated) or ordered from the Bloomington *Drosophila* Stock Center (BDSC). Fly lines used are listed in table 2.1 and figure 2.1, 2.2 and 2.3 details the insertion plasmids used to create the transgenic strains.

2.2 Computational IRE search

To search for predicted IREs within a gene, the transcript sequence was taken from Flybase and the FASTA sequence uploaded to the SIRE program¹⁴³ and given a predicted readout on the strength and characteristics of the predicted IRE. A more detailed summary is available in chapter 4.4.1.

2.3 Cloning IRP-1A and IRP-1B for injections

cDNA samples were ordered from the DGRC *Drosophila* gold collection (IRP-1A: LD36161, IRP-1B: LD13178) and transformed into chemically competent cells. Plasmids that contained the cDNA were based on pOT2¹⁴⁴ (a standard plasmid used for creating cDNA libraries). Transformations were performed by adding 50µL of 1X TE to the paper disc containing the dissolved plasmid and pipetted up and down two times. TE was immediately removed to avoid loss of DNA. 50µL of competent cells were added and incubated on ice for 30 minutes with a single one sec vortex half way through the incubation. Cells were heat-shocked for two min at 37°C and the cells (not the disc) were transferred into one mL of LB medium and incubated with shaking at 37°C for one hour. Cells were then spread after recovery on plates containing chloramphenicol (34 µl/ml) and left overnight at 37°C in 5 ml of LB+ chloramphenicol (34 µl/mL).

A mini-prep was performed on the 5 ml cultures using the GeneJet Plasmid Miniprep Kit (Thermo Fisher Scientific, catalog number: K0502). Isolated plasmids were then digested with restriction enzymes to verify identity using Fast Digest enzymes EagI, BSiwI, EcoI, KpnI and SmaI with their associated protocols (Thermo Fisher Scientific). To further verify identity, genes were sequenced (Ch. 2.6) and confirmed by comparing gene sequence to validate sequences to their gold clone counterpart.

IRPP-1A/B were then TOPO cloned into pENTR-DTM using the pENTRTM Directional TOPO Cloning Kit and associated protocol (Thermo Fisher Scientific, Catalog number: K240020) by first PCR amplifying *IRP-1A/B* with primers that add the sequence “CACC” 5' of the open reading frame cDNA sequence. PCR fragments were gel-extracted using the Qiaquick Gel Extraction Kit and associated protocol (Qiagen, catalog number:28704). Topoisomerase directionally inserted *CACC-IRP-1A/B* cDNA fragments were gel excised. The reaction was then transformed into OneShot Top10 competent cells from the TOPO kit as per the associated protocol. Successfully transformed colonies were grown in 5 ml cultures and Mini-prep procedure performed as above. Fast Digest enzymes EagI and BSiWI were then used as above to directionally verify the insert of *IRP-1A/B* cDNA into pENTR. I then performed site-directed mutagenesis (Ch. 2.4) on *IRP-1A* before further gateway cloning.

An LR clonase II gateway reaction was then performed to recombine *IRP-1A*, *IRP-1A^{C450S}* (Ch. 2.4) and *IRP-1B* cDNA into pBID vectors. pBID vectors containing *attB* and *attP* sites for recombination and are able to tag the genes with a sequence encoding three repeated FLAG sequences that can be recognized by specific antibodies once translated. As well, the pBID vectors are fully functional expression vectors capable for injection into *Drosophila* via the Φ C31 injection method¹⁴⁵. The reaction was performed as per product manual: LR clonase II (Thermo Fisher Scientific, catalog number: 11791-020). Successfully transformed colonies were then isolated and sequence verified prior to injection (Ch. 2.14). Primers used are listed in table 2.2.

2.4 Site-directed mutagenesis of *IRP-1A* to create a form of IRP-1A that is always RNA-binding

The three key cysteine residues required for ISC binding to human IRP⁸⁰ (amino acids: 437, 503, 506;) were aligned within *Drosophila*, chicken and mouse homologues using clustal omega¹⁴⁶ (Fig. 2.4). All three cysteines were conserved within each of the species analyzed and therefore the 450th amino acid (cysteine) was chosen because previous work has illustrated that when amino acid 437 is mutated in IRP1, it loses all aconitase functionality.

The following protocol is courtesy of Virginia Pimmet from the Simmonds lab (University of Alberta) and was used for Site Directed Mutagenesis (SDM) of *IRP-1A*. In a single reaction 10 µl of 5x Reaction buffer, 50 ng of plasmid template (IRP-1A), 100 ng of Forward Primer #1 (1 µl of 10 µg/µl working stock), 100 ng of Forward primer #2 (1 µl of 10 µg/µl working stock), 1 µL of 10 µg/µl dNTP mix, 0.5 µL Phusion polymerase (NEB, catalog number: M0530) and ddH₂O was added to a final volume of 50 µl. Primers were designed using QuickChange primer design for SDM. The reaction is cycled in a PCR machine as follows: 95°C for 30 sec, 12 cycles of 95°C for 30 sec, 55°C for 1 min and T_M-3°C for 1 min/kb of plasmid length. Afterwards 75°C for 10 min and a 4°C hold.

A *DpnI* digestion was then performed to digest unmutated PCR product by digesting all methylated DNA (newly synthesized DNA via PCR is not methylated). I began by adding 1 µl of Fast Digest *DpnI* and 5.7 µl of enzyme buffer to each sample tube and mixed thoroughly followed by incubation for at least one hour at 37°C. The product was sequence verified and then transformed into OneShotTopTen cells as above and followed with gateway cloning (Ch. 2.3). Primers used are listed in table 2.2.

2.5 Competent Cells

To make cells for transformations when OneShot TopTen cells were not used, the following procedure was used and was adapted from Inoue, *et al* (1990)¹⁴⁷. 100mL of SOB media and 100µl of a 5ml overnight DH5α culture were added together and shaken at room

temperature until a density of OD₆₀₀ of around 0.5 was achieved (approximately 1.5 days). The culture was poured into pre-chilled tubes on ice for 10 minutes and then centrifuged at 2500 g for 10 minutes at 4°C. The supernatant was discarded and the pellet was suspended in 30 mL of Trituration buffer (TB) (contains calcium and magnesium) (0°C). 600 µL of DMSO and the solution were mixed gently and placed on ice for 10 minutes. The culture was dispensed in 200 µL aliquots into 1.5 mL Eppendorf tubes and flash frozen and stored at -80°C. Solutions are listed in table 2.3.

2.6 Sequencing Reaction

Sequencing reactions were carried out in the following two ways: 1) BigDye Sequencing reaction was PCR amplified by myself using the BigDye Terminator v3.1 Cycle Sequencing Kit (Thermo Fisher Scientific, Catalog number: 433754) and the Molecular Biology Service Unit (MBSU) at the University of Alberta then sequenced using a Sanger DNA Sequencer (ABI 3730) or 2) the MBSU facility receives a sample containing 250 ng DNA, 2.5 pmoles of primer filled to 10 µL with H₂O and performed all BigDye reactions and sequencing also using the Sanger DNA Sequencer (ABI 3730).

Sequencing results were analyzed using FinchTv (Geospiza inc.) to determine sequencing readout and accuracy¹⁴⁸. Sequencing primers are listed in table 2.2.

2.7 RNA extraction from dissected tissue

Larva were dissected in 1% phosphate-buffered saline (PBS) to maintain cellular pH in solution and transferred to 100 µL TRIzol on ice (if the sample was not used right away, it was flash-frozen and stored at -80°C). The sample was homogenized using a mechanical pestle for one minute followed by the addition of TRIzol to a final volume of 1 mL. Next, 200 µL of chloroform was added and vortexed for 15 sec and let sit for one minute. Samples were centrifuged at max speed for 10 min at 4°C. The aqueous phase (top) was transferred to a fresh RNase-free Eppendorf tube followed by the addition of an equal volume of ethanol and mixed by pipetting up and down. 700 µL of the sample was transferred to an RNeasy Mini spin column

placed in a 2 ml collection tube and centrifuged for 30 sec at speeds greater than 8,000 g. The flow through was discarded and 700 μ l of Buffer RWI was added to the column and spun again for 30 sec at \geq 8,000 g. The flow-through was again discarded and 500 μ l of Buffer RPE was then added and spun for 2 minutes at \geq 8,000 g. The column was then transferred to a 2 ml collection tube and centrifuged for one minute at max speed to dry the membrane. The column was placed in a new 1.5 ml Eppendorf tube and 30 μ l of RNase-free water was added to the membrane of the column and centrifuged for one minute at \geq 8,000 g to elute the RNA. Note: it takes approximately 30 RGs or 10 BRGCs per RNA tissue sample to have sufficient RNA concentrations for cDNA synthesis and qPCR analysis. Kit components used are from Qiagen's RNeasy Mini kit (Catalogue number: 74104).

2.8 RNA extraction of whole body samples

Five wandering larva were flash frozen, transferred to 100 μ l of TRIzol and homogenized using a mechanical pestle for one minute. The volume was brought up to 1ml TRIzol and vortexed. The sample was incubated at room temperature (RT) for 5 min, and then 200 μ l of chloroform was added. The sample was shaken vigorously by hand for 15 sec followed by a 3-minute incubation at RT. Afterwards, samples were centrifuged for 15 min at 4°C at 12,000 rpm. The aqueous phase was transferred to a 1.5 ml microfuge tube followed by the addition of 500 μ L of isopropanol and inverted five times. The samples were incubated at RT for 10 min and then centrifuged for 15 min at 4°C at max speed. The supernatant was removed and the pellet was washed with 1 ml of 70% ethanol and vortexed. The samples were centrifuged again for 5 min at 4°C at max speed. The supernatant was removed again and the pellet was air dried at room temperature for 3 min.

The pellet was then dissolved in 120 μ l of RNase-free water and incubated for 5 min at room temperature. 200 μ l of chloroform was then added and shaken vigorously by hand for 15 sec. Samples were incubated at RT for 3 min and then centrifuged for 15 min at 4°C at 12,000 rpm. The aqueous phase was removed and placed into a new 1.5 ml Eppendorf tube. 10 μ l of 8M RNase free LiCl solution was added and mixed by inversion. 300 μ l of 100% technical grade ethanol was then added and incubated on ice for \geq 2minutes or overnight at -20°C. Samples were

then centrifuged for 30 min at 0°C at max speed followed by the removal of the supernatant. The pellets were washed gently with 1 mL of 70% ethanol and then centrifuged again at max speed for 2 min at 4°C. The supernatant was then removed and the pellet was air dried at RT for 20 min. The procedures outlined in this paragraph were repeated once before dissolving the RNA pellet in 10 µl of RNase-free water.

2.9 RNA quality verification

RNA sample quantities were determined using the Qubit high-sensitivity RNA kit with a Qubit fluorometer and RNA quality was measured using a 2100 Bioanalyzer instrument from Agilent in combination with the Agilent RNA 6000 Nano Kit.

2.10 cDNA synthesis

cDNA was synthesized using RNA from whole body or tissue extractions with the High-Capacity cDNA Reverse Transcription Kit (Thermo Fisher Scientific, catalog number: 4368814) following manufacturer's instructions.

2.11 qPCR primer validation

Primers were designed by Roche's online primer design database¹⁴⁹ and ordered through Integrated DNA Technologies (IDT)¹⁵⁰. To validate the accuracy and specificity of the primers a primer validation experiment was performed. Whole body larval cDNA from *w¹¹¹⁸* was serially diluted into samples of the following concentrations :1/4, 1/16, 1/64, 1/256, 1/1024 using 20 µl of cDNA and 60 µl of water. A single primer master mix containing both primers at a final concentration of 3.2 µM was prepared. 5 µl of Sybr Green master mix (Thermo Fisher Scientific), 2.5 µl primer master mix and 2.5 µl of cDNA are combined for each dilution in triplicate. The standard curve is performed on a QuantStudio™ 6 Flex Real-Time PCR System. The amplification plot, standard curve and melt curve were all analyzed and compared to *rp49*, a

gene constantly transcribed at all times. This allowed for comparisons to be made with respect to fluctuations in the experimental PCR products. Primers used are listed in table 2.2.

2.12 qPCR analysis

cDNA samples were diluted at a ratio of 1:20 for 1000 ng of input RNA to the cDNA reaction. Kappa Sybr Green (5 μ l), primer master mix (2.5 μ l) and cDNA sample (2.5 μ l) were mixed together per reaction. Each biological sample was tested in triplicate with another triplicate of technical samples per biological sample. The reaction was run in a QuantStudio™ 6 Flex Real-Time PCR System at 40 cycles per run. $\Delta\Delta C_t$ values were calculated using *rp49* for normalization and error was calculated using the standard deviation of the fold change values. Primers used are listed in table 2.2.

2.13 pIRES reactions/Gibson

The plasmid pIRES2 contains an EMCV IRES flanked by *RFP* and *GFP*¹⁵¹ and my goal was to clone the *ferritin HCH1* iron response element 5' of *RFP*. PCR fragments were generated of both the plasmid and the IRE, and Gibson cloning as per the manufacturer's instructions (NEB, catalog number: NEB E2611S).

2.14 *Drosophila* embryo injections

pBID-UASC injection plasmids (Ch. 2.3 and Fig. 2.1, 2.2, 2.3) were cultured in the host *Escherichia coli* and plasmid DNA with the transgene was isolated using PureLink™ HiPure Kit (Thermo Fisher Scientific, catalog number:K2100-07) and concentrated to 1 μ g/ μ L suspended in RNase- and DNase-free water. DNA was stored at 4°C until required.

To make sure embryos stuck to the slide for injections, I made glue by adding double sided scotch tape (Scotch 665) and heptane together and leaving it overnight in a sealed vial. I ensured that the glue was adhesive enough to mount embryos to a microscope slide, but viscous enough to pipette with a micropipette.

Next, *y,w,nos phiC31 nls integrase; attP40, y+* flies were expanded into 10-12 bottles and then added into a cage created from PVC pipe the same diameter of a 90 mm Petri dish. The cage was lined with filter paper to create surface area for the flies to mate. One end of the cage had a mesh hole for air circulation and the other end has a cap where a 90 mm petri dish containing grape juice agar (Ch. 2.21) and yeast was placed for embryos to be laid upon. The grape plate was swapped out for new eggs every 45 minutes to ensure embryos were the correct stage.

Needles for injections were prepared using a flaming/brown micropipette puller, model P-87 on the following settings: heat-590, pull-250, vel-250, time 170. The needles were then broken by force against a coverslip edge to obtain a beveled edge. Using a fine tipped P20 pipette tip, 5 μ l or less of DNA was added. Needle was loaded and mounted to the microscope and submersed in halocarbon oil until needed.

Embryos were dechorionated in a 50% bleach solution (must be made fresh each time) for one minute in an egg filter cup created out of a PBC pipe with mesh at the bottom to retain embryos and allow the bleach to enter. Embryos were removed from bleach and rinsed with water three times. Two rows of 50 embryos were lined up on grape agar with the germ region all facing one direction. Two glue strips were added to a microscope slide and gently pressed onto the embryos on the grape agar, the embryos became glued to the microscope slide, with the posterior end facing outwards, for injection. Posterior regions were determine based on visual identity that of the “bean” shape of the embryo, the larger side contains the germ cells.

Next I desiccated the embryos in a desiccation chamber for approximately five min, or until sufficiently dried. Afterwards the embryos were submersed in just enough halocarbon oil to cover all embryos.

Embryos were then horizontally lined up with the injection needle and injected with DNA. Afterwards, all embryos were analyzed under a dissecting scope with a light source at the bottom and screened for any band patterning signifying development and differentiation of the embryonic cells. Any embryos these signs of development were removed. A Vaseline wall was then placed around all the embryos and filled with halocarbon oil. The embryos were placed at 18°C for approximately 18 hours until they hatched. L1 larva were placed on broken up food for easy feeding.

Larva were reared to adulthood and crossed into the injection line and F1 progeny were screened for red eyes, indicating that the *miniwhite* transgene (which is associated with my

transgenes of interest) has been inserted into the germ line. All plasmids were successfully transformed. Flies with the transgene were selected for and the Φ C31 integrase enzyme on the X chromosome was crossed out and the transgene was made homozygous. Each line was sequence verified. Ultimately the following transgenic lines were produced: *UASC-IRP-1A*, *UASC-3XFLAG-IRP1A*, *UASC-myc-RFP-IRP1A*, *UASC-IRP-1A^{C450S}*, *UASC-3XFLAG-IRP-1A^{C450S}*, *UASC-IRP-1B* and *UASC-3xFLAG-IRP-1B*. The tagged-cDNA lines were planned for use for future experiments.

2.15 Immunoprecipitation of GFP-tagged ribosomes

The following procedure was adopted from Michelle Arbeitman (Florida State University) who has used the Translating Ribosome Affinity Purification technique to study gene translation in *Drosophila* adult brains. Before immunoprecipitating GFP-tagged ribosomes from samples, a bead preparation was done. Antibody aliquots of 50 μ g were spun at 13,000 g for 10 min at 4°C. 150 μ l of Dyna Protein G beads (Thermo Fisher Scientific, catalog #10003D) were placed in a 1.5 ml centrifuge tube, placed in a magnet for one min and then removed the supernatant. The tube was removed from the magnet and the beads were suspended in 1000 μ l of 0.15M KCl IP Wash Buffer. This was repeated two more times. Afterwards beads were suspended in 275 μ l of 0.15M KCl IP Wash buffer. 50 μ g of both GFP antibodies (19F7 and 19C8, from the Memorial Sloan-Kettering Monoclonal Antibody Facility) were added to the beads and incubated with end-over-end mixing for one hr at RT. The supernatant was removed after one min magnet exposure and washed with 1000 μ l of 0.15M KCl IP Wash Buffer three times. The beads were finally suspended in 200 μ l 0.15M KCl IP Wash Buffer.

150 larvae expressing the GFP-tagged ribosome in the PG were flash frozen in liquid nitrogen and then homogenized in a two ml tube with a stainless steel bead and 1.5 ml Lysis Buffer and shaken at 30 Hz for two min, re-arranged and shaken again for two min. The homogenized solution was then transferred to a 1.5 ml Eppendorf tube and spun at 4°C for 10 min at 2,000 g. The supernatant was transferred to a new 1.5 ml tube on ice and DHPC was added to a final concentration of 30 mM. Solution was mixed gently by inversion and 1/9th sample volume of 10% NP-40 was added and mixed by inversion. The solution was stored on ice

for five min. Post mitochondrial-supernatant was prepared by centrifuging at 4°C for 10 min at 20,000 g. 40 µl was taken for input fraction RNA samples and solution was transferred to a new 1.5 ml tube.

To immunoprecipitate the ribosomes I added 200 µl of prepared antibody-bound beads and incubated at 4°C for 30 minutes with end over end mixing. Beads were then collected with a magnet in the ice bucket (to keep beads cold) for one min. Supernatant can be kept for future analysis but is not necessary. Beads were resuspended with 1000 µl of 0.35 KCl IP Wash Buffer and the supernatant was collected with the magnet for one min. This was repeated three times.

Beads were re-suspended in TRIzol at RT and incubated for 5 min at RT with end over end mixing and then removed the TRIzol solution after one min magnet exposure. This IP was stored at -80°C until a standard RNA TRIzol extraction was performed as in chapter 2.7. See table 2.4 for reagents.

2.16 NO detection

Larvae were dissected in phosphate-buffered saline with 0.1% Triton X (PBT) buffer and placed into a 1.5 ml tube containing PBT. After RG's were dissected, PBT was removed and 500 µl of DAFII-DA solution was added (DAFII-DA is 1:500 in PBS) and incubated at room temperature for two hrs in the dark with end over end mixing. Tubes were left standing for two min for tissue to fall to the bottom. The stain was removed and 500 µl of 4% paraformaldehyde (PFA) solution was added. Sample was rotated in the dark at RT for 20 min. PFA was then removed and the tissue was quickly washed three times with 500 µl PBT. Three additional washes with PBT followed, and each wash was rotated in the dark at RT for 15 min. The tissues were then mounted in PBT and a 1:1 glucose/DAPI stain mixture. Samples were then imaged immediately using epifluorescence (Nikon Digital Sight DS-U3) on a Nikon Eclipse 80i microscope at 40x magnification (Nikon Pan Fluor) with a Nikon Confocal C2 camera and stored at -80°C. The positive control heat shock was performed for one hr at 37°C and allowed to recover for six hrs prior to dissection, the negative control was placed under the same conditions as the positive control but lacked stain.

2.17 Holidic medium and BPS iron food

Holidic media was synthesized as described in *Piper, et al* 2014. The only differences were that the buffer base was added after the autoclave step and that iron was added in the final step, so that it could be distributed across multiple aliquots in various concentrations. BPS was added at the same time as iron.

2.18 Vial analysis for iron-feeding, IRP rescue experiments

Embryos were collected from cages containing grape fruit plates with yeast. Grape plates were swapped twice daily and embryos were collected from grape plates with embryos less than six hrs old. 50 embryos were transferred to a vial containing 10 ml of either NutriFly or holidic media. Vials were placed in 25°C and scored for pupae formation and adult eclosion once per day at 5:00 pm.

For RG images, larvae were removed from vials using a brush and dissected in 1% PBS prior and mounted on a 1% PBS/glucose/DAPI medium. Images were immediately taken using epifluorescence. Whole body images of larvae were taken by washing larvae in water and placing them on a slide at -20°C for two minutes and then imaged. Adult flies were flash-frozen in liquid nitrogen and subsequently imaged by placing into a light box using the Lecia MZ 16F microscope with a Lecia DFC 500 camera.

2.19 DNA extractions

DNA was extracted from 50 adult flies that were flash-frozen in liquid nitrogen. They were ground manually over liquid nitrogen until turned into a fine white powder. 200 µl of DNAzol (Thermo Fisher Scientific, catalog number 10503027) was added and using a motor pestle, ground for two min. The final volume of DNAzol was brought to 800 µl and incubated at RT for five min. Samples were centrifuged at max speed for five min at 4°C. The viscous phase (middle) was transferred to a new tube and chloroform was added at a 1:1 ratio. Tubes were

inverted six times for mixing and then centrifuged at max speed for two min at 4°C. The upper phase was then transferred to a new 1.5 ml tube and 500 µl of 100% ethanol was added. The tubes were end to end rotated for three min at RT and then centrifuged at max speed for two min at 4°C. The pellet was washed with 800 µl of 70% ethanol and inverted four times to mix. The sample was then centrifuged at max speed for one min. The supernatant was discarded and the pellet was dried for three min. The pellet was then dissolved in 100 µl of water for 20 min on a horizontal shaker. 200 µl of chloroform was then added, inverted five times and centrifuged at max speed for two min. The upper phase is transferred into a new 1.5 ml Eppendorf tube and 4 µl of 5M NaCl is added to each tube. 500 µl of 100% ethanol is also added and rotated with end to end mixing for three min. The samples were then spun at max speed for two min, the supernatant was discarded and the pellet was washed with 70% ethanol. The sample was inverted six times and then centrifuged at max speed for one min. The supernatant was removed, the pellet dried and then dissolved in 200 µl NaOH.

2.20 PCR purifications

To purify PCR reactions, 1/10th volume of sodium acetate (pH5.2) was added. Next two to three volumes of 100% ethanol was added and then incubated at -20°C for one hr. Samples were centrifuged for 15 min at 13,000 rpm at 4°C. The supernatant was removed and 250 µl of cold 70% ethanol was added to the pellet and centrifuged for five min at 4°C. The supernatant was removed and the pellet was air-dried for 10 minutes and suspended in water.

2.21 GRAPE plates

Grape plates for *Drosophila* embryo collection were made as follows. 700 mL of H₂O was mixed with 35 g of agar and autoclaved. 20 ml ethanol methyl paraben solution (0.5g methyl paraben dissolved in 20 ml of 100% ethanol) was added to the autoclaved mixture. ~175 ml of Welches grape juice concentrate mixture was added to the solution. Once dissolved, the mixture was placed into petri dishes and allowed to cool. Plates were stored at 4°C until needed. Yeast was added on the grape plate to increase *Drosophila* embryo production rate.

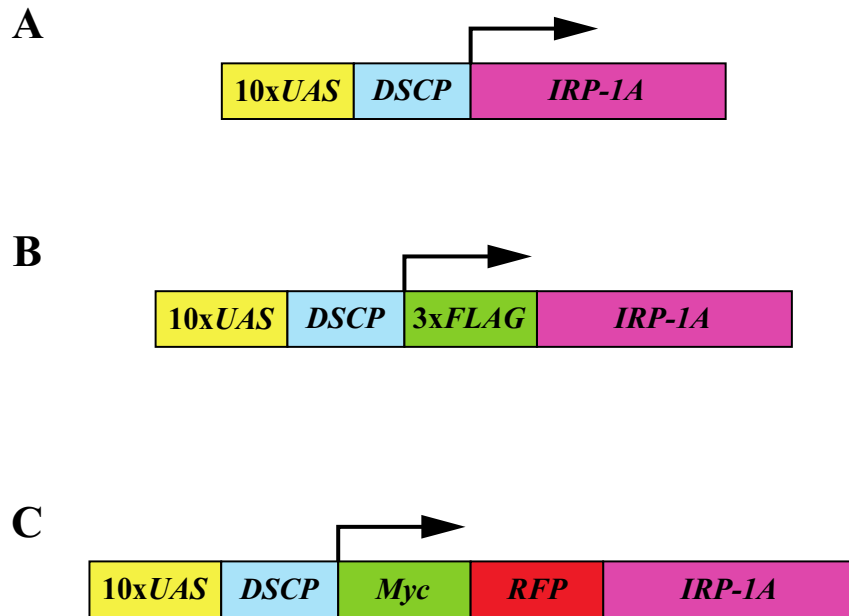


Figure. 2. 1. Illustration of the *IRP-1A* transgenic lines used in this thesis. A) pBID-UASC-*IRP-1A*. B) pBID-UASC-3xFLAG-*IRP-1A* C) pBID-UASC-mcy-*IRP-1A*. *DSCP*: *Drosophila* core promoter. *RFP*: *Red Fluorescent Protein*.

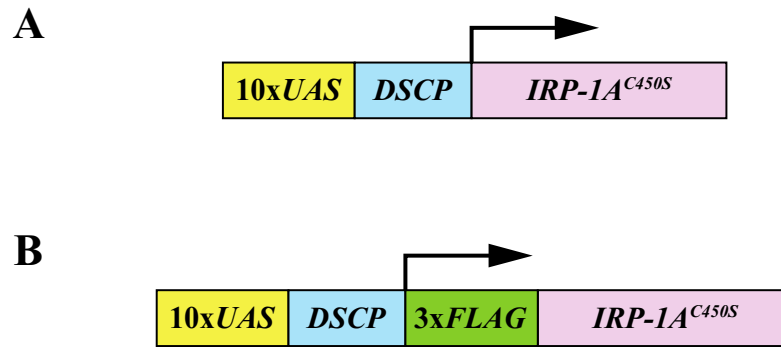


Figure. 2. 2. Illustration of the *IRP-1A*^{C450S} transgenic lines used in this thesis. A) pBID-UASC-*IRP-1A*^{C450S}. B) pBID-UASC-3xFLAG-*IRP-1A*^{C450S}. *DSCP*: *Drosophila* core promoter.

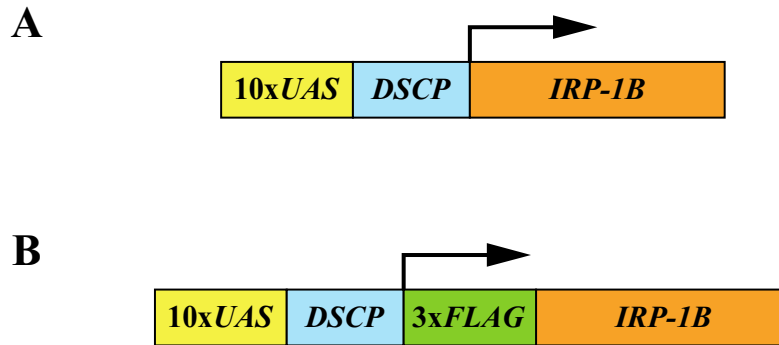


Figure. 2. 3. Illustration of the *IRP-1B* transgenic lines used in this thesis. A) pBID-UASC-*IRP-1B*. B) pBID-UASC-3xFLAG-*IRP-1B*. *DSCP*: *Drosophila* core promoter.

Table 2. 1. *Drosophila melanogaster* lines used to obtain the results embodied in this thesis. Lines were either obtained from the Bloomington *Drosophila* Stock Center (BDSC), Oren Schuldiner :Weizmann Institute of Sciences, Henry Krause: University of Toronto, Patrick O’Farell :University of California San Francisco or generated by me, in the King-Jones Lab.

Genotype	Flybase ID	Obtained from
<i>w[*]; P{UAS-GFP-RpL10Ab}BF27</i>	FBti0150332	BDSC
<i>NOS-Full deletion, hoA,G13,Ch,Bw</i>	N/A	Oren Schuldiner
<i>UAS-Spz5 RNAi; hsNOS^{MAC}</i>	N/A	Henry Krause
<i>E2671 (NOSD¹⁵ parental line)</i>	N/A	Patrick O’Farell
<i>NOSD¹⁵</i>	N/A	Patrick O’Farell
<i>y,w,nos phiC31 nls integrase;attP40, y+</i>	FBti0077396	BDSC
<i>canton S</i>	FBsn0000274	BDSC
<i>w¹¹¹⁸</i>	FBst0005905	BDSC
<i>UASC-IRP-1A</i>	N/A	Generated in the King-Jones lab
<i>UASC-3XFLAG-IRP-1A</i>	N/A	Generated in the King-Jones lab
<i>UASC-IRP-1A^{C450S}</i>	N/A	Generated in the King-Jones lab
<i>UASC-3XFLAG-IRP-1A^{C450S}</i>	N/A	Generated in the King-Jones lab
<i>UASC-myc-RFP-IRP-1A^{C450S}</i>	N/A	Generated in the King-Jones lab
<i>UASC-IRP-1B</i>	N/A	Generated in the King-Jones lab
<i>UASC-3XFLAG-IRP-1B</i>	N/A	Generated in the King-Jones lab
<i>UAS-NOS^{IR-X} -RNAi</i>	N/A	Henry Krause
<i>UAS-NOS^{IR-X} -RNAi; UASC-IRP-1A</i>	N/A	Generated in the King-Jones lab
<i>UAS-NOS^{IR-X} -RNAi; UASC-IRP-1A^{C450S}</i>	N/A	Generated in the King-Jones lab
<i>phantom22-Gal4</i>	N/A	Michael O’Connor

Table 2. 2. Primers for qRT-PCR, cloning and sequencing.

PCR	Sequence	Brief Description
IRP-1A Forward	5'-AGC CAG CTC GTG TTA TAT TGC-3'	
IRP-1A Reverse	5'-GGA TTG ATT TTC TCA GGA TTG C-3'	
IRP-1B Forward	5'-CGC CCA GTT CGA GAA AAC-3'	
IRP-1B Reverse	5'-GGA TCG AGT AGG GCA GTT GA-3'	
Cloning		
IRP-1A- topo Forward	5'-CAC CAT GTC CGG CTC CGG CGC C-3'	Primer used for Topo PCR
IRP-1A- topo Reverse	5'-CGC ACT AAC TAA TCC AGC ATT TTG CGT-3'	Primer used for Topo PCR
IRP-1A SDM Forward	5'-GCC GCC ATC ACC TCG TCC ACG AAC ACT TCG AAT CCC TCG GTG ATG TTG G-3'	Primer used for site directed mutagenesis of IRP-1A
IRP-1A SDM Reverse	5'-CCA ACA TCA CCG AGG GAT TCG AAG TGT TCG TGG ACG ACG TGA TGG CGG G-3'	Primer used for site directed mutagenesis of IRP-1A
IRP-1B topo Forward	5'-CAC CAT GTC AAG GGC CAA TCC CTT C-3'	Primer used for Topo PCR
IRP-1B topo Reverse	5'-AAG ATG AGT TGC TTA AGA GAG CAT TTT GCG-3'	Primer used for Topo PCR
Sequencing		
DSCP-F	5'-GAG CTC GCC CGG GGA TC-3'	Sequences from the <i>Drosophila</i> core promoter of pBID to transgene insert
SV40pA-R	5'-GAA ATT TGT GAT GCT ATT GC-3'	Sequences from the SV40 region towards end of transgene insert
RFP	5'-AAC CTT CAT CAA CCA CAC CC-3'	Sequences from the RFP of pBID onwards
IRP-1A-550	5'-AAC CTG GAG TAT CTG GCC CG-3'	Sequences starting at 550bp of IRP-1A
IRP-1A-1100	5'-CAG GAT CCC CAA TAC ACG-3'	Sequences starting at 1100bp of IRP-1A
IRP-1A-1650	5'-AAT CGC AAT TTC GAG GGT CG-3'	Sequences starting at 1650bp of IRP-1A
IRP-1A-2200	5'-TAT GAC TCG TGC GCT GCC-3'	Sequences starting at 2200bp of IRP-1A
IRP-1A-2750	5'-TGC TGG ATT AGT TAG TGC-3'	Sequences starting at 2750bp of IRP-1A
IRP-1B-550	5'-AAT TTG AGC GCA ACA AGG-3'	Sequences starting at 550bp of IRP-1B
IRP-1B-1100	5'-GAA GAT CGA CAT CAT TCG CCA G-3'	Sequences starting at 1100bp of IRP-1B
IRP-1B-1650	5'-GCA TTG GTA ACT CGG TTC C-3'	Sequences starting at 1650bp of IRP-1B
IRP-1B-2200	5'-GCC TGC TGC CCG ATT CTT GT-3'	Sequences starting at 2200bp of IRP-1B
IRP-1B-2750	5'-CCT ACT ACA AGA ATG GTG G-3'	Sequences starting at 2750bp of IRP-1B

Table 2. 3. Solutions used for Chemically Competent Cells

Solution	Amount
SOB	
Tryptone	20 g
Yeast extract	5 g
0.58 NaCl	0.58 g
KCl	0.19 g
HCl	up to 990 ml
MgCl ₂ + (2M)	10 mL (after autoclave)
MgCl	
MgCl ₂ -6H ₂ O	40.7 g
MgSO ₄ -7H ₂ O	
H ₂ O	up to 200 ml
TB	
PIPES	1.5 g
CaCl ₂ -2H ₂ O	1.1 g
KCl	9.3g
KOH	to pH 6.7
MnCl ₂ -4H ₂ O	5.4 g

Table 2. 4. Solutions used for the Translating Ribosome Affinity Purification experiment.

Solution	Reagents	Amount
Lysis Buffer	20 mM HEPES-KOH pH 7.4	200 uL 1M
For 10mL	5 mM MgCl ₂	50 uL 1M
	150 mM KCl	1.5 mL 1M
	DEPC-Water	8.25 mL
	Add immediately before use:	
	0.5 mM DTT	5 uL 1M
	Protease Inhibitors (Roche Complete, EDTA-Free) 25X solution	0.4 mL 25X
	100 ug/mL cyclohexamide	10 uL 1000X
	40 U/mL Rnasin (Promega)	10 uL 40 U/uL
0.15M KCl IP Wash Buffer	20 mM HEPES-KOH pH 7.4	600 uL 1M
for 30 mL	5 mM MgCl ₂	150 uL 1M
	150 mM KCl	4.5 mL 1M
	1% NP-40	3 mL 10%
	DEPC-Water	21.75 mL
	Add immediately before use	
	0.5 mM DTT	15 uL 1M
	100 ug/mL cyclohexamide	30 uL 1000X
0.35M KCl IP Wash Buffer	20mM HEPES-KOH pH 7.4	600 uL 1M
for 30 mL	5 mM MgCl ₂	150 uL 1M
	350 mM KCl	10.5 mL 1M
	1% NP-40	3 mL 10%
	DEPC-Water	15.75 mL
	Add immediately before use	
	0.5mM DTT	15 uL 1M
	100ug/mL	30 uL 1000X

3.0 Results

3.1 Comparing transcriptional regulation of *IRP-1A* and *IRP-1B* in the ring gland and brain ring gland complex before and during the major L3 ecdysone pulse

A recent study found that the *Drosophila* genome contains two *IRP* genes: *IRP-1A* and *IRP-1B*, both are conserved with mammalian *IRP1*¹¹⁰. Both encode a functional aconitase enzyme, however, *IRP-1B* lacks the ability to bind to IREs, whereas *IRP-1A* can¹¹⁰. As previously mentioned (Ch. 1.9), my hypothesis stated that an NO pulse in the RG was required to transition *IRP-1A* from the aconitase form to the IRE-binding form. *IRP-1A* would then bind *ferritin HCHI* mRNA, likely resulting in a decreased translational rate of *ferritin* mRNA. Fewer ferritin proteins would lead to an increase in cellular iron levels to be incorporated into heme, a cofactor for the P450 enzymes that are required to synthesize ecdysone. Therefore, I also proposed that NO acted through *IRP-1A* to upregulate ecdysone production at the late L3 stage. To further understand how *IRP-1A* functioned in the RG, I examined *IRP-1A* transcription levels in the larval RG, as only whole body expression studies have previously been reported¹¹⁰.

I predicted that during the mid-L3 (~30 hours after the L2/L3 molt, where ecdysone concentrations are low), *IRP-1A* functioned as an aconitase and then switched to its RNA-binding form immediately prior to the late L3 ecdysone pulse to promote cellular iron availability. This switch could encompass one or both of two proposed mechanisms: **1)** increased transcription and translation of *IRP-1A*, generating more protein which should outnumber available ISCs. The resulting excess of *IRP-1A* would not have available ISCs and thereby take on the RNA-binding form. Cellular iron concentrations would then be increased via the IRE regulatory effects of *IRP-1A*; or **2)** *IRP-1A* was regulated post-translationally in which transcript levels should remain constant over time. For increased levels of *IRP-1A* in its RNA-binding form to exist, *IRP-1A* could be altered or induced by a signal, which was predicted to be NO. Overall, *IRP-1A* was a likely candidate for increasing cellular iron for ecdysone synthesis, but another means to increase cellular iron may exist.

To determine whether *IRP-1A* transcription increased (mechanism 1) or stagnated (mechanism 2) I performed a qRT-PCR analysis on RG samples isolated from larvae staged to 30 and 44 hrs after the L2/L3 molt (which will be referred to as the 30 and 44 hr stages). The 30 hr stage was chosen because it precedes the initiation of the major L3 ecdysone pulse and lacks

the presence of NO, which might suggest that IRP-1A would function as an aconitase at that time. I chose the 44 hr stage because it occurs during the late L3 ecdysone pulse and NO has been reported to be present at this time, therefore IRP-1A was predicted to be RNA-binding. To determine whether the suspected NO/IRP/ecdyson pathway was occurring primarily in the RG, which was attached to the BRGC, I determined transcript levels in both RG and BRGC separately. I predicted that IRP-1A transcription would be more localized to my tissue of interest, the RG (which contains the PG), as opposed to the BRGC, which would have suggested that the RG had a higher demand for IRP-1A. Comparing the two tissues had the potential to demonstrate whether IRP-1A was more dynamically regulated in the RG or not. If a change in *IRP-1A* transcripts occurred between the 30 and 44 hr stages in the RG, but not the BRGC, it would suggest that the RG expresses IRP-1A for the speculated purpose of increasing cellular iron levels for ecdysone production. Lastly, *IRP-1B* transcript levels were analyzed in concert with *IRP-1A*, primarily as a control since *IRP-1B* had no RNA-binding activity and transcription levels should have been unaltered in relation to the state of ecdysone production. Alternatively, it was possible that as IRP-1A shifted to its RNA-binding form, the resulting reduction in aconitase activity could cause *IRP-1B* upregulation in order to compensate.

I collected control samples of w^{1118} and performed a qRT-PCR (Fig. 3.1). *IRP-1A* had a 1.5-fold increase in transcript levels from the 30 to 44 hr stages within the RG. A similar trend was seen in the BRGC, although this was not significant (Fig 3.1). *IRP-1B* transcript levels were similar at the 30 and 44hr stages in both the RG and BRGC. Also, *IRP-1B* transcript levels were slightly higher in the RG compared to the BRGC at both times tested. (Fig. 3.1). Finally, *IRP-1B* transcript levels in all cases were 2-3-fold higher compared to *IRP-1A* (Fig. 3.1).

These results suggested that mechanism 1 and 2 may both have contributed to the proposed shift in IRP-1A activity. The 1.5-fold increase of *IRP-1A* transcript levels supported that higher production rates of IRP-1A could outcompete ISCs as described in mechanism 1, whereas minimal differences in transcript levels between the RG and the BRGC supported mechanism 2. The slight increase of *IRP-1A* transcripts between the 30-44 hr stages in the BRGC could imply that a shift in IRP-1A towards its RNA-binding form was occurring in the BRGC as well as in the RG (where I believed it was required for making cellular iron available for heme production). Alternatively, the increase in *IRP-1A* transcript abundance in the RG could have been of biological importance but may not have been relevant for ecdysone production.

Finally, I proposed that if IRP-1A was RNA-binding, it would not be functioning as an aconitase and that IRP-1B would have to accommodate for decreasing aconitase activity. However, *IRP-1B* transcript levels did not increase when I speculated that IRP-1A was RNA-binding, suggesting that either IRP-1B did not need to accommodate for a loss of aconitase activity or that aconitase levels were not dropping below a level in which the cell must intervene.

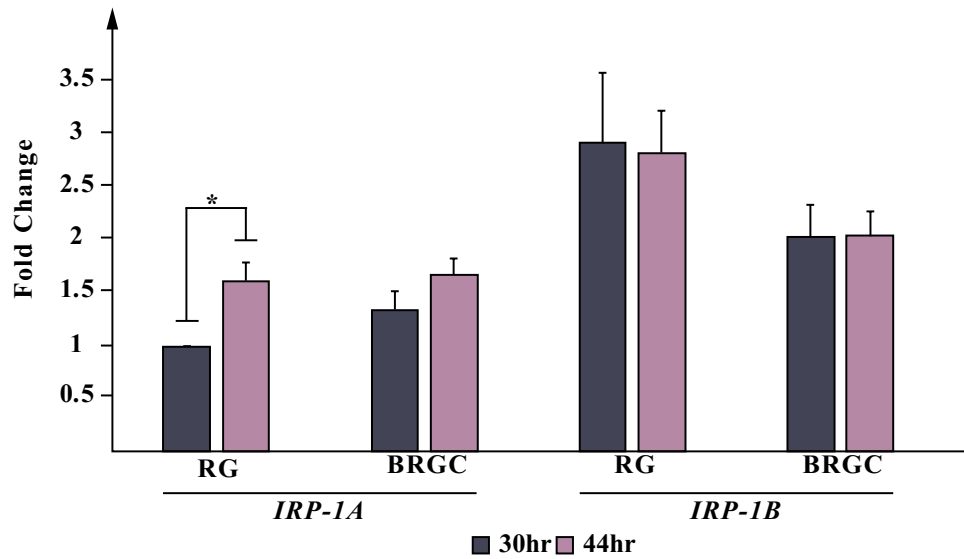


Figure 3. 1. *IRP-1A* and *IRP-1B* expression within the RG and BRGC at 30 and 44 hr post L2/L3 molt. Transcript abundance is relative to *IRP-1A* at 30 hrs after the L2/L3 molt in the RG. *IRP-1A* transcript levels were significantly upregulated in the RG from the 30 hr stage to the 44 hr stage and *IRP-1B* transcript levels were 1-3 fold higher than *IRP-1A* in all comparisons. Genotype used: *w¹¹¹⁸*, RG: ring gland, BRGC: Brain Ring Gland Complex, *IRP-1A/B*: *Iron Response Protein-1A/B*. hr: hours, L2/L3: second/third instar larva, *: $p < 0.05$.

3.2 NO pulses coordinate with ecdysone signaling and has three distinct staining patterns in the ring gland

I wanted to see if NO had a time coordinated role with respect to ecdysone signaling based on two previous findings. First, NO has been shown to affect the conformation of IRP *in vitro*, suggesting that it may play an important role *in vivo* to activate the RNA-binding activity of IRP-1A¹⁵²⁻¹⁵⁴. And second, feeding developmentally arrested *phm22>NOS^{IR-X}-RNAi* animals ecdysone, rescues them to adulthood². Tying these points together, controlled pulses of ecdysone trigger developmental transitions in the larvae and are synthesized by P450 enzymes, which have increased levels of their associated transcript prior to the major L3 ecdysone pulse¹. This apparent increase in protein levels would require one heme cofactor per protein molecule, and each molecule of heme requires an iron atom. And so, I predicted that an NO pulse occurred when ecdysone was required. NO might shift IRP-1A to the RNA-binding form to increase cellular iron levels for the suspected large heme demand during ecdysone pulses. Qiuxiang Ou, a postdoc in the lab, performed preliminary tests and detected an NO signal during and just prior to the late L3 ecdysone pulse from 40-44 hr after the L2/L3 molt and was unable to detect NO 30 hrs after the L2/L3 molt. This coordinated with the late L3 ecdysone pulse that occurs around 44 hrs after the L2/L3 molt and led myself to suspect that NO may indeed play a signaling role corresponding to ecdysone. I set out to further explore the link between NO, IRP and ecdysone biosynthesis by characterizing NO signaling in the RG in relation to development.

To detect NO I used two stains, DAF-2 diacetate (aka DAF2-DA) and DAR4M-AM. The former reacts with NO in the presence of oxygen¹⁵⁵ whereas the latter has been reported to react with reactive nitrogen species (RNS) as opposed to NO itself¹⁵⁶. I originally decided to look at NO using both markers because it was possible that RNS, as well as NO, could result in IRP-1A losing its ISC. NO donors often create RNS, and thus RNS could be responsible for shifting IRP1 to its RNA-binding form in previous experiments looking into how the presence of NO causes vertebrate IRP1 to bind IREs^{87,88}. However, in my hands, all instances with DAR4M-AM resulted in fluorescence regardless of the presence of NO or RNS, making it an unreliable detection method. Therefore, the following experiments were performed using DAF2-DA.

The NO staining protocol can be completed in two ways. The first method involves dissecting the RG and imaging directly after incubation with the DAF2-DA stain. Using this

method, I was unable to detect fluorescence, despite the procedure working previously in our lab. The previous DAF2-DA staining was performed with *phm22>w¹¹¹⁸* whereas I used *w¹¹¹⁸*, which had a different genomic background and any further differences could be the batch lots of reagents used or microscope settings. Ideally, future experiments following this method of DAF2-DA staining would compare both *phm22>w¹¹¹⁸* and *w¹¹¹⁸* as well as compare the outcomes using both old and new reagents, to ensure all reagents used in the procedure were and are functional. If the DAF2-DA NO detection is still unsuccessful and neither genetic background nor replacing old reagents and materials can explain the lack of NO detection, then perhaps the differences between previous DAF2-DA results and my results could be related to microscope settings resulting in increased or false detection.

The second method for NO detection with DAF2-DA is to fix the tissue directly after incubation with the stain, and then image. Fixing the sample dampens the signal from DAF2-DA, however, I was able to reliably detect fluorescence using this method, and thus the following experiments follow this procedure.

I performed a developmental time course of NO staining in four hour intervals starting at 12 hours after the L2/L3 molt. Samples were collected, fixed and stained with DAF2-DA and acquired until pupariation began, approximately 48 hours after the L2/L3 molt (Fig. 3.2A). NO was detected in 46-73% of samples from 16-24 hrs, possibly corresponding with the minor ecdysone pulses of the L3 larvae (Fig. 1.1)¹⁰. I was also able to detect a 40-44 hr signal of NO in 65-87% of samples, which occurred just prior to the late L3 ecdysone pulse and corresponds with previous NO detection data from the King-Jones lab. This data suggested a correlation between the timing of NO production and ecdysone production. Interestingly, the detection of NO in the RG was not as uniform as previously seen in the lab or literature and appeared to have three distinct tissue distribution patterns: 1) the entire PG, 2) half of the PG, or 3) the CA. The reasons for these patterns of signaling is currently unknown, however, previous reports have shown that NADPH diaphorase (NADHPd), a molecule that always co-precipitates with active NOS, was also present in the CA¹⁵⁷ (more detail in chapter 4.4), consistent with the idea that NO had a role in this tissue. The multiple signaling patterns did not appear to correlate with one particular time in development and were recovered randomly (Figure 3.2 only represents a single signaling pattern per 4-hour interval). Figure 3.2B shows that the multiple signaling patterns of NO in the

RG were also seen to occur in tandem, in this case both the CA and half of the PG were fluorescing.

Unfortunately, I detected fluorescence in only 40-80% of the samples per stage. In the positive control, NO was detected 44% of the time, perhaps because of the dampening effect of the signal from fixation. This data provided evidence to support the idea that NO was produced at the 16-24 hrs and 40-44 hrs stages, but the presence of NO in the RG is the only confirmed result. It was possible that due to the short lived nature of NO that detecting it at a reliable rate using my staining procedure was a limiting factor^{158,159}. Previous experiments that did not use fixation in the King-Jones lab showed consistent NO presence in the RG at the 40-44 hr stage, however, after several attempts where I omitted fixation, I was unable to detect NO.

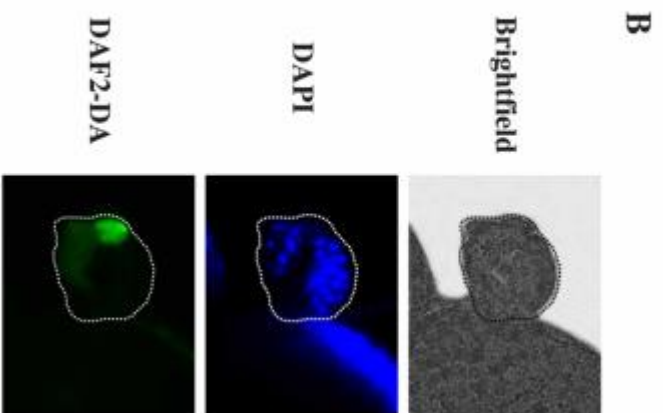
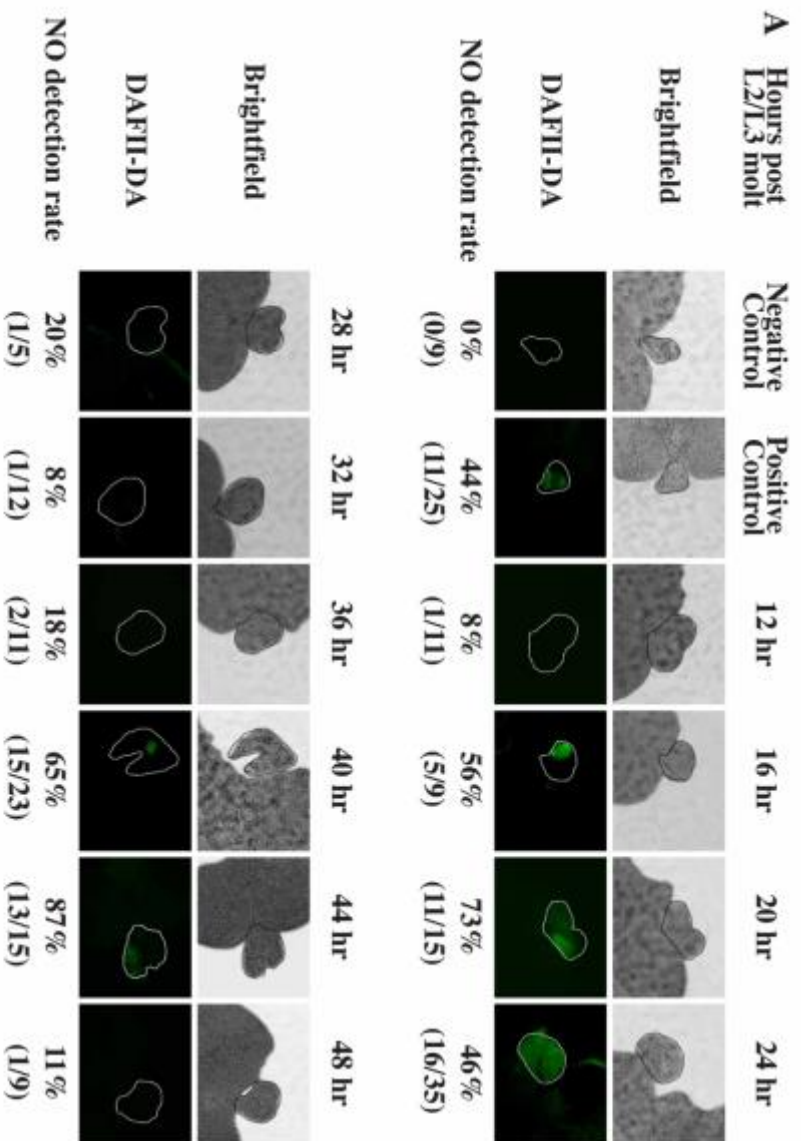


Figure 3. 2. NO was present in the RG during and prior to ecdysone pulses in three distinct patterns within the L3 larval stage. *w¹¹¹⁸* larvae were collected in 4-hour intervals starting at 12 hours after the L2/L3 molt. Each sample was stained with DAF2-DA and fixed prior to imaging. NO detection rate refers to the percentage of samples that fluoresced as a result of NO reacting with DAF2-DA and the “n” value is represented below in parenthesis. Not all RG’s had the same pattern of fluorescence. There were three distinct types of fluorescence: whole PG was fluorescing, half of the PG was fluorescing, or the CA was fluorescing. **A)** NO was present during and just prior to the minor ecdysone pulses (16-24 hrs) and during the major L3 ecdysone pulse (40-44 hrs). The positive control *NOS^{MAC}* encodes a constitutively active form of NOS, the negative control was also *NOS^{MAC}* but with no DAF2-DA staining. **B)** NO signaling occurred in both the CA and the PG. A 40 hr RG stained with DAF2-DA and DAPI which was used to show the distinction between the PG and CA. NO staining occurred in the left half of the PG with a stronger signal in the CA. L2/L3: second/third instar larva, hr: hour. NO: nitric oxide. NOS: Nitric Oxide Synthase DAF2-DA: DAF-2 diacetate. CA: corpus allatum. PG: prothoracic gland.

3.3 Variable iron concentrations in the diet and the associated phenotypes

3.3.1 Decreasing iron concentrations through the diet does not rescue *phm22>NOS^{IR-X}-RNAi* animals

phm22>NOS^{IR-X}-RNAi animals displayed a giant L3 arrest phenotype with large red RGs that was caused by the accumulation of heme precursors in the tissue. This suggested that heme production was impaired, raising the possibility that iron –a key component of heme- was inaccessible or unavailable in the RG. As mentioned previously, it has been shown that NO can trigger a conformational change in vertebrate IRP1 from the aconitase form to the RNA-binding form⁸⁸. Therefore, I predicted that without NO being produced to shift IRP-1A into its RNA-binding form in *phm22>NOS^{IR-X}-RNAi* animals, free cellular iron would not be available for heme, red fluorescent precursors would build up and result in decreased ecdysone production. The only known trigger of this switch *in vivo* is when cellular iron concentrations are low, the lack of ISCs cause IRPs to become RNA-binding. The King-Jones lab has previously shown that *Drosophila* IRP-1A cDNA overexpression within the PG in a *phm22>NOS^{IR-X}-RNAi* background rescued larvae to adulthood, linking IRP-1A and NO *in vivo* for the first time. The idea was that an excess or overabundance of IRP-1A resulted in all the available ISCs being bound to the protein. Once all the ISCs were being used by IRP-1A, the continuing production of IRP-1A from the cDNA overexpression resulted in the remaining IRP-1A to be without an ISC and thus in the RNA-binding form. If my prediction that NO was required in the PG to cause this shift in IRP-1A activity was correct, overexpressing IRP-1A to achieve the RNA-binding form should bypass the presumptive need for an NO signal in *phm22>NOS^{IR-X}-RNAi* animals. As a result, available cellular iron levels should increase, providing sufficient amounts of iron for heme production needed in ecdysone synthesis, rescuing the animal.

I wanted to further investigate the link between NO and IRP-1A by generating an excess of RNA-binding IRP-1A in a *phm22>NOS^{IR-X}-RNAi* background. The goal was to feed the animals a low iron diet to deplete available ISCs as opposed to transgenically manipulate IRP-1A. This decrease in ISCs should cause IRP-1A to shift to its RNA-binding form. This would

subsequently increase cellular iron (because ferritin would be no longer produced for iron storage), which in turn may rescue animals in a similar manner to *IRP-1A* overexpression.

Recent work has provided a method to produce a defined holidic diet for *Drosophila* consumption in which each compound in the food is added separately, allowing researchers to alter and control the concentrations of amino acids, sugar, lipids, nucleic acids, salts, vitamins, and metals (specifically iron for my experiments) within the diet¹⁶⁰. This is significant in *Drosophila* research as the diet plays an important role for gene expression and survival. Previous work has shown the optimal concentration of critical components in the diet such as amino acids, sugars, etc, but was unable to achieve the level of control seen in the holidic diet described above¹⁶¹. Traditionally, researchers have fed a primarily cornmeal or yeast diet to the flies, each batch with undefined quantities of various components (sugars, lipids and metals, etc) that could affect the outcome of the experiment. The holidic defined media eliminates these variables, therefore, I chose to rear flies on this medium for the following experiments, allowing for the manipulation of precise quantities of iron.

First, I compared survivability of the control strain *w¹¹¹⁸* on standard fly kitchen medium to that of stock holidic medium to determine the effect of this new diet on *Drosophila* on the rates of puparium formation and adult eclosion (Fig 3.3). Larvae displayed a delayed growth period of five days (Fig. 3.3B), likely because holidic diet is not as rich in nutrients as the standard media. However, once a healthy pupa was produced, adult eclosion rates were comparable to flies on standard media (Fig 3.3A). Therefore, any delay on the holidic diet of five days was a result of the nutritional composition of the holidic medium itself and not experimental conditions. With respect to my focus on iron, Piper *et al* (2014) designed the holidic diet with a 1mM iron concentration, which provided the optimal egg laying rates and survival for the flies¹⁶⁰.

phm22>NOS^{IR-X}-RNAi animals reared on a holidic media containing standard 1 mM iron concentrations showed no change in the rate of adult survival compared to standard fly kitchen media (Fig. 3.4A). This showed that the differences in iron concentration between the holidic diet and standard fly kitchen media were insufficient to induce a phenotypic rescue, and so the next step was to systematically alter the iron concentrations within the holidic media.

In an attempt to induce IRP-1A RNA-binding activity by decreasing cellular iron concentrations, *phm22>NOS^{IR-X}-RNAi* animals were reared on a holidic diet ranging from 0 to 1

mM iron concentrations (Fig. 3.4B). I also tested iron concentrations up to 100 mM to determine whether increased iron in the diet could result in increased cellular iron in the PG for incorporation into heme and subsequently produce ecdysone via P450s to rescue the *phm22>NOS^{IR-X}-RNAi* larvae. I observed no rescue in any of the conditions for *phm22>NOS^{IR-X}-RNAi* animals. Therefore, it appeared that dietary iron levels had no influence on the *NOS^{IR-X}-RNAi* phenotype. However, control samples were still viable on media containing no iron, giving rise to the possibility that maternal egg storages of iron might have been sufficient to maintain cellular iron levels regardless of iron concentration within the media. And so, it is possible that *phm22>NOS^{IR-X}-RNAi* larvae were not rescued because they did not experience low cellular iron due to maternal iron stores.

Realizing that *Drosophila* raised on media containing no iron could survive similar to that of flies raised with iron, I wanted to know how long *Drosophila* could survive on iron depleted media. Therefore, if the parental generation of *phm22>NOS^{IR-X}-RNAi* animals were raised on media with minimal or no iron, perhaps the maternal stores of iron predicted to be sufficient for offspring survival, could be minimized to allow for a phenotypic rescue to occur in subsequent generations. To determine how long *Drosophila* could survive without iron, Megan Malach, an undergraduate student under my supervision, reared control flies on iron-depleted media. Embryos were transferred to each vial and raised to adulthood, adults were then transferred to a fresh vial and given time to lay embryos for the next generation. Once a sufficient number of eggs were laid, the adults were removed and embryos were allowed to develop into the next generation of adults. The procedure was repeated until all generations in the iron-depleted media had died (Fig. 3.4C). Megan found that after one full generation, flies began to die and that after four generations the flies were incapable of surviving without iron in the diet, suggesting that at that point, maternal iron had become limiting. She also noticed that the flies were “slower” and less active than their counterpart raised on media containing iron, suggesting that the lack of iron resulted in less energy production and overall decreased health of the fly. Perhaps repeating the *phm22>NOS^{IR-X}-RNAi* low iron-feeding experiments and having the parental generation raised on low iron media, could yield a noticeable phenotypic rescue because of a reduced maternal storage of iron being present.

To circumvent the issues of using low iron, Megan introduced the iron chelator bathophenanthroline disulfonic acid (BPS) into the food. A low iron diet had no effect on the

survival of *phm22>NOS^{IR-X}-RNAi* animals and we suspected that the lack of rescue was due to maternal iron levels preventing low cellular iron levels from occurring. This prevention of low cellular iron could have resulted in IRP-1A proteins being bound to ISCs and not in the RNA-binding form. As a result, cellular iron was thought to not be made available in the PG for the production of heme, which was required for P450s to synthesize ecdysone. Therefore, we wanted to chemically induce a low iron environment by feeding the flies the iron chelator BPS. This should chelate both dietary and maternal iron stores and create low iron conditions within the larvae to induce the RNA-binding form of IRP-1A, which I predicted was required to rescue *phm22>NOS^{IR-X}-RNAi* animals to adulthood. Previous studies have shown that at concentrations of 100 to 250 μM BPS, *Drosophila* had no developmental defects but in the latter concentration had a detectable 50% decrease in cellular iron stores^{162,163}. Therefore, the iron chelator BPS should have reduced the maternal and dietary iron to initiate the shift in IRP-1A conformation.

A previous iteration of this experiment was attempted in the King-Jones lab by Qiuxiang Ou with 100 μM BPS in NutriFly (a highly nutritional diet) with encouraging results. *phm22>NOS^{IR-X}-RNAi* were rescued to adulthood in three of six vials tested. The effect was all or nothing, such that either all animals remained arrested at the L3 stage, or all larvae were capable of reaching adulthood. This indicated that a threshold for cellular iron stores may exist where the animals can either commit to adult development or continue to feed as larvae. The 50% success rate of this trial led us to pursue our experiments on holidic media in an effort to get maximum distribution of BPS, because making the holidic media ourselves provided the opportunity to optimally distribute the iron chelator.

In figure 3.4D, *phm22>NOS^{IR-X}-RNAi* flies reared on a holidic diet containing 0, 100 or 250 μM BPS, showed no increase in survival to adulthood. Although there is previous evidence linking IRP-1A to NO signaling, altering iron concentrations in the diet could not further bolster this connection. Furthermore, we repeated our experiments on NutriFly and the standard fly kitchen media and all results were the same as Figure 3.4D with the only difference being increased adult survival for control lines. We were ultimately unable to confirm that BPS feeding is capable of rescuing *phm22>NOS^{IR-X}-RNAi* larvae to adulthood.

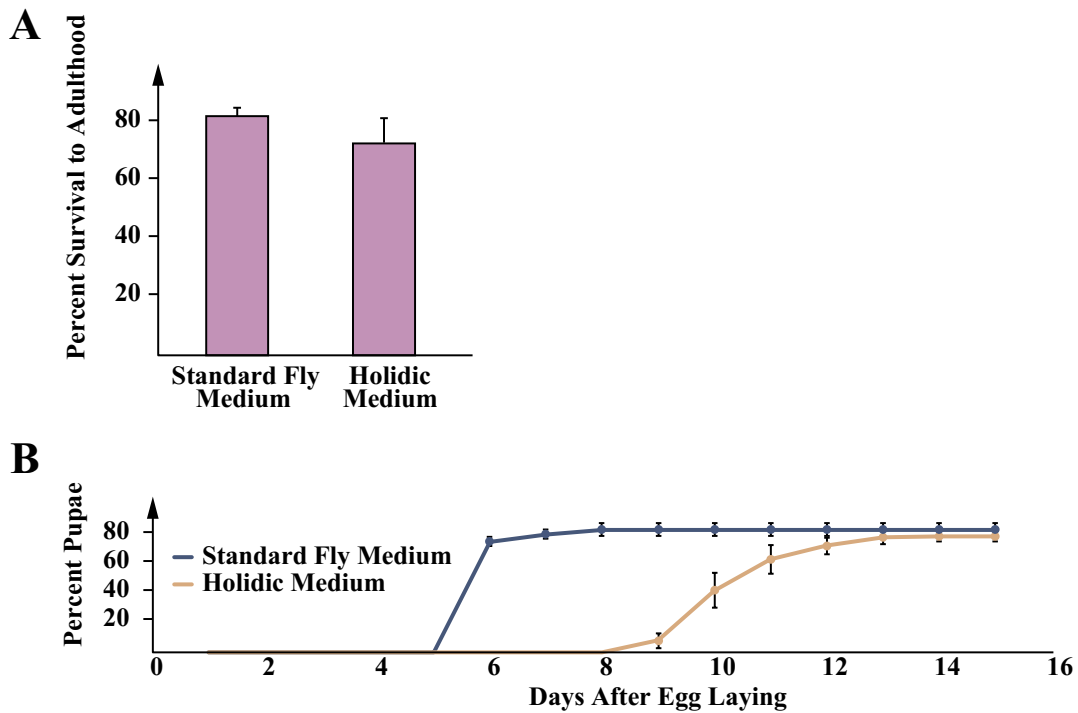


Figure 3. 3. *Drosophila* reared on a defined holidic diet had similar adult survival rates compared to controls reared on standard fly medium, but with a four to five-day delay to pupal formation. A) Adult survival represents the number of healthy adults that eclosed. B) Larvae had a delayed growth on a holidic diet, pupa formation occurred approximately five days later compared to animals reared on standard media. All flies were w^{1118} , Fly kitchen medium was produced at the University of Alberta.

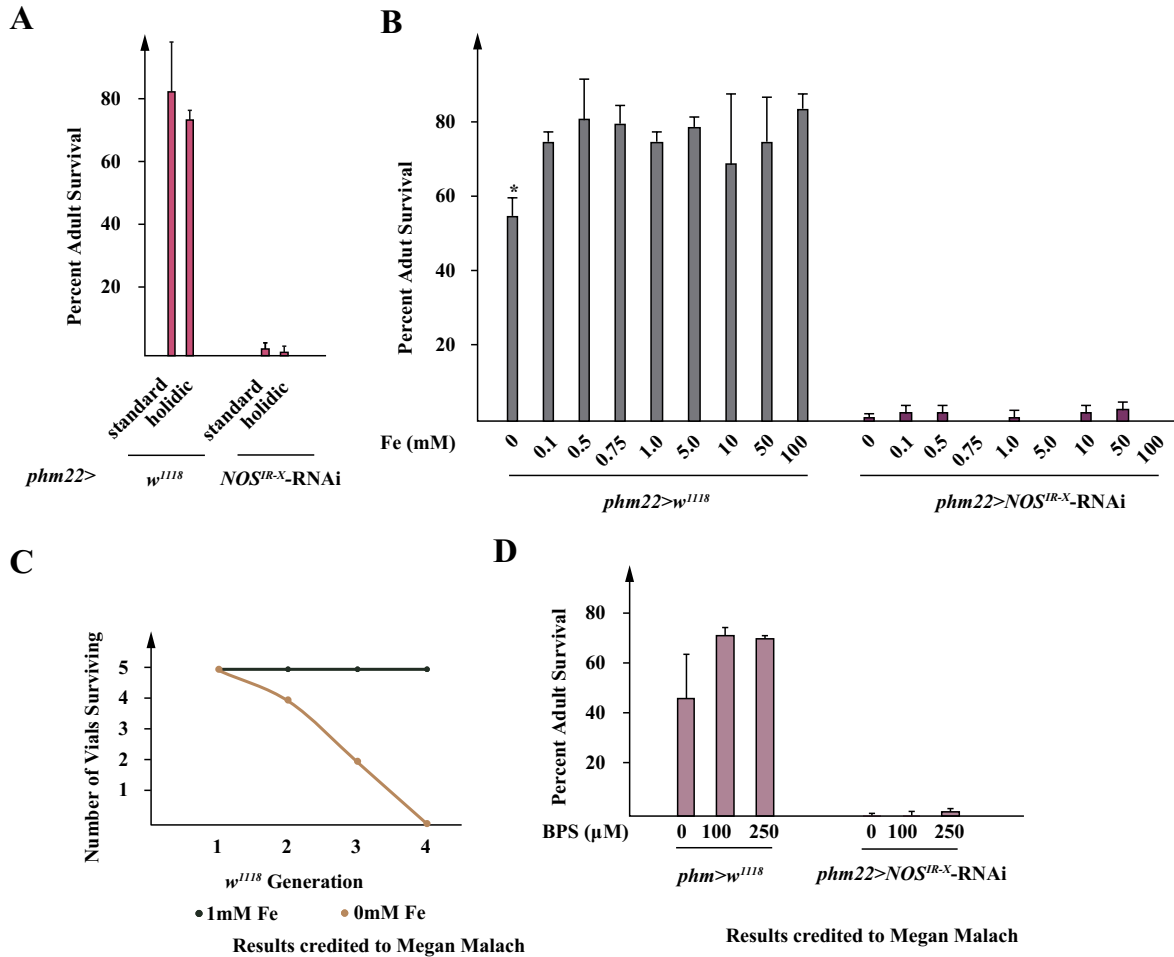


Figure 3.4. *phm22>NOS^{IR-X}-RNAi* animals were not phenotypically rescued when fed an iron manipulated holidic diet. **A)** *phm22>NOS^{IR-X}-RNAi* animals had no difference in adult survival on holidic media compared to standard fly kitchen media. The differences between nutrients, specifically that of iron within the holidic medium compared to fly kitchen medium appeared to exert no phenotypic rescue or have any effects on *phm22>NOS^{IR-X}-RNAi* animals, represented via percent survival to adulthood. **B)** *phm22>NOS^{IR-X}-RNAi* animals were not rescued to adulthood under variable iron concentrations ranging from 0-100 mM. *phm22>w¹¹¹⁸* control treatments showed no varying survival to adulthood on the various iron concentrations except when iron was absent in the media. In that case, an approximate 20% decrease in survival to adulthood occurred. However, for *phm22>NOS^{IR-X}-RNAi* animals, no change was observed in adult survival to adulthood across all concentrations tested. All media was holidic. **C)** *Drosophila* can survive up to four generations when reared on iron-depleted media. The strain used was *w¹¹¹⁸* and adult progeny from each generation were added to a fresh vial containing holidic media with either an iron solution or water. After one generation the flies on the media lacking iron began to perish. Data attributed to Megan Malach. **D)** *phm22>NOS^{IR-X}-RNAi* animals exposed to various concentrations of BPS to reduce cellular iron concentrations did not rescue larvae to adulthood. Animals were grown on holidic media on either 0, 100 or 250 µM BPS. Control flies *w¹¹¹⁸* had no significant increase or decrease in viability nor did *phm22>NOS^{IR-X}-RNAi* flies. Data attributed to Megan Malach. BPS: bathophenanthroline disulfonic acid.

3.3.2 *NOS* mutants fed BPS have increased viability

I had access to two *NOS* mutant lines and wanted to see if there was any corresponding phenotype related to the *phm22>NOS^{IR-X}-RNAi* animals in hopes of further validating the *NOS^{IR-X}-RNAi* phenotypic rescue.

I had two mutant lines to test: 1) A *NOS* full deletion CRISPR line which I will be referring to as *NOS^{FD}* from Oren Schuldiner¹⁶⁴ and 2) a deletion line removing amino acids 1-757 which includes the oxygenase, heme-binding and substrate-binding domains: *NOS^{Δ15}* was from Patrick O'Farrell¹⁶⁵. *NOS^{FD}* flies are reported as viable with phenotypes related to neuronal pruning¹⁶⁴, whereas *NOS^{Δ15}* is only reported as viable¹⁶⁵.

Despite the reported viability of both *NOS^{FD}* and *NOS^{Δ15}*, I wanted to examine these lines for the presence of phenotypes that may have been previously missed. Perhaps the strains were viable but not as healthy as their corresponding control lines, and if *NOS* was indeed involved in iron regulation, perhaps altering dietary iron concentrations could result in a phenotype. Each line was reared on a holidic diet with varied iron concentrations and compared to their appropriate controls, *w¹¹¹⁸* for *NOS^{FD}* and the parental line, *E2761*, that was used to generate *NOS^{Δ15}* (Fig. 3.5AB). *NOS^{FD}* flies, while viable as a stock, had an approximate survival rate of 20% to adulthood compared to controls (*w¹¹¹⁸*) which showed a ~55% survival rate. The control line usually has an 80-90% survival rate on holidic medium and this decrease was likely caused by unforeseen variations between batches of the holidic media. However, when normalized to controls, *NOS^{FD}* flies exhibited a 60% decrease in survival (Fig. 3.5A). Future experiments could be performed alongside a separate batch of holidic medium to determine if there is a difference between survival of controls based on the batch tested. Furthermore, these experiments should be carried out alongside a highly nutritious food source, such as Nutrifly, to ensure the flies are capable of surviving at typical rates of 80-90% for controls. Finally, *NOS^{Δ15}* had a viability comparable to that of controls, consistent with previous reports¹⁶⁵ (Fig. 3.5B).

In regards to *NOS^{Δ15}*, limited resources at the time of the experiment allowed for only two replicates of the 1 mM iron concentration and therefore no standard deviation could be calculated, leaving the results ambiguous (Fig. 3.5B). The results therefore appeared to show no differences in survival based on the range of iron concentrations tested and will have to be repeated in order to draw further conclusions or confirm these results. At the time of this

experiment, *NOS^{FD}* (Fig. 3.6B) showed more promising results and I did not follow up on *NOS^{AI5}* any further.

NOS^{FD} flies showed a decreased viability, approximately 60% compared to controls, and appeared to not be affected by iron concentrations in the diet (Fig. 3.5A). Although the flies were not tested on diets completely lacking iron, decreasing dietary iron levels from 1 to 0.5 mM appeared to have no effect on survival rates. As mentioned with the *w¹¹¹⁸* iron-depleted feeding, perhaps maternal iron stores prevented a phenotype related to dietary iron from occurring and, therefore, I wanted to see if BPS could reduce cellular iron levels and rescue *NOS^{FD}* mutant viability. I predicted that the viability of *NOS^{FD}* animals suffered due to a lack of IRP-1A RNA-binding activity, perhaps related to embryogenesis as all surviving larvae developed to adulthood. Therefore, *NOS^{FD}* flies were fed a holidic diet containing 0, 100 or 250 μ M BPS concentrations (Fig. 3.5C), which resulted in a significant increase in viability from less than 40% to over 60%, a 1.5 fold change. This suggested a link between NOS, NO and iron and supported the hypothesis that iron is connected to NOS and NO. Perhaps ecdysone regulation was affected in these animals and a disruption in NO and iron regulation through the mutant *NOS* caused the decrease in viability seen.

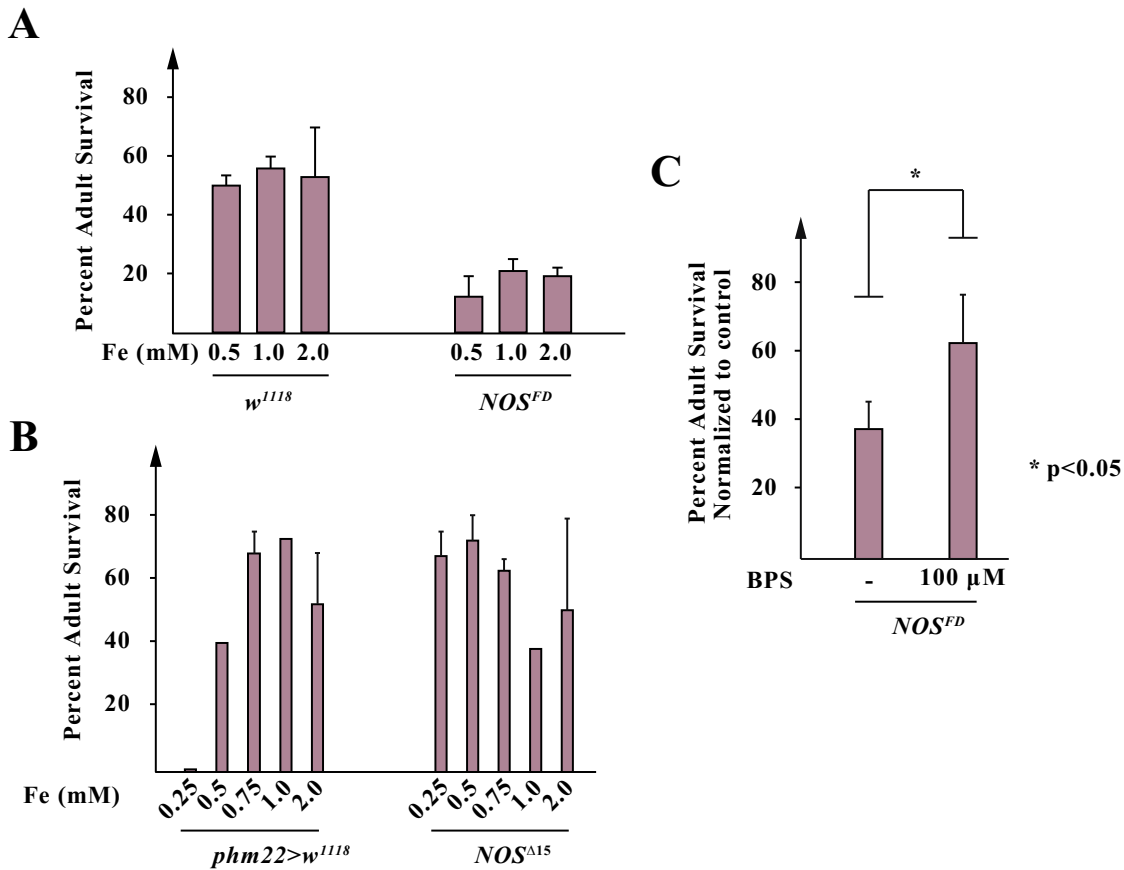


Figure 3.5. *NOS^{FD}* mutants appeared to have an iron related phenotype whereas *NOS^{Δ15}* did not. **A)** *NOS^{FD}* mutants had a decreased rate of survival compared to adults, regardless of iron concentration in the diet. Flies were reared on holidic media; control survival was sub-par in this variation of food. When compared to control flies of *w¹¹¹⁸*, *NOS^{FD}* mutants still exhibited a 60% decrease in survivability to adulthood. **B)** *NOS^{Δ15}* mutants reared on various iron-concentrated media showed no decrease in viability compared to control, regardless of iron concentration. Due to lack of materials, some vials were only done in two replicates, resulting in a lack of error bars in particular conditions. **C)** *NOS^{FD}* mutants had increased viability when reared on a holidic diet containing 100 μM BPS. The data has been normalized to the control to better represent the data. The shift is statistically significant with a p value being less than 0.05. The control line used was *w¹¹¹⁸*, BPS: bathophenanthroline disulfonic acid.

3.4 Constitutively active IRP-1A in the prothoracic gland rescues *phm22>NOS^{IR-X}-RNAi* animals to adulthood

As previously mentioned (Ch. 1.9), overexpressing an *IRP-1A* cDNA in the PG of *phm22>NOS^{IR-X}-RNAi* animals rescued both the L3 arrest and giant red ring gland phenotype. The variable iron dietary experiments were not consistent with these data and therefore I took another approach to artificially induce IRP-1A RNA-binding activity. I wanted to see if overexpressing a transgene encoding constitutively active RNA-binding IRP-1A could bypass the presumptive need for the NO signal lost in *phm22>NOS^{IR-X}-RNAi* animals (Fig. 1.9). I used my transgenic lines from chapter 2.1: *UASC-IRP-1A* and *UASC-IRP1A^{C450S}*, in combination with the *NOS^{IR-X}-RNAi* for the rescue experiment.

I speculated that the RNA-binding form of IRP-1A was responsible for rescuing the *NOS^{IR-X}-RNAi* phenotype in previous experiments. Since my model proposed that NO was required for activating IRP-1A RNA-binding activity in the PG, ultimately for ecdysone production, then overexpressing the RNA-binding form of IRP-1A should bypass the presumptively lost NO signal in *phm22>NOS^{IR-X}-RNAi* animals. Therefore, I wanted to compare the effectiveness between IRP-1A and IRP-1A^{C450S} in rescuing *phm22>NOS^{IR-X}-RNAi* animals. IRP-1A^{C450S} should always be active and result in a greater rescue compared to wild type IRP-1A when expressed in a *phm22>NOS^{IR-X}-RNAi* background.

First, I needed to see if *phm22>IRP-1A* and *phm22>IRP-1A^{C450S}* animals could survive. Both showed an approximate 30-50% survival rate compared to the control cross *phm22>w¹¹¹⁸* (Fig. 3.6A). Overexpressing the transgenes caused embryonic lethality and the larvae that survived were viable until adults with no apparent visual defects. *phm22>NOS^{IR-X}-RNAi; mcd8:GFP, EGFP* animals displayed L3 arrest. *mcd8:GFP* was associated with the RNAi for tissue expression visualization of the RNAi and EGFP ensured that the number of transgenes remained constant between the control and experimental lines (so GAL4 was equally distributed in both cases). I will be referring to *NOS^{IR-X}-RNAi, mcd8: GFP* as *NOS^{IR-X}-RNAi* and will not be mentioning *EGFP* hereafter.

phm22> NOS^{IR-X}-RNAi; IRP-1A larvae displayed an L3 arrest phenotype similar to *NOS^{IR-X}-RNAi*: L3 arrest and giant red RGs (Fig 3.6AB). This was unexpected because previous reports in the lab showed that *IRP-1A* overexpression rescued *NOS^{IR-X}-RNAi* animals to

adulthood. I believed this was due to positional effects because my *IRP-1A* line had the transgene inserted in the *attP40* location on the second chromosome, which likely had differential expression characteristics than that of the random P-element *IRP-1A* line that the King-Jones lab obtained¹¹⁰. Additionally, the P-element *IRP-1A* transgene had a *hsp70* promoter which had leaky and variable expression¹¹⁰, compared to the *Drosophila* core promoter contained in the *IRP-1A* transgenic lines I created, which could have added another variable in transgene expression differences.

Interestingly, when *IRP-1A^{C450S}* was expressed in a *NOS^{IR-X}-RNAi* background, the animals were rescued to adulthood at a rate of 20% (Fig. 3.6AB). The only difference between *phm22>NOS^{IR-X}-RNAi; IRP-1A* and *phm22>NOS^{IR-X}-RNAi; IRP-1A^{C450S}* was a single point mutation resulting in a C450S substitution. As mentioned in chapter 2.4, this was predicted to prevent *IRP-1A* from binding an ISC, forcing *IRP-1A* to assume the RNA-binding form at all times. These results showed that the constitutively active form of *IRP-1A* (*IRP-1A^{C540S}*) rescued *NOS^{IR-X}-RNAi* animals, whereas the transgenically expressed wild type *IRP-1A*, which was not dedicated to the RNA-binding form at all times, did not rescue the animals to adults. This supported my prediction that the RNA-binding form of *IRP-1A* was capable of bypassing the NO signal lost in *phm22>NOS^{IR-X}-RNAi* animals, allowing them to develop into adults.

Whole body phenotypes were documented (Fig. 3.6B) and showed that only *phm22>NOS^{IR-X}-RNAi* and *phm22> NOS^{IR-X}-RNAi; IRP-1A* had an L3 larval arrest and giant red RG phenotype, which was visible to the naked eye. In the case of *phm22>NOS^{IR-X}-RNAi; IRP-1A^{C450S}*, not all larva reached the L3 stage, and rather died as wandering L2.

RGs were dissected and analyzed, revealing not only that body size and survival to adulthood was rescued in *phm22> NOS^{IR-X}-RNAi; IRP-1A^{C450S}* animals, but that the giant red RG phenotype was also rescued in both size and fluorescence. Why the size of the RG was rescued is currently unknown. On the other hand, the loss of red fluorescence in the RG indicated that heme precursors were no longer accumulating, which suggested that heme molecules were being successfully synthesized for their role as a cofactor for P450s in ecdysone biosynthesis. (Fig. 3.6C). This demonstrated that *IRP-1A* RNA-binding activity may have aided in the production of heme, likely by increasing available cellular iron for the final step of heme biosynthesis and further implied a link between *NOS*, *NO* and *IRP-1A*. As previously mentioned, *IRP-1A* could not rescue *phm22> NOS^{IR-X}-RNAi* to adulthood, nor the RG phenotype. This was interesting as it

further indicated the RNA-binding role of IRP-1A in the predicted NOS, NO, IRP-1A, ecdysone pathway (Fig. 1.9).

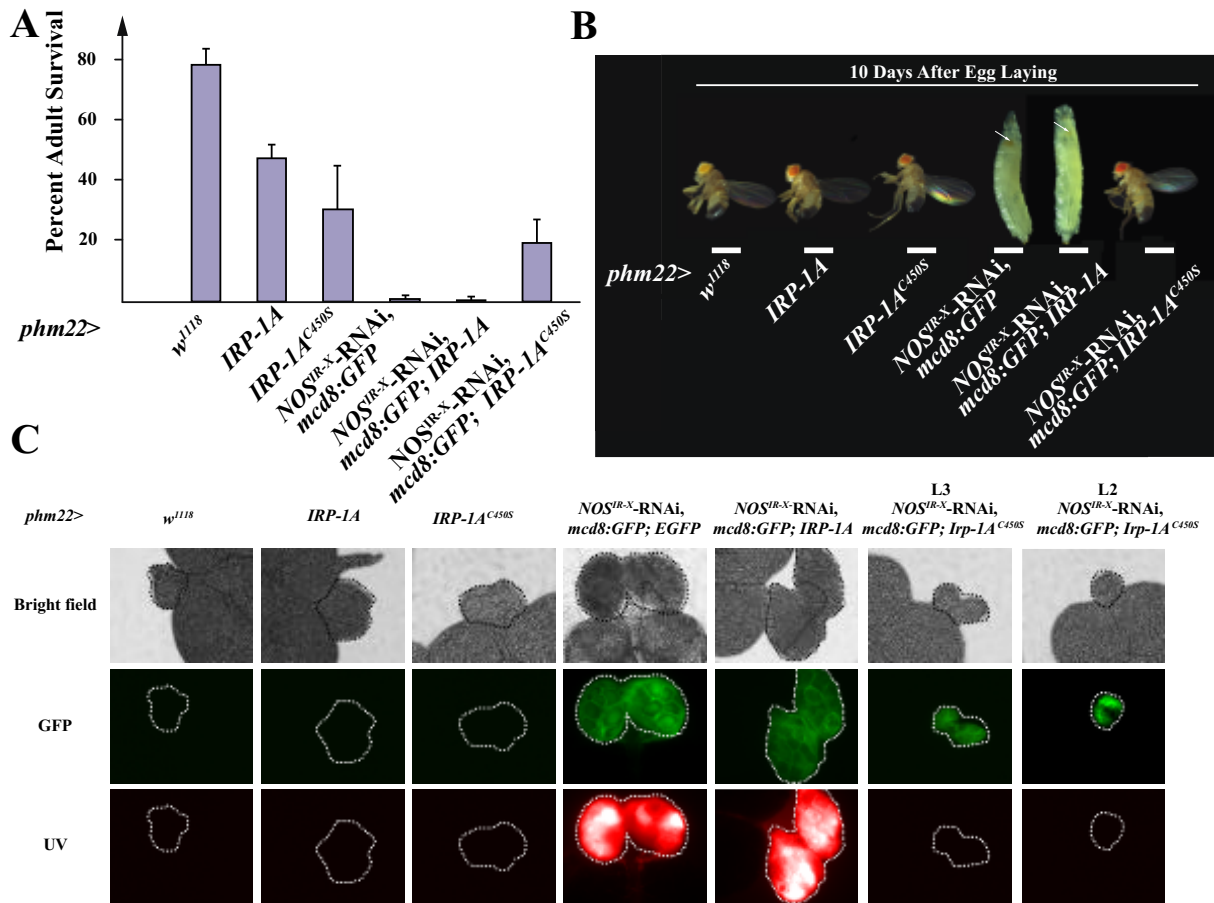


Figure 3. 6. Overexpressed constitutively active IRP-1A in the RG rescued *phm22> NOS^{IR-X}-RNAi* giant red RG phenotype and L3 arrest. **A)** Constitutively active IRP-1A in the RG rescued *phm22> NOS^{IR-X}-RNAi* to adulthood. *phm>w¹¹¹⁸* was the control strain and showed an 80% survival to adulthood. *phm22>IRP-1A* and *IRP-1A^{C450S}* had a 30-60% survival rate to adulthood and all embryos that hatched survived to adulthood. *phm22>NOS^{IR-X}-RNAi* showed the standard L3 arrest phenotype of no adult survival. *IRP-1A* expressed in the PG in a *phm22>NOS^{IR-X}-RNAi* background showed no change in phenotype compared to the standard *phm22>NOS^{IR-X}-RNAi* L3 arrest. When *IRP-1A^{C450S}* was expressed in the PG in a *phm22>NOS^{IR-X}-RNAi* background the animal was rescued to adulthood at a rate of 20%. **B)** Whole body analysis showed that *IRP-1A^{C450S}* expression in the PG rescued the *phm22>NOS^{IR-X}-RNAi* animals to adulthood. Arrows indicate visible red RGs in whole larvae. **C)** RG analysis showed that *IRP-1A^{C450S}* expression rescued the *phm22>NOS^{IR-X}-RNAi* giant red ring RG phenotype which was seen fluorescing under UV light. *mcd8:GFP*, was located on the X chromosome with *NOS^{IR-X}-RNAi* for tissue visualization of RNAi expression. *UAS-EGFP* was used as a transgene control to ensure that GAL4 molecules were distributed equally across all transgenes. All images are L3 larvae unless otherwise indicated RG: Ring Gland, PG: Prothoracic Gland. Medium used is Nutri-Fly. L3: third instar.

3.5 *NOS^{IR-X}*-RNAi phenotype is the result of an off-target effect

The main caveat of RNAi-associated phenotypes is the potential for off-target effects¹⁶⁶, causing an unintended gene to be knocked down instead or in addition to the actual target gene, in this case *NOS*. *NOS^{Δ15}* and *NOS^{FD}* mutants and TRIP *NOS*-RNAi were reported viable with no L3 arrest or giant red ring glands^{164,165}, raising concerns that *NOS^{IR-X}*-RNAi may indeed have had an off-target. Fortunately, previous work showed that *NOS^{IR-X}*-RNAi animals had no detectable NO fluorescence using the DAF2-DA stain and that NOS's 100 kd band could no longer be detected in a western blot, suggesting that if there was an off-target it was in addition to *NOS* knockdown².

To determine whether the *NOS^{IR-X}*-RNAi phenotype was a result of a *NOS* knockdown, I crossed the RNAi line into a *NOS^{FD}* mutant background. If *NOS^{IR-X}*-RNAi only targets *NOS*, then the giant L3 larva with large red RG phenotype seen in *phm22*> *NOS^{IR-X}*-RNAi should not occur. The idea was that the *NOS^{IR-X}*-RNAi would no longer have an mRNA target and thus should not cause lethality. Therefore, animals expressing *NOS^{IR-X}*-RNAi in a *NOS^{FD}* background should have the same viability and phenotype as *NOS^{FD}*, and should be largely viable to adulthood. The phenotypes of this experiment for *phm22*>*NOS^{IR-X}*-RNAi; *NOS^{FD}* were the same as *phm22*>*NOS^{IR-X}*-RNAi, indicating that *NOS^{IR-X}*-RNAi had an off-target, likely in addition to *NOS* (Fig. 3.7).

An NCBI blast analysis using the 698 bps of the RNAi construct revealed four potential off-targets: *N(alpha)-acetyltransferase 60 (Naa60)* and *CG31950* with an E-value of 7.8 and *CG13667* and *CG5577* with an E value of 0.18. *Naa60* is a histone acetyl-transferase (RNAi is predicted to be capable of binding 22 bases in a 24 base range), *CG31950* is known to have an LSM domain and with the RNAi suspected of binding 22 bases in a span of 24. *CG5577* is a haloacid dehalogenase with phosphatase activity and the RNAi is capable of bonding with 29 bases within a span of 32. Neither *Naa60*, *CG5577* or *CG31950* have obvious connections to NOS or ecdysone biosynthesis and are unlikely to be the off-target. The most likely phenotypically related off-target however, with potential connections to P450s and NOS was *CG13667*, an NADPH-hemoprotein reductase in which the RNAi was predicted to bind 33 bases in a 40 base range. Currently, we only know the predicted molecular functions of this gene as it has not yet been studied. NOS and P450's both require NADPH and heme, and this protein is

predicted to be necessary for electron transfer from NADPH to heme, therefore, if this gene is knocked down by RNAi, then NO production could be disrupted. However, this does not answer why I saw L3 arrest and giant red RGs in *phm22>NOS^{IR-X}-RNAi; NOS^{FD}* animals when NOS was absent and the RNAi was active. NOS could not have been affected by CG13667 if it was not present, therefore setting forth more unknowns. Perhaps the *NOS* gene, while deleted in its native location, could have become inserted elsewhere in the genome during the generation of the *NOS^{FD}* line. If this was the case, my primers for detecting the deletion would be incompatible with the new insertion site and would render it undetectable unless new primers were designed or perhaps even a southern blot could be performed to detect the *NOS* gene.

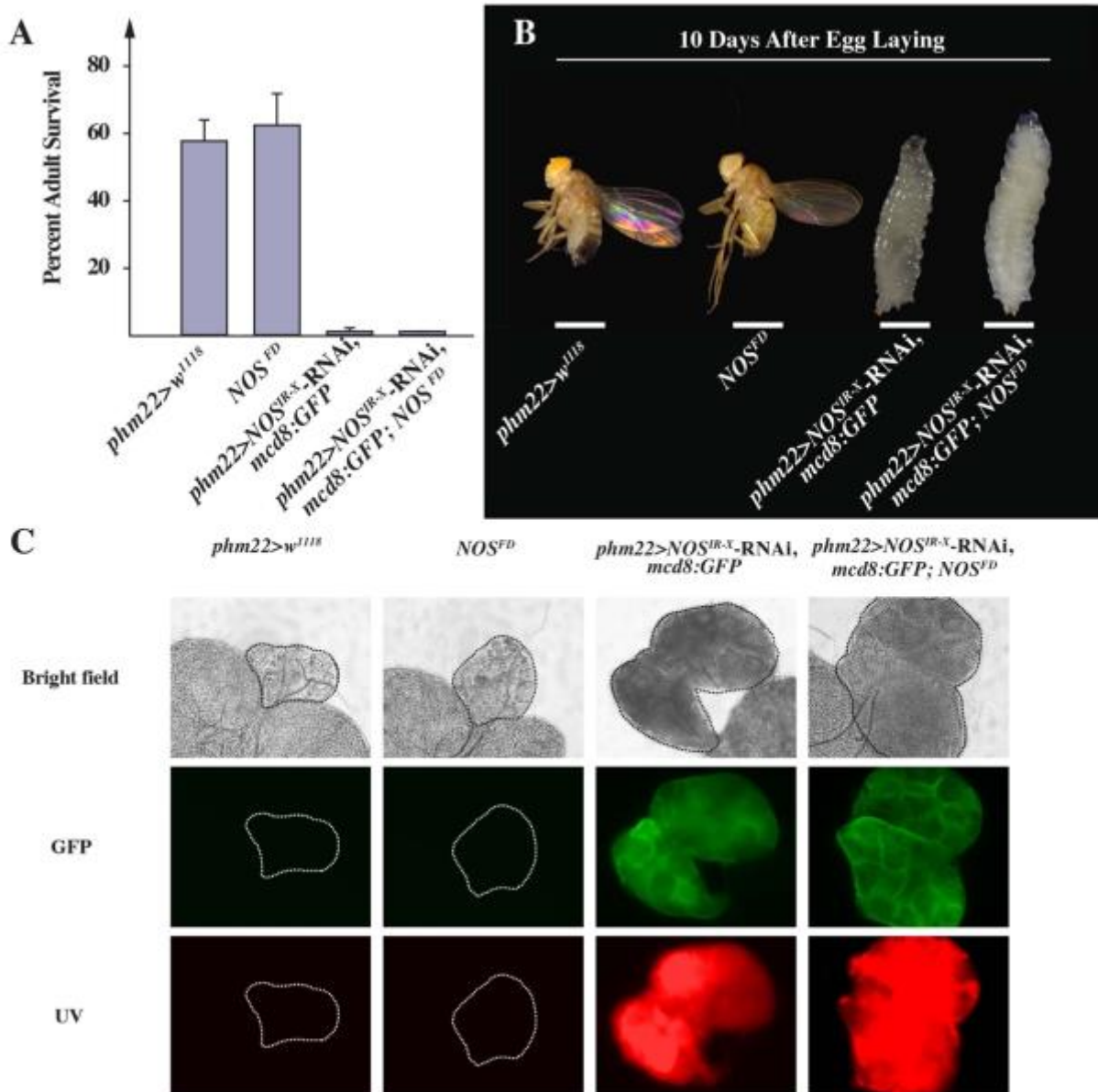


Figure 3.7. *NOS^{IR-X}-RNAi* had an off-target effect instead of or in addition to NOS. **A)** *NOS^{FD}* mutants in this experiment had 60% survival to adulthood and when *phm22> NOS^{IR-X}-RNAi* is introduced into the *NOS^{FD}* line, all animals arrested during L3. This suggested that the RNAi targeted mRNA other than NOS, otherwise it was expected to have the same phenotype as *NOS^{FD}* because there would be no target for the RNAi to bind to. **B)** Whole body images representing the L3 arrest phenotype of *phm22> NOS^{IR-X}-RNAi* in a *NOS^{FD}* background. **C)** RG images representing the L3 arrest phenotype of *phm22> NOS^{IR-X}-RNAi* in a *NOS^{FD}* background. *mcd8:GFP*, was located on the X chromosome with *NOS^{IR-X}-RNAi* for tissue visualization of RNAi expression. *UAS-EGFP* was used as a transgene control to ensure that GAL4 molecules were distributed equally across all transgenes. RG: Ring Gland. L3: third instar. UV used to view red fluorescence.

4.0 Discussion

4.1 The importance of IRP in the mammalian brain and the *Drosophila* ring gland

Drosophila only has IRP-1A and IRP-1B, whereas mammals have IRP1 and IRP2, with differential expression patterns over the animal¹⁶⁷. For example, IRP1 is highly expressed in the kidneys, liver, and brown fat and is implicated in pulmonary and cardiovascular functions. IRP2's act mainly in the duodenum and the central nervous system and are widely considered the primary regulator of iron homeostasis¹⁶⁷. I have shown that IRP-1A is expressed and/or upregulated in the RG and BRGC during development (Fig. 3.1), in line with mammalian studies that show IRP2 being largely responsible for neuronal regulation of iron¹⁶⁸. IRP2 is only found in the evolutionary chain after *Danio rerio*, suggesting it had never evolved in *Drosophila*. This making it possible that IRP-1A's function encompasses that of both IRP1 and IRP2 in mammalian systems. Alternatively, studies have shown a role for IRP1 in the brain, suggesting that flies do not require the level of iron regulation that IRP2 provides, since flies only have one known IRE-binding protein. For example, the amyloid precursor protein associated with Alzheimer's, contains a 5' UTR IRE in human neuronal cells, and researchers have demonstrated that IRP1, not IRP2, could bind and regulate the IRE of the *amyloid precursor protein* mRNA¹⁶⁹. Fly Atlas shows that IRP-1A is highly expressed in the gut, likely to process dietary iron, but also shows moderate *IRP-1A* expression in the central nervous system¹⁷⁰. This suggests that *IRP-1A* may play an important role here, part of which could be for my proposed link with ecdysone biosynthesis. Therefore, IRP-1A's role in the RG may encompass similar features to that of both IRP1 and IRP2 as well as additional roles in ecdysone production.

In regards to *IRP-1A* expression in the PG, I have shown that when ecdysone biosynthesis is occurring, *IRP-1A* expression increases in the RG (Fig. 3.1). This suggests that in times of hormonal regulation, IRP-1A was increasingly necessary for proper animal development. This data does not include whole body samples and so the relative amount of *IRP-1A* increase in the brain compared to the whole body at the times tested is currently unknown. Additionally, expressing *IRP-1A^{C450S}* specifically in the PG rescued *phm22>NOS^{IR-X}-RNAi* animals to adulthood (Fig. 3.6), further demonstrating the activities of IRP-1A within the PG.

The data also implies the importance of the RNA-binding activity of IRP-1A in the PG because the wild type *IRP-1A* transgene was unable to rescue *phm22>NOS^{IR-X}-RNAi* animals, only the constitutively active form was capable.

Together, these data provide evidence that IRP-1A has important functions in the *Drosophila* PG. Future studies determining protein levels and a more detailed analysis of transcript levels over time in the RG would provide useful information of IRP-1A's regulation in relation to proper development. Additionally, research in rats has shown that a limited iron diet decreased the levels of P450 enzymes in the intestine¹⁷¹. Therefore, it would be interesting to know if affecting iron regulation through IRP-1A in the PG could limit P450 generation, thereby limiting ecdysone production. A qRT-PCR looking at P450 transcript levels when *IRP-1A* is over- and underexpressed, to see if P450 transcripts increase or decrease respectively, could tell us if IRP-1A's RNA-binding activity has a direct relation to P450 production. Similarly, simply measuring ecdysone concentrations or performing a western blot to detect P450 protein concentrations could also give a readout to the degree as to which steroid hormone biosynthesis is disrupted.

4.2 IRP-1A RNA-binding activity activated through transgene manipulation as opposed to dietary iron manipulation rescues *phm22>NOS^{IR-X}-RNAi* animals to adulthood

My primary goal was to bypass the loss of a late third instar NO signal in *phm22>NOS^{IR-X}-RNAi* flies that I believed was required to shift IRP-1A from the aconitase to RNA-binding form (Fig. 1.9). This NO signal was thought to be required for an increase in cellular iron by disrupting the ISC bound to IRP-1A, causing it to become RNA-binding. As a result, IRP-1A was predicted to translationally downregulate *ferritin* mRNA, making more iron available for incorporation into heme. Heme should then be required in large quantities as a cofactor for cytochrome P450 enzymes in order to synthesize ecdysone for pupariation. To try and bypass the loss of the predicted NO signal in *phm22>NOS^{IR-X}-RNAi* animals and induce the RNA-binding form of IRP-1A I believed was necessary to rescue the animal, I depleted iron within the diet and fed an iron chelator to the animals. I hypothesized that decreasing ISC concentrations would result, thereby shifting IRP-1A to the RNA binding form. *IRP-1A* transgenes were also used: a wild type form and a constitutively active RNA-binding form. The wild type form was used with the idea of outcompeting available ISCs, thereby leaving many IRP-1A proteins without an ISC which would cause it to become RNA-binding. The constitutively active form relinquishes the need to decrease cellular iron levels to achieve IRP-1A RNA-binding activity. It is also important to note that I hypothesized that the cells for all purposes other than producing ecdysone, had sufficient levels of free cellular iron. I believed it was only due to the high heme demand required by P450s that the PG essentially lacked free cellular iron at that time and instead required higher levels of free iron than other tissues generally would. Of the attempts to rescue developmentally arrested *phm22>NOS^{IR-X}-RNAi* animals, ectopically expressing the constitutively RNA-binding IRP-1A was the only means by which rescue occurred.

My first approach was to decrease or diminish iron in the diet in order to shift IRP-1A to its RNA-binding form in an attempt to rescue *phm22>NOS^{IR-X}-RNAi* animals (Fig. 3.4). If the cause of the giant red RG seen in the *phm22>NOS^{IR-X}-RNAi* L3 arrest phenotype was caused by a lack of free cellular iron, feeding the animals increasing levels of iron to alleviate the symptoms was logical. This was performed and no rescue occurred, perhaps because ferritin was simply storing the excess iron as it normally would and that the PG cells were essentially

unaware of the iron demand from P450's heme cofactors. Therefore, to bypass the suspected NO signal that was absent in *phm22>NOS^{IR-X}-RNAi* animals, I reduced iron in the diet in an attempt to shift IRP-1A to the RNA-binding form in order to rescue the animal. If cellular iron levels were low, ISCs should have been limiting and IRP-1A should have become RNA-binding because it would no longer be bound to an ISC. This would then cause IRP-1A to block ferritin translation, preventing the storage of iron, thereby increasing cellular iron levels for incorporation into heme and ecdysone production. However, this was unable to rescue *phm22>NOS^{IR-X}-RNAi* animals, even when cellular iron levels were chelated using 100 μ M BPS in the diet, a method previously shown to decrease cellular iron stores by 50%^{162,163}. Perhaps BPS was not an optimal chelator of iron in animals for this study. It was originally chosen because of previously published results but other iron chelators such as 2,2 -bipyridyl (BIP), desferrioxamine (DFO), 3-(2-pyridyl)-5,6-bis (4-phenylsulfonic acid)-1,2,4-triazine (ferrozine), or even preclinical chemotherapeutic iron chelators may be better suited for *Drosophila* feeding and iron chelation in the RG or perhaps a different method of introducing the chelator was necessary, such as injection.

Although shown effective in previously mentioned studies, characteristics of BPS that could be disadvantageous are that it binds iron outside of the cell, is impermeable to the cell layer¹⁷², the longer it is active the less effective it becomes¹⁷³, and has limited effectiveness from pH 6-7¹⁷³. Comparably, DFO, commonly used in IRP-1A studies *in vitro* to initiate RNA-binding activity, also cannot penetrate the cell layer¹⁷⁴. However, DFO binds to iron in a 1:1 ratio, whereas BPS binds in a 3:1 ratio, so less DFO is necessary to achieve equivalent rates of chelation. Another enticing reason to test DFO is its use in clinical trials as a metal chelator, showing limited side effects in biological systems¹⁷⁵. An advantage to the limited mobility of BPS and DFO could be that if a chelator enters the cell, it could become so effective that the chelation becomes lethal. Alternatively, both BIP and ferrozine can penetrate the membrane^{172,173} and have greater access to cellular iron, therefore their chelation ability should be more potent. Both BIP and ferrozine bind iron at the same ratio of BPS, 3:1 with ferrozine having a faster mode of chelation than BPS¹⁷²⁻¹⁷⁴. Interestingly in a cell culture study, researchers compared the rate at which IRP1 RNA-binding form was activated in response to ferrozine or BPS and both activated IRP1 at the same rate *in vitro*, regardless of the speed of iron chelation¹⁷³. This suggests that the effectiveness of the chelator is more important than the rate of action. Finally, it may be

valuable to look at new cancer chemotherapeutic iron chelators. Many drugs are being developed for human use that are all cell permeable, giving a wide variety of additional drugs that can be tested for iron chelation effectiveness in rescuing *phm22>NOS^{IR-X}-RNAi* animals¹⁷⁶ that have direct clinical ties.

The myriad of possibilities that could limit BPS efficiency, perhaps resulted in BPS being unable to reach the PG to chelate iron. It is possible the low iron diet treatment only affected IRP-1A in the gut, where it was ingested. Alternatively, perhaps the PG maintained some form of priority, and so iron could not have been depleted there until absolutely necessary. If a rescue with an iron chelation treatment occurs, it is important to know whether the rescue is specifically due to the inactivation of iron as opposed to other metals, or off-target effects. For example, DFO can bind both aluminum and iron¹⁷⁵ and it is common for these chelators to have a high affinity for copper and zinc as well¹⁷⁷. Any observed rescue seen should be controlled for by outcompeting the chelator with iron in the media, bringing back the L3 arrest and giant red RG phenotype originally observed in *phm22>NOS^{IR-X}-RNAi* animals, which would demonstrate that iron chelation specifically rescues the animal.

The biological and environmental methods of reducing iron in the animal to trigger IRP-1A RNA-binding activity in hopes of rescuing *phm22>NOS^{IR-X}-RNAi* larvae was unsuccessful. Therefore, IRP-1A transgenes were directly expressed in the PG, bypassing the need for altering dietary and biological iron. I expressed the constitutively active RNA-binding form of IRP-1A and was able to fully rescue *phm22>NOS^{IR-X}-RNAi* animals (Fig. 3.6). IRP-1A and IRP-1A^{C450S} had a semi-lethal effect on embryonic development in this study, similar to previous studies demonstrating the importance of IRP1 and IRP2 in the embryo¹⁷⁸. This lethality was seen throughout the study and reduced survival to 50-70% of control when expressed in the PG. The RNA-binding form of IRP-1A led to more lethality in the population compared to its wild-type cDNA counterpart, suggesting that the RNA-binding activity of IRP-1A was responsible. Furthermore, only IRP-1A^{C450S} was capable of rescuing *phm22>NOS^{IR-X}-RNAi* animals showing that the RNA-binding form of IRP-1A bypassed the presumptive loss of the NO signal. Ultimately, this supported my hypothesis that the mobilization of cellular iron can rescue the heme-precursor buildup seen in the large red ring glands of *phm22>NOS^{IR-X}-RNAi* larvae.

IRP-1A^{C450S} expression rescues both size and fluorescence in *phm22>NOS^{IR-X}-RNAi* PGs (Fig. 3.6C). The King-Jones lab has been able to show that the red fluorescence matches the

fluorescent excitement peaks of heme precursors (Ch. 1.9). Therefore, the loss of red fluorescence showed that heme precursors no longer accumulated, suggesting they were successfully synthesized into heme.

Why the RG was enlarged in the first place is unknown, making it difficult to come to conclusions as to how IRP-1A RNA-binding activity rescued the size of the RG. Researchers have shown that the large size of the PG can be due to endoreplication and oncogenic studies have reported that NO can have a negative effect on cell growth, so perhaps the loss of NO in *phm22>NOS^{IR-X}-RNAi* animals is related to the giant ring glands^{2,179}. One means to test this would be to compare the average concentration of nuclear DNA in an enlarged red RG to the amount of mitochondrial DNA in the same tissue, because mitochondrial DNA should not be undergoing endoreplication. Comparing this data to control RGs should show an increased ratio of nuclear DNA to mitochondrial DNA. However, if the large red RGs have increased amounts of mitochondria present, this comparison would suggest an overall increase in cell growth. Another means to test if endoreplication is occurring would be to measure the amount of DNA relative to tissue size using a Qubit and compare the ratios seen in giant red RGs to control RGs. Overall, if endoreplication is occurring, these two methods should provide evidence of such. It has also been shown in *Drosophila* that ecdysone is also cell size-limiting in the fat body so this may have added to the size of the RGs seen because ecdysone was not being synthesized in *phm22>NOS^{IR-X}-RNAi* animals¹⁸⁰. It may be possible that the successful production of ecdysone brought about by IRP-1A RNA-binding activity bypassed the loss of the NO signal and repressed abnormal growth rates in the PG, keeping cell size in check for proper developmental progression. This however, is purely speculative.

Although 20% of the *phm22>NOS^{IR-X}-RNAi* animals were rescued from *IRP-1A^{C450S}* expression (Fig. 3.6A), the remainder of the surviving embryos were L2 larvae, wandering for four days after egg laying and unable to pupariate, eventually dying on the walls of food vials. Perhaps in these animals, *IRP-1A^{C450S}* RNA-binding activity was lethal, interrupting proper ecdysone signaling, causing the organism to take on early wandering behavior. As well, the L2 RGs (Fig. 3.6C) showed no sign of overgrowth or red fluoresce five days after egg laying. While this may have been a partial rescue of the animal, perhaps the PG was not developing enough to even begin to accumulate heme precursors. Conversely, Qiuxiang Ou from the King-Jones lab has shown that *updo*-RNAi (one of the enzymes in the heme biosynthesis pathway) expressed in

the PG had L2 arrest and giant red RGs because heme biosynthesis was disrupted and fluorescent precursors accumulated. This shows that it is possible to see heme precursor build up at the L2 stage, perhaps implying that this too was rescued with *IRP-1A^{C450S}* expression.

One difference between my Φ C31 *IRP-1A* transgenic line and the one previously used in our lab was that my Φ C31 line was incapable of rescuing *phm22>NOS^{IR-X}-RNAi* animals. The location of the transgenes likely altered their expression as both mine and the previous experiment were done with the *phm22-GAL4* driver. It would be interesting to see, through qRT-PCR, which line has greater expression of *IRP-1A*. Perhaps my Φ C31 *IRP-1A* line is capable of rescuing *phm22>NOS^{IR-X}-RNAi* animals, but requires a stronger driver. Increased transcription should result in increased protein, outcompeting available ISCs, and a greater portion of IRP-1A would be without an ISC and thus RNA-binding. However, it would also be beneficial to create a new line capable of expressing the P-element IRP-1A transgene with the exact generations of *NOS^{IR-X}-RNAi* line I have been using. This would allow a direct comparison of the rate at which my transgenic line vs the P-element transgenic line can rescue *phm22>NOS^{IR-X}-RNAi* animals. Furthermore, sequence verifying the P-element IRP-1A, and showing that it is indeed as reported would ensure previous results were accurate. Perhaps this transgene is not a reliable representation of IRP-1A and is functioning by a different means than my Φ C31 IRP-1A transgenic line.

Ultimately, I have shown here that IRP-1A RNA-binding activity can bypass the suspected NO signal lost in *phm22>NOS^{IR-X}-RNAi* animals (Fig. 3.6). The RNA-binding activity appeared to be required in order to make iron available for heme. Heme is likely produced in large quantities in times of high ecdysone synthesis and must be used as a cofactor for P450s upon production because free heme is toxic¹⁸¹. Iron availability via IRP-1A RNA-binding activity supplies sufficient quantities of iron for heme and thereby ecdysone production, which is ultimately lost in *phm22>NOS^{IR-X}-RNAi* animals. This data can support my original hypothesis that NO is utilized in the PG to disrupt ISCs and induce IRP-1A RNA binding activity, because when *phm22>NOS^{IR-X}-RNAi* animals are supplemented with transgenic expression of IRP-1A RNA-binding activity, they survive to adulthood.

Although this data provides some evidence to my proposed model, it is important to consider that my iron feeding experiments were accurate in their results. Perhaps past experiments involved with restricted iron diets in the King-Jones lab that were capable of

rescuing *phm22>NOS^{IR-X}-RNAi* animals had inaccuracies. Previous BPS feeding experiments used a Nutrifly diet, as such the concentration of iron in each vial would not have been consistent, regardless of a consistent usage of BPS. Furthermore, I have performed many replicates, all with the same conclusions demonstrated in this thesis whereas previous experiments done had only two replicates, with six biological trials at most. As such, my model comes into question, mainly, why did the transgenic manipulations of *IRP-1A* rescue the animal, yet the limited iron feeding was incapable. As shown in Chapter 3.5, the *NOS^{IR-X}-RNAi* had an off-target, that likely in combination with a knockdown of *NOS*, resulted in the giant red ring gland L3 arrest phenotype. It was possible that the RNAi-binding activities of IRP-1A was rescuing the animal by an alternative means. Perhaps iron was being made available for heme production as previously suspected, and IRP-1A was affecting IRE-associated transcripts which resulted in a rescue of the off-target effect. One could measure iron concentrations in the rescued animal compared to controls, which would argue for the former.

The implications of the off-target effect are discussed further next chapter but some conclusions can be made regarding the *phm22>NOS^{IR-X}-RNAi* rescue experiments. First, it is clear that dietary manipulations are incapable of rescuing the animal and while I previously discussed how the dietary iron manipulations could have been flawed, the evidence suggests that my data is accurate. And second, the constitutively active form of IRP-1A can rescue the *phm22>NOS^{IR-X}-RNAi* animal whether or not the phenotype was a result of *NOS* knockdown. What can ultimately be concluded here is that whatever the effect of the *NOS^{IR-X}-RNAi* is on the animal, manipulating IRE-associated transcripts via IRP-1A can rescue the animal at a rate of ~20%. Therefore, identifying the underlying cause of the red RGs, which could be a result of the off-target is important to discover. The data still suggests that IRP-1A played an important role related to the giant red RG phenotype.

4.3 Exploring the role of NOS and NO in ecdysone production

Previous evidence has shown that *phm22>NOS^{IR-X}-RNAi* animals lack NO in the PG and that the NOS protein is not synthesized², providing evidence that the RNAi results in NOS knockdown. However, there was still the potential of an off-target effect occurring, likely in conjunction with NOS (Ch. 3.5). Although it does appear that a lack of NOS and NO in the RG has detrimental effects for the animal, it is unclear why mutants appear to be healthy and relatively viable (Ch. 3.3.2). Since NOS did not appear to be an essential protein, it may have assisted with alternative pathways and development. For example, when PTH, a regulator and initiator of ecdysone is knocked-down, the animals are still capable of reaching adulthood, but are delayed in development⁴¹. Furthermore, mammals, including mice, have three *NOS* genes (*eNOS*, *iNOS* and *nNOS*) that when triply deficient are still viable, albeit with phenotypes including obesity and diabetes that reduces lifespan to 10 months (three of 13 triply *NOS* deficient mice survived whereas all control mice survived)^{24,182}. It appeared that NOS is not completely essential for survival, but did play a critical role in how healthy the mice were. It is unknown whether the actions of NO can be achieved through other cellular means but both fly and mouse *NOS* knockout studies suggest that perhaps the mice were receiving NO from an alternative source to sustain life. Alternatively, perhaps NOS and NO are not necessary for fly survival as the *NOS^{FD}* mutant suggests. Therefore, two possibilities arose: **1)** NO was still a critical component of the *NOS^{IR-X}-RNAi* phenotype (explored in the following paragraph) and **2)** NOS and NO did not play a critical role (explored at the end of the chapter).

In *Drosophila*, two options for NOS-independent NO synthesis arise. First, since mammals have three different *NOS* genes, perhaps flies have an additional gene with NOS activity that has not yet been discovered. This is unlikely because researchers have already made unsuccessful attempts to find sequences related to *NOS* in the *Drosophila* genome¹⁸³. Second, NO could be synthesized through other means in the animal. For example, microbes and mitochondria can synthesize NO by reducing nitrite without NOS¹⁸⁴, showing that it was possible for these animals to generate or obtain NO without having a *NOS* gene. Another example is that *Caenorhabditis elegans* lack a *NOS* gene and obtain their NO from ingested bacteria⁸⁹. And so, simply deleting *NOS* may not be enough to completely disrupt NO signaling in an animal and other means may be necessary to replicate the phenotype seen in

phm22>NOS^{IR-X}-RNAi. Conflicting research in *Drosophila* has shown that a particular glycine mutation in *NOS* abolishes enzymatic activity and resulted in lethality during embryonic and larval stages¹⁸⁵ leading some researchers to believe that *NOS* is required. This however, leads to conflicting reports because of mutations that delete all or some of *NOS* are reported in this thesis to be viable and suggests that the glycine mutant of *NOS* may have been enacting some form of lethal activity within the animal.

It would be interesting to know what effects *NOS* mutations have in *Drosophila* when solely expressed in the PG. Therefore, by focusing on the PG with *NOS* mutations, it may be possible to replicate the *phm22>NOS^{IR-X}-RNAi* phenotype. Perhaps when disrupted in the PG as opposed to the whole body, the animal is unable to compensate for the loss of NO in just one tissue, or the lack of NO is not sensed by the animal until it is too late. Previous work in the King-Jones lab has shown that when *timeless (TIM)* is knocked down in the PG it was lethal, whereas a null mutant was not¹⁸⁶. This showed that tissue specific knockdowns can be more severe, which may be the case with *NOS*. To do this, GAL4/UAS Cas9 CRISPR technology can be utilized¹⁸⁷, where guide RNA's that specifically target the *NOS* gene can have PG-specific expression of *Cas9*. This would allow for tissues-specific mutations and would constitute an alternative to PG-specific *NOS*-RNAi. Furthermore, FRT sites flanking *NOS* in the genome can be excised via heat shock induced FLT-FRT flippase activity to initiate a temporal knockdown¹⁸⁸. And so, multiple transgenic approaches are still available to determine the effect of *NOS* mutations in the PG.

If transgenic means of deleting *NOS* do not produce the *phm22>NOS^{IR-X}-RNAi* phenotype, a chemical approach to affect NO may be necessary. One commonly used compound in *NOS* research is N-nitro-L-Arginine Methyl Ester (L-NAME), which is an enzymatic inhibitor of *NOS*. This compound can be fed to larvae with the idea that it would disable *NOS* throughout the organism, although the *NOS^{FD}* phenotype suggests this would be ineffective. However, if the minimalistic phenotype in the *NOS^{FD}* mutants is due to an additional source of NO, L-NAME will have no effect, and maybe an NO scavenger would be more appropriate. For example, hemoglobin and cobinamide are NO scavengers capable of alleviating NO-induced sepsis in mice and *Drosophila*¹⁸⁹⁻¹⁹¹. Such scavengers could be fed to either *w¹¹¹⁸*, or the *NOS^{FD}* mutants to scavenge and repress NO present in the animal. If neither the transgenic or chemical approach to disable NO result in the *phm22>NOS^{IR-X}-RNAi* phenotype, perhaps a combination of both

treatments could affect the PG and remove all sources of NO in the PG, while also minimizing NO throughout the whole body. Any replicated phenotypes of L3 arrest and giant red RGs should be tested for ecdysone rescue to ensure that the effect generated is ultimately related to ecdysone production. Alternatively, one could overexpress *NOS* in the PG and look at the rate of *ferritin* or *sdhb* translation. The idea is that excessive NO would trigger the switch in IRP-1A to become RNA-binding. When this occurs, IRP-1A should be active and thereby decrease the translation of *ferritin* and *sdhb*, which can be detected using the TRAP method described in chapter 4.4.2.

With the data present in this thesis, regardless of the proposed experimental procedures, it seems likely that the proposed model (Fig. 1.9) is not as predicted. The presence of the off-target effect indicates that the phenotype observed in *phm22>NOS^{IR-X}-RNAi* animals could be completely related to an off-target knockdown. What can be concluded from the data is that heme production was impaired, however the means by which this occurred is currently unknown. The NOS protein requires heme cofactors to function, therefore if the off-target gene, when knocked down, was disrupting heme production, then NOS would be nonfunctional. And so, it seems logical that without the heme cofactors, NOS may have become unstable, degraded and unable to synthesize NO. This would explain why previous experiments could not find either NOS or NO in the RG². The lack of NO and ecdysone production in *phm22>NOS^{IR-X}-RNAi* animals may be due to secondary RNAi effects. Therefore, the lack of ecdysone could directly correspond to the lack of heme. My data demonstrating that the RNA-binding form of IRP-1A was capable of rescuing the *phm22>NOS^{IR-X}-RNAi* animals is still valid and likely suggests that iron mobilization into heme is the reason the animals were rescued. However, NO's role upstream of IRP-1A in my proposed model may not be how the natural biological system works. Furthermore, IRP-1A may not be part of the proposed pathway either, but the actions of the RNA-binding form of IRP-1A is a means to rescue the animal and aid in heme production.

To validate the idea that NOS and NO are not involved with the giant red RG and L3 arrest seen in *phm22>NOS^{IR-X}-RNAi* animals a NO feeding experiment could be performed. If *phm22>NOS^{IR-X}-RNAi* animals were fed an ingestible NO donor such as S-nitroso-N-acetylpenicillamine (SNAP)¹⁹² and the animals were rescued to adulthood, this would demonstrate that a lack of NO was indeed the reason that the L3 arrest and giant red RG phenotype that occurred. However, if when fed NO, the animal still maintains the lethal

phenotype, then one would be able to surmise that an off-target is the reason for the phenotype and that a lack of NO is a result of the knockdown and not the cause of the phenotype. One would also have to verify that NO is present in the SNAP fed *phm22>NOS^{IR-X}-RNAi* animals, which could be tested using the DAF2-DA stain as previously discussed.

A major link that is not backed up by data in the originally proposed pathway is the connections between IRP-1A and heme through ferritin. If one is able to show that *ferritin* mRNA regulation is critical to the rescue of *phm22>NOS^{IR-X}-RNAi* animals, it would cement IRP-1A with the downstream components of the proposed pathway. This could be explored by deleting the IRE component of *ferritin* using CRISPR technology. If *phm22>NOS^{IR-X}-RNAi* animals lacking the 5' UTR IRE within the *ferritin* transcript cannot be rescued by *IRP-1A^{C450S}* overexpression, it would show that ferritin regulation was critical to heme biosynthesis and ultimately ecdysone production. However, if this mutation proved lethal, a conditional CRISPR mutant could be created in the RG to circumvent the issue. Furthermore, if the IRE deletion line could still be rescued in a *NOS^{IR-X}-RNAi* background, this would suggest that IRP-1A is affecting alternative IRE-associated transcripts to produce heme and rescue the animal. The only other known IRE in *Drosophila* is located within the 5' UTR of *sdhb*, and any other IRE's are yet to be elucidated (discussed further in Ch. 4.4.1).

Overall, being able to show that a lack of NOS is not causing the phenotype would solidify the newly proposed idea that NOS and NO disruptions are a result of the phenotype and not a cause of the phenotype. This leads to the importance of determining the link IRP-1A RNA-binding activity has to the ecdysone biosynthetic pathway that is ultimately disrupted in *phm22>NOS^{IR-X}-RNAi* animals. Testing whether IRP-1A RNA-binding activity is capable of rescuing other genes from the screen in chapter 1.9 that result in giant red ring glands or show if the IRE associated with *ferritin* is necessary for rescue would validate the role of iron regulation in ecdysone production.

4.4 A novel patterning of NO signaling in the RG

I have shown that NO was present in the RG during and prior to the minor ecdysone pulses from 16-24 hours after the L2/L3 molt and just prior to the major ecdysone pulse at 40 hours after the L2/L3 molt (Fig. 3.2). This was done in the control strain *w¹¹¹⁸* to determine the normal timing and expression of NO in the PG. The limited efficiency of the staining procedure with DAF2-DA would be valuable to repeat in order to obtain more consistent staining during the NO pulses. However, as mentioned before, this may be difficult due to the short half-life of NO. It would be interesting to quantify the amount of NO in the RG, but this can only be done by measuring nitrates as opposed to NO directly. DAF2-DA is an enticing option to measure fluorescence, but the signal is not proportional to the concentration of NO detected¹⁵⁵.

I observed NO during the 16-24 hr and 40-44 hr stages after the L2/L3 molt, which appeared to correlate with known ecdysone pulses at those developmental time points. Those NO signals were thought to be required to activate IRP-1A in order to increase cellular iron for incorporation into P450s. Alternatively, due to *NOS^{IR-X}*-RNAi having an off-target, the presence and/or absence of NO in the RG may not be related to the originally proposed pathway and could be a downstream effect of the off-target. Either way, it was important to look at NO signaling based on its presumptive importance in the RG and its known role in binding E75². It is likely, based on previous reports that NO signaling is playing a role in the RG, and so understanding its role in relation to ecdysone still yields valuable information, albeit information that is likely not a cause of the red RG and L3 arrest phenotype of *phm22>NOS^{IR-X}*-RNAi animals.

As previously reported, NO was lost in late L3 larvae of *phm22>NOS^{IR-X}*-RNAi animals² and being able to show that the rescued animals of *phm22>NOS^{IR-X}*-RNAi; *IRP-1A^{C450S}* have lost all L3 NO signals could further support the original hypothesis. This is because if *IRP-1A^{C450S}* overexpression is enabling the production of heme, then one would predict that NOS would be functional, and therefore producing NO. However, because the RNAi is likely causing a *NOS*-knockdown in addition to an off-target, NO signaling should theoretically also be disrupted. Taken together, this experiment could reveal whether the off-target is knocking down *NOS* in addition to an off-target or not because an off-target specific effect would result in NO signaling being present in *phm22>NOS^{IR-X}*-RNAi; *IRP-1A^{C450S}* animals.

Another result from the NO time course experiment was the patterning of NO seen in Figure 3.2B. The biphasic PG staining where only half the PG was stained has never been shown in the literature to my knowledge and appeared to be randomly observed throughout the time course (although not all images reflect the biphasic signaling, it did not appear at any one specific time). Interestingly, Nhan Huynh, another grad student in the lab, is studying genes discovered in our lab's giant red RG screen as mentioned in chapter 1.9, and noticed that the red fluorescence can either comprise the full PG, or just half of the gland, at least in *phm22>CG17985-RNAi* animals. *CG17985* has yet to be the focus of a study but has a predicted lysine domain¹⁹³. The meaning of this is unknown, but the notion that this observation is related to red RGs is interesting because perhaps this newly uncovered method of biphasic PG signaling is related to ecdysone biosynthesis. However, the biphasic patterning may just be a general means of PG signaling, where the PGs are not fully synchronized and both halves of the PG, at least for NO and *CG17985* related signaling/patterning of NO and heme are slightly off base in their signal timing. Alternatively, the biphasic behaviors could also be evidence of a wave type signaling, or perhaps the cells are not equivalent and release NO on an unequivocal basis, such that each half of the PG runs on its own signaling schedule, off-kilt to the other cells of the PG. Ultimately, the reasoning to this unequal and apparently random rate of full vs half PG NO staining is unknown but provides evidence of a novel means for signaling in the PG.

How the presence of NO in the CA can be reconciled with my originally predicated functions for NOS, NO, and IRP-1A in the ecdysone pathway is currently unclear and may be entirely unrelated to ecdysone signaling. The CA signal for NO was likely not an artifact because previous research has shown that NOS is active in the CA¹⁵⁷. This was accomplished through NADPH diaphorase (NADPHd) staining, a method of detecting NOS activity that worked in both the locust and *Drosophila*^{194,195} and was used prior to widespread acceptance of the DAF2-DA stain. Essentially, NADPHd co-precipitates with NOS, proportional to the amount of NOS in the sample. Thus, using NADPHd histochemistry staining, researchers were able to infer that NOS was active in whichever tissue showed NADPHd activity^{194,195}. Therefore, since NOS activity was inferred through NADPHd presence in the CA of *Drosophila*, it seems reasonable to have found NO staining in the CA¹⁵⁷.

The primary function of the CA, as currently known, is to release the juvenile hormone (JH), which is responsible for maintaining insects in their juvenile state, thus opposing the

function of ecdysone, which promotes maturation. *Drosophila* with an ablated CA, have shown a decrease or loss in JH production, resulting in pupal lethality¹⁹⁶. Furthermore, animals with half the CA removed and decreased JH levels were more susceptible to stress-related damages¹⁹⁶, ultimately showing that the CA played an important role in regulating hormones, specifically JH. How this pertains to NO is currently unknown, perhaps NO aids in iron regulation for a potential iron demand in JH production or blockage. It would be interesting to study functional relationships between NO and JH, perhaps NO signaling aids in JH production as I predict it aids in ecdysone production. JH biosynthetic enzymes, like ecdysone producing enzymes, are partially composed of P450s, and thus, heme and iron regulation is also important for JH biosynthesis and regulation¹⁹⁷, suggesting that NO could coordinate JHs production to some extent. Alternatively, the NO staining in the CA could be an unrelated function, and therefore more studies are required.

4.4 Future directions

4.4.1 Searching for novel IREs in *Drosophila*

My first major goal was to discover novel IREs in *Drosophila* because of the apparent shortage of IRE abundance when compared to mammals since *Drosophila* have two known IREs and mammals have at least 13. I reasoned that since mammalian transcripts contain IREs without obvious ties to iron regulation such as the Alzheimer's amyloid precursor protein transcript¹⁹⁸, that perhaps additional transcripts involved with the predicted NO/IRP/ecdysone pathway may harbor IREs.

The first approach I used to identify novel IREs was with a computational search using the SIRE IRE tool¹⁴³. An mRNA sequence was uploaded to the web program and analyzed for transcript potential to fold and produce an RNA stem loop similar to the canonical IRE. This program allowed me to analyze transcripts that are associated with iron regulation and potentially my proposed pathway. I built a list of targets related to iron regulation based on their obvious connections to iron metabolism, NO and ecdysone in the literature. After including the eight genes required for heme production (chosen due to both their connection to iron regulation and the fact that in mammals ALAS2 has an IRE), a list of 20 likely candidates for SIRE analysis was compiled (Table 4.1). This was a pilot study; therefore, I chose to start with only 20 genes. For future studies, a Flybase query for "iron regulation" yields 257 genes, all of which can be computationally analyzed. Each of the 20 gene sequences were uploaded into SIRE and four possible outcomes existed ranging from no IREs detected or an IRE of high, medium or low quality. High quality IRE predictions had every component of an experimentally validated IRE: hexa-apical hairpin loop and two stem sequences with a cysteine bulge in the middle. Medium and low quality targets had experimentally unconfirmed alterations to their sequence.

To determine the rate of IRE detection based on random chance, I uploaded 300kb of random DNA, from this, 4 high, 8 medium and 13 low quality IREs were predicted, giving a rate of 8.3×10^{-2} IREs per kb (1.3×10^{-2} high quality, 2.6×10^{-2} medium quality IREs or 4.3×10^{-2} low quality IREs per kb). From the list of 20 likely candidates, totaling 191,642 bases, I expected to see 2 high quality, 5 medium quality and 8 low quality IREs, totaling 15 IREs detected. What I found was 13 IRES: 2 high, 5 medium, and 6 low quality, very close to what one would expect to

occur by chance (Table 4.1). However, from the list of 20 likely candidates, a high quality IRE was predicted to be present in the 5'UTR mRNA of the heme biosynthesis gene *PBGD* and a medium quality IRE in the 3'UTR mRNA of *mfrn*, raising the possibility that a true IRE occurs in these transcripts (the reasoning of their likelihood is discussed next paragraph). In regards to the IREs detected in intron regions, it would be interesting to know if they are a new means of IRE binding, however, it has never been seen before and could just be non-functional.

ALAS2 contains a 5' UTR IRE in mammals to regulate heme production, which is logical because heme requires iron in its final biosynthetic step (Fig. 1.4). *Drosophila*, however, lacks an IRE in its *ALAS* transcript, appearing to have lost or never acquired IRP regulatory control over heme production. Perhaps an IRE has evolved in *PBGD* to regulate heme production in *Drosophila* because of the 5'UTR location of the IRE, making up for the lack of IRE control in *ALAS*. *Drosophila* lacks the Transferrin Receptor, which in mammals is involved with iron uptake and regulated via a 3' UTR IRE within its transcript. There are currently no known IREs in *Drosophila* affecting iron uptake which makes *mfrn* an interesting hit in the SIRE IRE search. *mfrn* is involved with iron uptake in the mitochondria for various purposes such as ISC and heme production, therefore having a 3' UTR IRE would fall in line with increased iron uptake in times of iron demand and IRP-1A RNA-binding activity. Although these candidates seem plausible to have true IREs based on the literature, this is only a computational approach and must be followed up with RNA-Immunoprecipitation sequencing (RIP-seq).

The tagged transgenic lines *3xFLAG-IRP-1A*, *3xFLAG-IRP-1A^{C450S}* and *3xFLAG-IRP-1B* were originally created for use with the RIP-seq experiment. 3xFlag tags on the N-terminus were chosen for IRP-1A, IRP-1A^{C450S} and IRP-1B because it was a small sequence tag that could bind with high specificity to the FLAG antibody and that N-terminus tags have been reported to maintain IRP-1A and -1B protein function¹¹⁰. Overexpressing constitutively active IRP-1A would allow for maximum binding to IRP targets, however, any hits with this form of IRP requires caution as they may be a result of hyper activity and therefore be non-specific. Finally, IRP-1B can be used as a negative control because it is a highly similar protein to IRP-1A but cannot bind IREs. Any hits from IRP-1B would be false positives, narrowing down the true list of IREs from the IRP-1A or IRP-1A^{C450S} RIP-Seq. Furthermore, any candidate IRE-containing mRNAs discovered in the RIP-Seq should be compared to the computational IRE search to have an extra degree of confidence in defining true IREs. The outcome of this search for IREs would

likely elucidate novel IREs that may play a role in my proposed pathway where the RNA-binding form of IRP-1A can rescue *phm22>NOS^{IR-X}-RNAi* animals. Since my data has suggested that NO does not cause the giant red RG with L3 arrest phenotype, it would be valuable to determine if IRP-1A has any targets related to heme biosynthesis in *Drosophila*. Any newly identified transcripts could further explain why the off-target effect may not be related to NO and NOS and is ultimately rescued by IRP-1A RNA-binding activity. Alternatively, it is still beneficial to know if only *sdhb*, and *ferritin* contain IREs within *Drosophila*, allowing us to search for alternative means of iron regulation outside of IRP.

Table 4. 1. Computational analysis of genes related to NO, iron, heme and ecdysone regulation. Sets of genes were organized with respect to their relation to heme biosynthesis, ecdysone synthesis or other functions related to iron. The SIRE program was used to analyze the entire gene region, looking for IREs. High quality IRE predictions had every component of an experimentally validated IRE: hexa-apical hairpin loop and two stem sequences with a cysteine bulge in the middle. Medium and low quality targets had experimentally unconfirmed alterations to their sequence. UTR: untranslated region.

CG	FlyBase ID	Symbol	Gene Name	IRE?	Predicted IRE Strength	Location
Heme						
CG3017	FBgn0020764	Alas	Aminolevulinate synthase	0		
CG10335	FBgn0036271	PBGS	Porphobilinogen synthase	0		
CG9165	FBgn0010786	PBGD	lethal (3) 02640	2	High, Medium	5'-UTR, Exon 1
CG1885	FBgn0030066	CG1885	UROS in animals	0		
CG1818	FBgn0033428	Updo	Updo	0		
CG3433	FBgn0021944	Coprox	Coproporphyrinogen oxidase	0		
CG5796	FBgn0020018	Ppox	Protoporphyrinogen oxidase	0		
CG2098	FBgn0266268	FeCH	Ferrochelatase	0		
Ecdysone synthesis						
CG12028	FBgn0000449	dib	disembodied	1	Medium	Intron 1
CG40050	FBgn0259697	nvd	neverland	4	Medium, Low (3)	Intron 2,3,4
CG6578	FBgn0004959	phm	phantom	2	High, Low	Intron 3, 5'-UTR
CG14728	FBgn0003312	sad	shadow	1	Low	Exon 1/Intron 1
CG10594	FBgn0003486	spo	spook	0		
CG41624	FBgn0086917	spok	spookier	1	Medium	Intron 1
Other						
CG7727	FBgn0000108	Appl	β amyloid protein precursor-like	0		
CG4205	FBgn0011769	Fdx1	Ferredoxin 1	0		
CG1319	FBgn0035529	Fdx2	Ferredoxin 2	1	Low	Intron 1/Exon 2
CG8971	FBgn0030092	fh	frataxin homolog	0		
CG4963	FBgn0039561	mfrn	mitoferrin	1	Medium	3'-UTR

4.4.2 Elucidating IRP-1A activity prior to the major L3 ecdysone pulse using the Translating Ribosome Affinity Purification assay

Since NO was present just prior to the late L3 ecdysone pulse, I originally predicted that NO caused IRP-1A to become RNA-binding in order to boost cellular iron levels for heme production. Therefore, at 40/44 hrs after the L2/L3 molt, when NO was present (Fig. 1.9 and 3.2) IRP-1A was thought to be RNA-binding and at 30 hrs after the L2/L3 molt, when NO was absent, IRP-1A was thought to be in the aconitase form. To test this, I planned on quantifying the levels of IRE-containing transcripts that were bound to ribosomes at various time points where I believed IRP-1A to either be an aconitase or RNA-binding. For example, IRP-1A should be binding the 5' UTR IRE of *ferritin* mRNA at the 40/44 hr stage and therefore fewer transcripts should be translated compared to the 30 hr stage. A method to test this is a technique known as TRAP (Translating Ribosome Affinity Purification)^{199,200}, which allows for the isolation of ribosome-bound mRNAs from specific tissues (Fig. 4.1). While the off-target, iron media and transgenic rescue data suggests NO may not be involved with the IRP-1A rescue, knowing the state of IRP-1A in relation to development and ecdysone could still be valuable.

Using TRAP, a *UAS*-controlled GFP-tagged ribosome can be expressed in the PG by expressing *phm22-GAL4*; allowing highly specific tissue activation. Using a GFP antibody, the GFP-tagged ribosomes can be isolated at any stage in development, in this case the 30 and 44 hr stages. RNA can then be extracted from the immunoprecipitate and quantified using qRT-PCR to determine the levels of *ferritin* IRE transcripts which would be associated with the activity of IRP-1A at these two time points.

I was able to isolate samples, pull-down the GFP-tagged ribosome and isolate the RNA, resulting in 1.5 ug of RNA per 150 L3 larvae. The next stage in this experiment would involve testing an accurate reference gene for qRT-PCR analysis. I used the housekeeping gene *rp49* as a standard for regular qRT-PCR experiments, since it was ubiquitously expressed, however, its rate of translation over time was unknown and could not confidently be used as a reference. A list of housekeeping genes needs to be assessed at both the 30 and 44 hr stages to see if expression is altered and the most reliable ones chosen for analysis.

Once a reference gene is selected, a proof-of-concept preliminary experiment must be performed. Expressing the tagged ribosome in the whole body and comparing expression of

*sgs-3*¹¹, a gene that is highly expressed in wandering larva and promptly turned off at the larval to prepupal transition, could be used to confirm the TRAP experiment works. A positive result would show high levels of *sgs-3* translation in wandering larva and no translation in pupae. Once this is complete, *ferritin* and *sdhb* transcript levels can be accurately assessed.

Overall, using the TRAP method in a tissue-specific manner would allow for the analysis and quantification of *ferritin* and *sdhb* within the translome of the PG. This would determine if these genes are being translated at the 30 hr stage and blocked at the 44 hr stage, representing the corresponding activity of IRP-1A. And so, this could further support my hypothesis that IRP-1A was RNA-binding at these times, suggesting the necessity of IRP-1A to regulate iron in times heme demand.

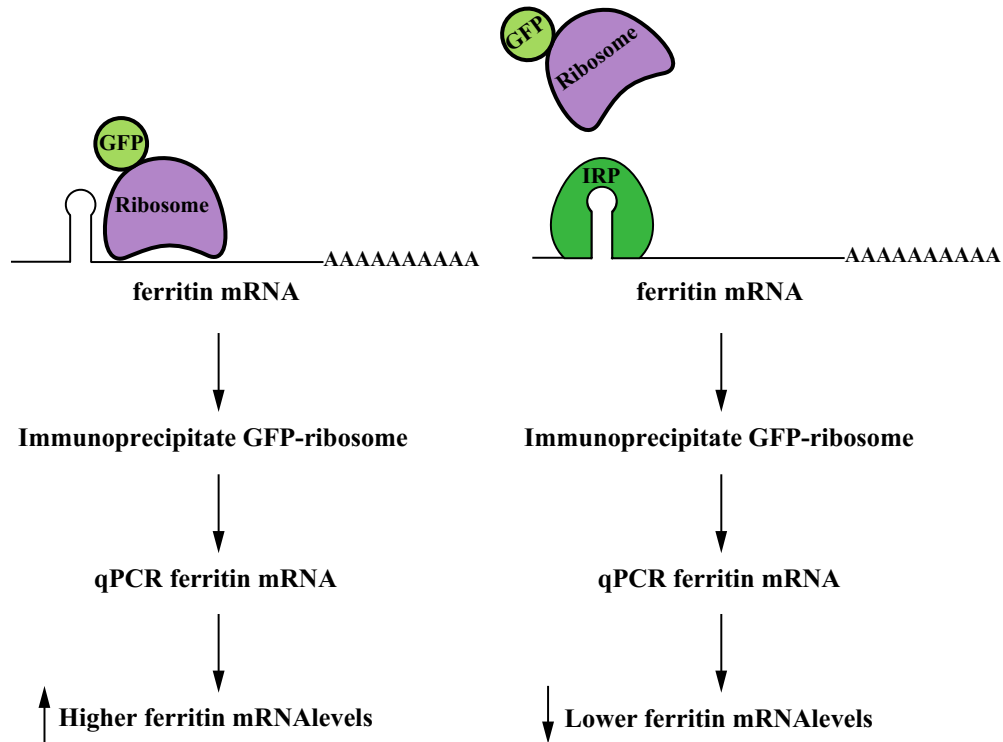


Figure 4. 1. Illustration of the translating ribosome affinity purification (TRAP) technique to identify whether IRP-1A is RNA-binding or not. GFP-tagged ribosomes are expressed in the PG. When *ferritin* mRNA is predicted to be actively translated by the GFP-tagged ribosome, it can be immunoprecipitated and then RNA-extracted to reveal hypothesized average to high levels of *ferritin* mRNA which should be bound to the GFP-tagged ribosome when IRP-1A is an aconitase. When *ferritin* mRNA is predicted to be bound to the RNA-binding form of IRP-1A, the GFP-tagged ribosome cannot bind the *ferritin* mRNA. Once immunoprecipitated and subsequently RNA-extracted, no *ferritin* mRNA should be detected. The experiment can then infer whether IRP-1A is RNA-binding or not. PG: prothoracic gland.

4.4.3 Using an Internal Ribosomal Entry Site to elucidate the timing of IRP-1A RNA-binding activity

Another approach to determine IRP-1A's activity between the 30 and 44 hr stages, as in chapter 4.4.2, is by taking advantage of the Internal Ribosomal Entry Site (IRES) sequence. An IRES refers to an RNA sequence originally found in the polio virus²⁰¹ that allows for cap-independent translation. Since its discovery, many viruses found in mammals, invertebrate and plants have been shown to have IRES sequences²⁰². However, this is not strictly a tool utilized by viruses and occurs in animals to be utilized in times of stress²⁰³. Therefore, scientists have taken advantage of this system for antiviral¹⁶⁹, oncogenic²⁰⁴ and IRP/IRE binding studies in mice¹⁶⁹. This made it an ideal system for IRP activity analysis because it would not be controlled by an enhancer region, thereby decreasing limitations in expression.

In the mouse studies, the authors designed a plasmid with an iron response element preceding an *RFP* sequence; following *RFP* was the IRES sequence accompanied by a *GFP* sequence. Therefore, *RFP* was regulated by IRP via the IRE and *GFP* was constitutively expressed via the IRES, independent of *RFP* regulation. *GFP* was then used as an internal control for *RFP* translation (Fig. 4.2). Using a virus, the plasmid (pJR-1) was transfected into mouse cells exposed to iron-limiting conditions, promoting IRP1 IRE binding activity. In iron-replete conditions, IRP1 had little or no IRE binding activity and consequently, *GFP* and *RFP* were expressed at equivalent levels. However, if IRP1 was in the RNA-binding form, it bound to the iron response element 5' of *RFP*, blocking the ribosome from binding the mRNA and translating *RFP*. IRES however, was not governed by an iron response element, allowing the ribosome to freely translate *GFP* without IRP1 interference. Thus, the ratios of GFP and RFP were used as a readout to establish which form of IRP-1A was present in the sample. My plan was to replicate this experiment in *Drosophila* by using the pBID injection plasmids previously described. To this date, I have acquired the pIRES2 plasmid, which has an IRES sequence shown to function in *Drosophila* S2 cells¹⁵¹ surrounded by both *RFP* and *GFP*. The next step was to use Gibson cloning technology to insert a *ferritin* iron response element upstream of the *RFP* open reading frame. This construct would then be cloned into pBID-UASC-G (a gateway vector) for injection and the production of a transgenic line. When crossed to *phm22-GAL4* and expressed in the PG, there should be a difference in GFP vs. RFP fluorescence between the 30 hr and 44 hr

stages. Specifically, there would be reduced *RFP* expression normalized to *GFP* at the 44 hr stage compared to the 30 hr stage, signifying that IRP-1A switched to an RNA-binding form at the 44 hr stage.

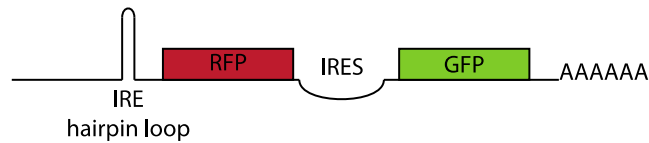


Figure 4. 2. An Internal Ribosomal Entry Site used as a tool for Iron Response Protein’s RNA-binding ability. The IRE hairpin loop is positioned in front of an *RFP* gene. In iron-replete conditions Iron Response Protein (IRP) does not bind Iron Response Elements (IREs, labeled as IRE hairpin loop). Under low iron conditions IRP undergoes a conformational switch, losing its ISC cluster and gaining the ability to bind RNA (IRE hairpin loops). With this tool IRP will bind the IRE hairpin loop preventing the ribosome from binding and translating the *RFP* transcript. The presence of the Internal Ribosomal Entry Site (IRES) directly downstream of *RFP* and upstream of *GFP* is not governed by an IRE hairpin loop; thereby the ribosome can freely bind the transcript between *RFP* and *GFP*, actively translating *GFP*. The ratio of RFP and GFP will fluctuate in the presence or absence of iron. GFP never has translational restrictions therefore, when iron levels are decreased and IRP binds the IRE hairpin loop, the ratio of RFP expression to GFP expression is decreased. This can then be imaged on a confocal microscope. ISC: iron-sulfur cluster.

4.4.4 Looking at ferritin degradation in relation to ecdysone production

During the late L3 ecdysone pulse, when I believed iron was made available for incorporation into heme for P450s, I wanted to know if ferritin released bound iron in addition to having decreased translation from IRP-1A RNA-binding. The current hypothesis on iron release from ferritin is through lysosomal degradation⁶⁷. If true, then ferritin should be degraded prior to the late L3 ecdysone pulse, increasing cellular iron levels for heme production. This can be tested using a native GFP-tagged ferritin fly line. Using the LysoTracker stain, the amount and location of lysosomes can be tracked and tested for co-localization with the GFP-ferritin line within the PG during the late L3 stage. This would provide evidence that increased cellular iron levels are required during ecdysone production. Next, I would test whether *phm22>NOS^{IR-X}-RNAi* animals had decreased ferritin degradation compared to controls as this could be the reason that heme precursors accumulated. Perhaps the ferritin turnover rate through lack of IRP-1A RNA-binding could be the rate-limiting factor in iron availability for *phm22>NOS^{IR-X}-RNAi* animals. Ultimately, iron release from ferritin is relatively unknown and this experiment would shed light on how ferritin and iron release relate to steroid hormone synthesis.

4.4.5 RNA-Seq to identify genes that are affected from IRP-1A overexpression

Conducting an RNA-Seq to search for potential genes that are affected when *IRP-1A* is upregulated, downregulated, or mutated, relative to *w¹¹¹⁸* may yield novel gene functions relating to IRP-1A, heme or ecdysone signaling. Using whole body expression with an *actin-GAL4* driver for *IRP-1A*, *IRP-1A^{C450S}*, and *IRP-1A*-RNAi would allow for maximum identification of genes. Whole larval samples can be used first to achieve results because of the large amounts of RNA contained within, leading to much faster RNA accumulation compared to dissecting an equivalently sized sample of RGs (dissecting this amount of RGs can take over 100 hours). After hits are found by determining the fold change of genes that are upregulated and downregulated in response to *IRP-1A* over- or underexpression, they can later be validated to play a role in the PG. Based on IRP-1A's RNA-binding activity, overexpression of IRP-1A and IRP-1A^{C450S} will result in decreased *ferritin* and *sdhb* mRNA levels as IRPs block translation and decrease their half-life²⁰⁵. I also predict the opposite to occur when IRP-1A is knocked down with RNAi. If *ferritin* and *sdhb* levels are affected, they can be used as positive controls to ensure that the RNA-Seq is working as intended. IRP-1B should also be tested as a negative control due to its lack of RNA-binding activity as any results shared between IRP-1A and 1B should be false positives.

Results from the RNA-seq could then be systematically screened using the experiments previously discussed. First, all the significantly upregulated or downregulated genes affected in the RNA-seq could be compared to both the computational IRE search and the RIP-Seq results from chapter 4.4.1, any overlap between all three experiments would be highly promising IRE candidate genes. These candidates could then be tested using the TRAP approach to test if IRP-1A can affect their translational rate during the late L3 ecdysone pulse, which could indicate that they have biological importance with respect to their IRE. Furthermore, not all the results from RNA-Seq will yield a gene containing an IRE, but instead may be influenced by genes that contain IREs. Do these genes, when knocked down or overexpressed cause the animal to have ecdysone-deficient phenotypes? Or the opposite? Do the results overlap with the red RG screen from chapter 1.9? And are these genes capable of alleviating some of the phenotypes involved with *phm22>NOS^{IR-X}*-RNAi animals when overexpressed or knocked down? Answering these questions with the results of the RNA-seq could yield very interesting genes implicated in IRP-1A/heme/ecdysone pathway.

4.5 Conclusions

My original hypothesis was that NOS produced an NO signal required to shift IRP-1A from the aconitase form to the RNA-binding form in the PG prior to the late L3 ecdysone pulse that triggers puparium formation. IRP-1A would act to increase cellular iron levels to provide iron for heme biosynthesis. Heme would then be utilized as a cofactor for cytochrome P450 enzymes which in turn would be required to synthesize ecdysone. Ultimately, I have shown that the *phm22>NOS^{IR-X}-RNAi* phenotype of L3 arrest and giant red RGs is related to an off-target effect, perhaps in combination with *NOS*. This data, coupled with the results where I showed that limited iron feeding was incapable of bypassing the predicted loss of NO in *phm22>NOS^{IR-X}-RNAi* animals led me to rethink the original hypothesis. Interestingly, and in line with the original proposed model in which IRP-1A was involved with promoting ecdysone production, I have shown that *IRP-1A^{C450S}* transgenic expression can rescue the *phm22>NOS^{IR-X}-RNAi* phenotype. Therefore, my updated prediction lacks the involvement of NO, because it is no longer confirmed to be a cause of the phenotype, but the proposed model still involves each factor downstream and including IRP-1A involvement. Unfortunately, at this time it is unclear whether a lack of IRP-1A RNA-binding activity is involved with the *phm22>NOS^{IR-X}-RNAi* phenotype, or if overexpressing *IRP-1A^{C450S}* is just an alternative means to rescue the animal and must be explored through transgenic manipulations of the *ferritin* IRE (Ch. 4.3). Finally, the NO staining evidence I have accumulated suggests that NO plays a timely coordinated role in the RG, however this experiment requires further refinement to better elucidate the timing of NO in the RG with respect to development. The newest model can be seen in figure 4.3.

Although this research primarily focused on the role of NO and IRP-1A with respect to ecdysone, it is enticing to consider the therapeutic implications with respect to Alzheimer's disease. While the exact cause of the disease is unknown, and there is currently no cure, it is associated with the misregulation and buildup of both beta amyloid plaques and metal ions, such as iron, aluminum, zinc and copper²⁰⁶. Interestingly, in an effort to subdue the mental decline associated with Alzheimer's disease, a study treated patients with DFO to chelate the buildup of aluminum, and showed a noticeable delay in the onset of mental degredation¹⁷⁵. As well, researchers were able to decrease the neurodegenerative effects in mice with late onset Alzheimer's disease using a copper and zinc chelator in the diet²⁰⁶. A problem with these studies

is that chelators have the tendency to bind more than one metal ion, suggesting that instead of aluminum chelation resulting in a delay of mental degradation, iron may have been the therapeutic target. While it generally appeared that mismanagement of metals in the neurons was contributing in some part to Alzheimer's disease, the fact that the amyloid precursor protein associated with Alzheimer's disease had a functional 5'UTR IRE within its transcript, suggested IRP and iron have a role in the disease to some extent¹⁶⁹. The benefit from metal ion chelation may have been more related to the misregulation of iron homeostasis than other metals. Finally, research has shown that NO may cause the effects of Alzheimer's disease to worsen²⁰⁷. It is intriguing to think that the NO, IRP, and the iron regulatory network I have described throughout this study may play a role in Alzheimer's disease. The only link in my research able to connect iron regulation with NOS, is when BPS treatments improved *NOS^{FD}* mutant viability, connecting NO and IRP-1A together in some respect. Learning how NO and IRP interact in hormonal studies could create a base for further research of the mammalian systems, laying a new foundation for studying how to cure Alzheimer's disease and neuronal degradation.

Another interesting application of this research lies in the tools I have produced using IRP-1A^{C450S} as a transgenic means to rescue developmentally arrested larvae. I was able to show that a constitutively RNA-binding form of IRP-1A (IRP-1A^{C450S}) was capable of alleviating the heme precursor buildup in *phm22>NOS^{IR-X}-RNAi* larval RGs as well as the giant size. This led to the RNA-binding form of IRP-1A being able to rescue the L3 arrest and giant red RGs seen in these animals. One could test my transgenic lines for their ability to rescue developmentally arrested flies; genes associated with the giant red RG phenotypes that were identified in the King-Jones lab's screen would be an ideal starting point to flesh out the interactions between IRP-1A, heme and ecdysone biosynthesis (Fig. 1.9). If rescue occurs, it would demonstrate that iron regulation is perturbed in the animal. This could also reveal that ecdysone signaling is disrupted due to knockdowns prior to IRP-1A RNA-binding activation. Perhaps proteins that affect the phosphorylation of IRP-1A could also play a role in the regulation of ecdysone biosynthesis. It is exciting to think of the possibilities that this simple cDNA rescue could lead to in uncoupling how IRP-1A interacts to regulate ecdysone production.

Taking into account the knowledge that can be obtained from the future directions (Ch. 4.4) and the data shown here, I have implicated IRP-1A with ecdysone signaling. My work sheds light on a previously unknown component of hormone production and regulation. This is the first

time that IRP and iron regulation and heme have been proposed to act in concert to regulate the production of steroid hormones *in vivo*.

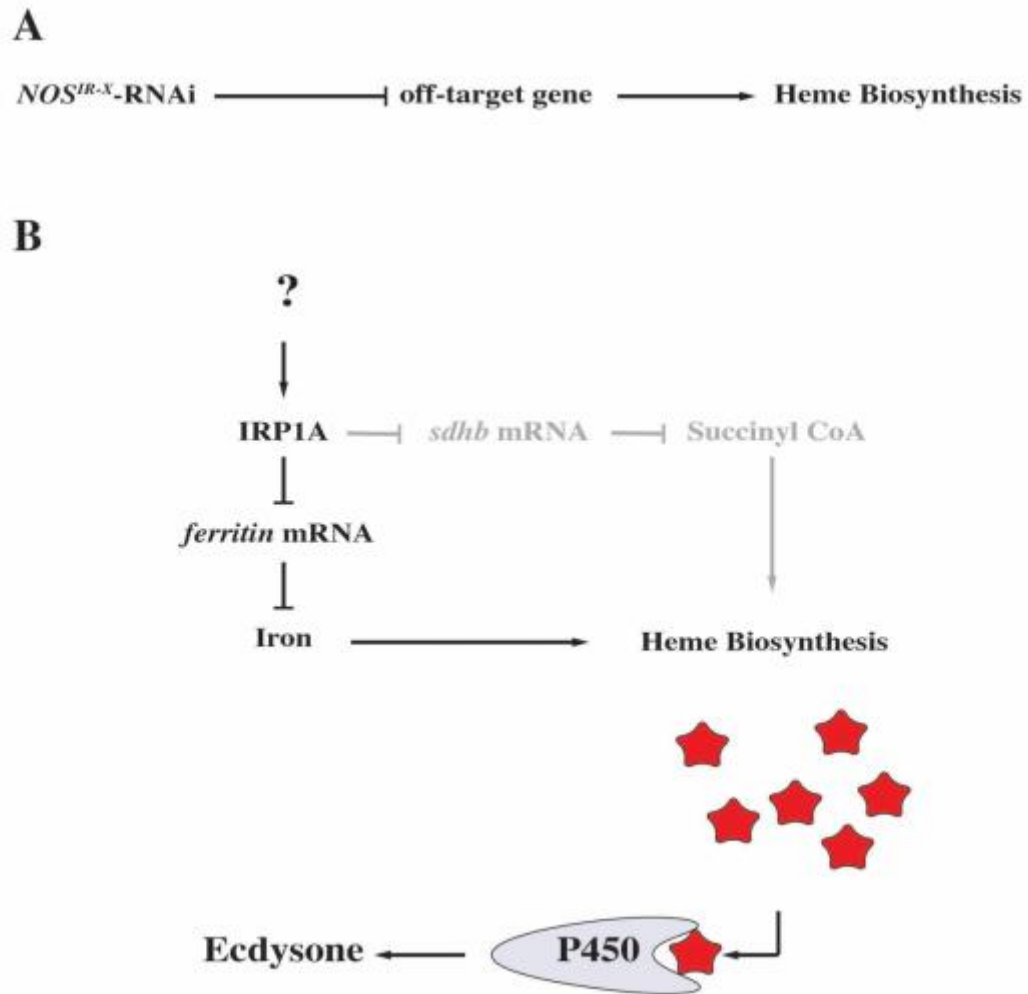


Figure 4. 3. An updated illustration of the predicted model for IRP-1A, iron regulation and heme production in the biosynthesis of ecdysone. **A)** The *NOS^{IR-X}-RNAi* construct was determined to have an off-target effect resulting in heme biosynthesis becoming disrupted. It is possible that the combination of a *NOS* knockdown and an off-target resulted in the giant red RG and L3 arrest phenotype, but the work embodied in this thesis suggests that NO may not have been involved as a driving factor. **B)** The original hypothesis that IRP-1A is involved with producing heme through iron regulation is still predicted and supported for by the evidence in this thesis. This proposed model requires further investigation, specifically involving *ferritin*, to determine if the transcripts 5' URT IRE is required for the IRP-1A^{C450S} rescue of *phm22>NOS^{IR-X}-RNAi* animals. However, *NOS* and NO are no longer suspected to be key players in this model as it appears likely that their disruptions were the result of the off-target knockdown. RG: ring gland. NO: nitric oxide. NOS: Nitric Oxide Synthase.

Works Cited

1. Ou Q, Zheng J, Yamanaka N, Brakken-Thal C, O'Connor MB, King-Jones K. The Insect Prothoracic Gland as a Model for Steroid Hormone Biosynthesis and Regulation. *Cell Reports*. 2016;(16):1-17. doi:10.1016/j.celrep.2016.05.053.
2. Cáceres L, Necakov AS, Schwartz C, Kimber S, Roberts IJH, Krause HM. Nitric oxide coordinates metabolism, growth, and development via the nuclear receptor E75. *Genes & Development*. 2011;25(14):1476-1485. doi:10.1101/gad.2064111.
3. Desvergne B, Héligon C. Steroid hormone pulsing drives cyclic gene expression. *Nat Cell Biol*. 2009;11(9):1051-1053. doi:10.1038/ncb0909-1051.
4. Stavreva DA, Wiench M, John S, et al. Ultradian hormone stimulation induces glucocorticoid receptor-mediated pulses of gene transcription. *Nat Cell Biol*. 2009;11(9):1093-1102. doi:10.1038/ncb1922.
5. Lightman SL, Conway-Campbell BL. The crucial role of pulsatile activity of the HPA axis for continuous dynamic equilibration. *Nature Publishing Group*. 2010;11(10):710-718. doi:10.1038/nrn2914.
6. Bourguignon J-P, Parent AS, Juul A, Skakkebaek NE, Teilmann G, Toppari J. The timing of normal puberty and the age limits of sexual precocity: variations around the world, secular trends, and changes after migration. *Endocrine Reviews*. 2003;24(5):668-693. doi:10.1210/er.2002-0019.
7. Sinha R, Morgan PT, Fox H, Hong K-I, Sofuoglu M, Bergquist KT. Sex steroid hormones, stress response, and drug craving in cocaine-dependent women: implications for relapse susceptibility. *Experimental and Clinical Psychopharmacology*. 2007;15(5):445-452. doi:10.1037/1064-1297.15.5.445.
8. Casto JM, Nolan V, Ketterson ED. Steroid hormones and immune function: experimental studies in wild and captive dark-eyed juncos (*Junco hyemalis*). *Am Nat*. 2001;157(4):408-420. doi:10.1086/319318.
9. Mirth C, Truman JW, Riddiford LM. The role of the prothoracic gland in determining critical weight for metamorphosis in *Drosophila melanogaster*. *Curr Biol*. 2005;15(20):1796-1807. doi:10.1016/j.cub.2005.09.017.
10. Richards G. The radioimmune assay of ecdysteroid titres in *Drosophila melanogaster*. *Molecular and Cellular Endocrinology*. 1981;21(3):181-197. doi:10.1016/0303-7207(81)90013-7.
11. Warren JT, Yerushalmi Y, Shimell MJ, O'Connor MB, Restifo LL, Gilbert LI. Discrete pulses of molting hormone, 20-hydroxyecdysone, during late larval development of *Drosophila melanogaster*: correlations with changes in gene activity. *Dev Dyn*. 2006;235(2):315-326. doi:10.1002/dvdy.20626.

12. Gilbert LI. Halloween genes encode P450 enzymes that mediate steroid hormone biosynthesis in *Drosophila melanogaster*. *Molecular and Cellular Endocrinology*. 2004;215(1-2):1-10. doi:10.1016/j.mce.2003.11.003.
13. Roth GE, Gierl MS, Vollborn L, Meise M, Lintermann R, Korge G. The *Drosophila* gene Start1: a putative cholesterol transporter and key regulator of ecdysteroid synthesis. *Proceedings of the National Academy of Sciences*. 2004;101(6):1601-1606. doi:10.1073/pnas.0308212100.
14. Yoshiyama-Yanagawa T, Enya S, Shimada-Niwa Y, et al. The Conserved Rieske Oxygenase DAF-36/Neverland Is a Novel Cholesterol-metabolizing Enzyme. *Journal of Biological Chemistry*. 2011;286(29):25756-25762. doi:10.1074/jbc.M111.244384.
15. Huang X, Warren JT, Gilbert LI. New players in the regulation of ecdysone biosynthesis. *Journal of Genetics and Genomics*. 2008;35(1):1-10. doi:10.1016/S1673-8527(08)60001-6.
16. Ono H, Rewitz KF, Shinoda T, et al. Spook and Spookier code for stage-specific components of the ecdysone biosynthetic pathway in Diptera. *Developmental Biology*. 2006;298(2):555-570. doi:10.1016/j.ydbio.2006.07.023.
17. Warren JT, Petryk A, Marques G, et al. Phantom encodes the 25-hydroxylase of *Drosophila melanogaster* and *Bombyx mori*: a P450 enzyme critical in ecdysone biosynthesis. *Insect Biochemistry and Molecular Biology*. 2004;34(9):991-1010. doi:10.1016/j.ibmb.2004.06.009.
18. McBrayer Z, Ono H, Shimell M, et al. Prothoracicotropic hormone regulates developmental timing and body size in *Drosophila*. *Developmental Cell*. 2007;13(6):857-871. doi:10.1016/j.devcel.2007.11.003.
19. He J, Cheng Q, Xie W. Minireview: Nuclear Receptor-Controlled Steroid Hormone Synthesis and Metabolism. *Molecular Endocrinology*. 2010;24(1):11-21. doi:10.1210/me.2009-0212.
20. Parvy JP, Blais C, Bernard F, et al. A role for β FTZ-F1 in regulating ecdysteroid titers during post-embryonic development in *Drosophila melanogaster*. *Developmental Biology*. 2005;282(1):84-94. doi:10.1016/j.ydbio.2005.02.028.
21. Sugawara T, Kiriakidou M, McAllister JM, Holt JA, Arkane F, Strauss JF III. Regulation of expression of the steroidogenic acute regulatory protein (STAR) gene: A central role for steroidogenic factor 1. *Steroids*. 1997;62(4):5-9.
22. Ou Q, Magico A, King-Jones K. Nuclear receptor DHR4 controls the timing of steroid hormone pulses during *Drosophila* development. Schneider DS, ed. *PLoS Biol*. 2011;9(9):e1001160. doi:10.1371/journal.pbio.1001160.
23. Bier E. *Drosophila*, the golden bug, emerges as a tool for human genetics. *Nat Rev*

- Genet.* 2005;6(1):9-23. doi:10.1038/nrg1503.
24. Tsutsui M, Shimokawa H, Morishita T, Nakashima Y, Yanagihara N. Development of Genetically Engineered Mice Lacking All Three Nitric Oxide Synthases. *J Pharmacol Sci.* 2006;102(2):147-154. doi:10.1254/jphs.CPJ06015X.
 25. Fortini ME, Skupski MP, Boguski MS, Hariharan IK. A Survey of Human Disease Gene Counterparts in the Drosophila Genome. *The Journal of Cell Biology.* 2000;150(2):F23-F30.
 26. Rubin GM, Spradling AC. genetic transformation of drosophila with thransposable element vectors. *Science.* 1982;218(4570):348-353.
 27. Brand AH, Perrimon N. Targeted gene expression as a means of altering cell fates and generating dominant phenotypes. *Development.* 1993;118(2):401-415.
 28. Xu T, Rubin GM. Analysis of genetic mosaics in developing and adult Drosophila tissues. *Development.* 1993;117(4):1223-1237.
 29. Golic KG, Golic MM. Engineering the Drosophila Genome: Chromosome Rearrangements by Design. *Genetics.* 1996;144(4):1693-1711.
 30. Carthew RW. Gene silencing by double-stranded RNA. *current opinion cell biology.* 2001;13(2):244-248.
 31. Clemens JC, Worby CA, Simonson-Leff N, et al. Use of double-stranded RNA interference in Drosophila cell lines to dissect signal transduction pathways. *Proc Natl Acad Sci USA.* 2000;97(12):6499-6503.
 32. Dietzl G, Chen D, Schnorrer F, et al. A genome-wide transgenic RNAi library for conditional gene inactivation in Drosophila. *Nature.* 2007;448(7150):151-156. doi:10.1038/nature05954.
 33. Boutros M, Kiger AA, Armknecht S, et al. Genome-Wide RNAi Analysis of Growth and Viability in Drosophila Cells. *Science.* 2004;303(5659):832-835.
 34. St Johnston D. THE ART AND DESIGN OF GENETIC SCREENS: DROSOPHILA MELANOGASTER. *Nat Rev Genet.* 2002;3(3):176-188. doi:10.1038/nrg751.
 35. Venken KJT, Bellen HJ. Emerging technologies for gene manipulation in Drosophila melanogaster. *Nat Rev Genet.* 2005;6(3):167-178. doi:10.1038/nrg1553.
 36. Bischof J, Maeda RK, Hediger M, Karch F, Basler K. An optimized transgenesis system for Drosophila using germ-line-specific phiC31 integrases. *Proceedings of the National Academy of Sciences.* 2007;104(9):3312-3317. doi:10.1073/pnas.0611511104.

37. Venken KJT, Bellen HJ. Transgenesis upgrades for *Drosophila melanogaster*. *Development*. 2007;134(20):3571-3584. doi:10.1242/dev.005686.
38. Bassett AR, Tibbit C, Ponting CP, Liu J-L. Highly Efficient Targeted Mutagenesis of *Drosophila* with the CRISPR/Cas9 System. *CellReports*. 2013;4(1):220-228. doi:10.1016/j.celrep.2013.06.020.
39. Xue Z, Wu M, Wen K, et al. CRISPR/Cas9 Mediates Efficient Conditional Mutagenesis in *Drosophila*. *G3 & Genes|Genomes|Genetics*. 2014;4(11):2167-2173. doi:10.1534/g3.114.014159.
40. Gilbert LI, Rybczynski R, Warren JT. Control and biochemical nature of the ecdysteroidogenic pathway. *annual review of entomology*. 2002;(47):883-916.
41. Rewitz KF, Yamanaka N, Gilbert LI, O'Connor MB. The Insect Neuropeptide PTTH Activates Receptor Tyrosine Kinase Torso to Initiate Metamorphosis . *Science*. 2009;326(5958):1403-1405.
42. Hentze JL, Bengtsson MS, Gilbert LI, et al. Accessory gland as a site for prothoracicotropic hormone controlled ecdysone synthesis in adult male insects. Palli SR, ed. *PLoS ONE*. 2013;8(2):e55131. doi:10.1371/journal.pone.0055131.
43. Lavrynenko O, Rodenfels J, Carvalho M, et al. The ecdysteroidome of *Drosophila*: influence of diet and development. *Development*. 2015;142(21):3758-3768. doi:10.1242/dev.124982.
44. Niwa R, Namiki T, Ito K, et al. Non-molting glossy/shroud encodes a short-chain dehydrogenase/reductase that functions in the “Black Box” of the ecdysteroid biosynthesis pathway. *Development*. 2010;137(12):1991-1999. doi:10.1242/dev.045641.
45. Chavez VM, Marques G, Delbecque JP, et al. The *Drosophila* disembodied gene controls late embryonic morphogenesis and codes for a cytochrome P450 enzyme that regulates embryonic ecdysone levels. *Development (Cambridge, England)*. 2000;127(19):4115-4126. <http://www.ncbi.nlm.nih.gov/pubmed/10976044>.
46. Warren JT, Petryk A, Marques G, et al. Molecular and biochemical characterization of two P450 enzymes in the ecdysteroidogenic pathway of *Drosophila melanogaster*. *Proceedings of the National Academy of Sciences*. 2002;99(17):11043-11048. doi:10.1073/pnas.162375799.
47. Niwa R, Matsuda T, Yoshiyama T, et al. CYP306A1, a Cytochrome P450 Enzyme, Is Essential for Ecdysteroid Biosynthesis in the Prothoracic Glands of *Bombyx* and *Drosophila*. *Journal of Biological Chemistry*. 2004;279(34):35942-35949. doi:10.1074/jbc.M404514200.
48. Petryk A, Warren JT, Marques G, et al. Shade is the *Drosophila* P450 enzyme that mediates the hydroxylation of ecdysone to the steroid insect molting hormone 20-

- hydroxyecdysone. *Proc Natl Acad Sci USA*. 2003;100(24):13773–11378.
49. Grogan G. Cytochromes P450: exploiting diversity and enabling application as biocatalysts. *Current Opinion in Chemical Biology*. 2011;15(2):241-248. doi:10.1016/j.cbpa.2010.11.014.
 50. Handschin C, Lin J, Rhee J, et al. Nutritional Regulation of Hepatic Heme Biosynthesis and Porphyria through PGC-1 α . *Cell*. 2005;122(4):505-515. doi:10.1016/j.cell.2005.06.040.
 51. Phillips JD, Kushner JP. Fast track to the porphyrias. *nature medicine*. 2005;11(10):1049-1050.
 52. Reinking J, Lam MMS, Pardee K, et al. The Drosophila nuclear receptor e75 contains heme and is gas responsive. *Cell*. 2005;122(2):195-207. doi:10.1016/j.cell.2005.07.005.
 53. Cappellini MD, Brancaleoni V, Graziadei G, Tavazzi D, Di Pierro E. Porphyrias at a glance: diagnosis and treatment. *Intern Emerg Med*. 2010;5(S1):73-80. doi:10.1007/s11739-010-0449-7.
 54. Poblete-Gutierrez P, Wiederholt T, Merk HF, Frank J. The porphyrias: clinical presentation, diagnosis and treatment. *Eur J Dermatology*. 2006;16(3):230-240.
 55. Hentze MW, Muckenthaler MU, Andrews NC. Balancing Acts: Molecular Control of Review Mammalian Iron Metabolism. *Cell*. 2004;117(3):285-297. doi:10.1016/S0968-0004(05)00043-5.
 56. Rouault TA. Iron metabolism in the CNS: implications for neurodegenerative diseases. *Nature Publishing Group*. 2013;14(8):551-564. doi:10.1038/nrn3453.
 57. Zhang D-L, Ghosh MC, Rouault TA. The physiological functions of iron regulatory proteins in iron homeostasis - an update. *Front Pharmacol*. 2014;5(June):124. doi:10.3389/fphar.2014.00124.
 58. Evstatiev R, Gasche C. Iron sensing and signalling. *Gut*. 2012;61(6):933-952. doi:10.1136/gut.2010.214312.
 59. Gunshin H, Allerson CR, Polycarpou-Schwarz M, et al. Iron-dependent regulation of the divalent metal ion transporter. *FEBS Letters*. 2001;(509):309-316.
 60. McKie AT, Barrow D, Latunde-Dada GO, et al. An Iron-Regulated Ferric Reductase Associated with the Absorption of Dietary Iron. *Science*. 2001;291(5509):1755-1759.
 61. Abboud S, Hailes DJ. A Novel Mammalian Iron-regulated Protein Involved in Intracellular Iron Metabolism*. *journal of biochem*. 2000;275(26):19906-19912.

62. Donovan A, Brownie A, Zhou Y, et al. Positional cloning of zebrafish ferroportin1 identifies a conserved vertebrate iron exporter. *Nature*. 2000;403(6771):776-781.
63. McKie AT, Marciani P, Rolfs A, et al. A Novel Duodenal Iron-Regulated Transporter, IREG1, Implicated in the Basolateral Transfer of Iron to the Circulation. *Molecular Cell*. 2000;5(2):299-309.
64. Fleming MD, Romano MA, Su MA, Garrick LM, Garrick MD, Andrews NC. Nramp2 is mutated in the anemic Belgrade (b) rat: Evidence of a role for Nramp2 in endosomal iron transport. *Proc Natl Acad Sci USA*. 1998;95(3):1148-1153.
65. Ohgami RS, Campagna DR, Greer EL, et al. Identification of a ferrireductase required for efficient transferrin-dependent iron uptake in erythroid cells. *Nat Genet*. 2005;37(11):1264-1269.
66. Theil EC. Ferritin protein nanocages-the story. *nanotechno percep*. 2012;8(1):7-16.
67. Asano T, Komatsu M, Yamaguchi-Iwai Y, Ishikawa F, Mizushima N, Iwai K. Distinct mechanisms of ferritin delivery to lysosomes in iron-depleted and iron-replete cells. *Molecular and Cellular Biology*. 2011;31(10):2040-2052. doi:10.1128/MCB.01437-10.
68. Brazzolotto X, Pierrel F, Pelosi L. Three conserved histidine residues contribute to mitochondrial iron transport through mitoferrins. *Biochem J*. 2014;460(1):79-89. doi:10.1042/BJ20140107.
69. Metzendorf C, Wu W, Lind MI. Overexpression of Drosophila mitoferrin in l(2)mbn cells results in dysregulation of Fer1HCH expression. *Biochem J*. 2009;421(3):463-471. doi:10.1042/BJ20082231.
70. Ye H, Rouault TA. Human iron-sulfur cluster assembly, cellular iron homeostasis, and disease. *Biochemistry*. 2010;49(24):4945-4956. doi:10.1021/bi1004798.
71. Hentze MW, Rouault TA, Klausner RD, et al. A model for the structure and functions of iron-responsive elements. *Gene*. 1988;72(1-2):201-208. <http://www.ncbi.nlm.nih.gov/pubmed/3266604>.
72. Piccinelli P, Samuelsson T. Evolution of the iron-responsive element. *RNA*. 2007;13(7):952-966. doi:10.1261/rna.464807.
73. Goforth JB, Anderson SA, Nizzi CP, Eisenstein RS. Multiple determinants within iron-responsive elements dictate iron regulatory protein binding and regulatory hierarchy. *RNA*. 2010;16(1):154-169. doi:10.1261/rna.1857210.
74. Sanchez M, Galy B, Muckenthaler MU, Hentze MW. Iron-regulatory proteins limit hypoxia-inducible factor-2 α expression in iron deficiency. *Nat Struct Mol Biol*. 2007;14(5):420-426. doi:10.1038/nsmb1222.

75. Hentze MW, Dandekar T, Hentze MW, et al. Identification of a novel iron-responsive element in murine and human erythroid delta-aminolevulinic acid synthase mRNA. *The EMBO journal*. 1991;10(7):1903-1909.
76. Garrick MD, Dolan KG, Horbinski C, et al. DMT1: A mammalian transporter for multiple metals. *Biometals*. 2003;16(1):41-54.
77. Mastrogiannaki M, Matak P, Keith B, Simon MC, Vaulont S, Peyssonnaud C. HIF-2 α , but not HIF-1 α , promotes iron absorption in mice. *J Clin Invest*. 2009;119(5):1159-1166. doi:10.1172/JCI38499.
78. Shah YM, Matsubara T, Ito S, Yim S-H, Gonzalez FJ. Intestinal hypoxia-inducible transcription factors are essential for iron absorption following iron deficiency. *Cell Metabolism*. 2009;9(2):152-164. doi:10.1016/j.cmet.2008.12.012.
79. Missirlis F, Kirby K, Hu J, Rouault TA, Hilliker AJ, Phillips JP. Compartment-specific protection of iron-sulfur proteins by superoxide dismutase. *Journal of Biological Chemistry*. 2003;278(48):47365-47369. doi:10.1074/jbc.M307700200.
80. Philpott CC, Klausner RD, Rouault TA. The bifunctional iron-responsive element binding protein/cytosolic aconitase: the role of active-site residues in ligand binding and regulation. *Proc Natl Acad Sci USA*. 1994;91(15):7321-7325. <http://www.pubmedcentral.nih.gov/articlerender.fcgi?artid=44391&tool=pmcentrez&rendertype=abstract>.
81. Rouault TA, Hentze MW, Caughman SW, Harford JB, Klausner RD. Binding of a cytosolic protein to the iron-responsive element of human ferritin messenger RNA. 1988;241(4870):1207-1210. <http://www.ncbi.nlm.nih.gov/pubmed/3413484>.
82. Kennedy MC, Mende-Mueller L, Blondin GA, Beinert H. Purification and characterization of cytosolic aconitase from beef liver and its relationship to the iron-responsive element binding protein. *Proc Natl Acad Sci USA*. 1992;89(24):11730-11734. <http://www.pubmedcentral.nih.gov/articlerender.fcgi?artid=50630&tool=pmcentrez&rendertype=abstract>.
83. Deck KM, Vasanthakumar A, Anderson SA, et al. Evidence that phosphorylation of iron regulatory protein 1 at Serine 138 destabilizes the [4Fe-4S] cluster in cytosolic aconitase by enhancing 4Fe-3Fe cycling. *Journal of Biological Chemistry*. 2009;284(19):12701-12709. doi:10.1074/jbc.M807717200.
84. Brown NM, Anderson SA, Steffen DW, et al. Novel role of phosphorylation in Fe-S cluster stability revealed by phosphomimetic mutations at Ser-138 of iron regulatory protein 1. *Proc Natl Acad Sci USA*. 1998;95(26):15235-15240. <http://www.pubmedcentral.nih.gov/articlerender.fcgi?artid=28026&tool=pmcentrez&rendertype=abstract>.
85. Clarke SL, Vasanthakumar A, Anderson SA, et al. Iron-responsive degradation of

- iron-regulatory protein 1 does not require the Fe-S cluster. *The EMBO Journal*. 2006;25(3):544-553. doi:10.1038/sj.emboj.7600954.
86. FILLEBEEN C, CALTAGIRONE A, Fillebeen C, Chahine D, Segal P. A Phosphomimetic Mutation at Ser-138 Renders Iron Regulatory Protein 1 Sensitive to Iron-Dependent Degradation. 2003;23(19):6973-6981. doi:10.1128/MCB.23.19.6973.
 87. Jaffrey SR, Cohen SA, Rouault TA, Klausner RD, Snyder SH. The iron-responsive element binding protein: A target for synaptic actions of nitric oxide. *Proc Natl Acad Sci USA*. 1994;91(26):12994-12998.
 88. Gonzalez D, Drapier JC, Bouton C. Endogenous nitration of iron regulatory protein-1 (IRP-1) in nitric oxide-producing murine macrophages: further insight into the mechanism of nitration in vivo and its impact on IRP-1 functions. *Journal of Biological Chemistry*. 2004;279(41):43345-43351. doi:10.1074/jbc.M401889200.
 89. Gusarov I, Shamovsky I, Gautier L, et al. Bacterial nitric oxide extends the lifespan of *C. elegans*. *Cell*. 2013;152(4):818-830. doi:10.1016/j.cell.2012.12.043.
 90. Stuehr DJ. Mammalian nitric oxide synthases. *Biochim Biophys Acta*. 1999;1411(2-3):217-230. doi:10.1016/S0005-2728(99)00016-X.
 91. Guo B, Yu Y, Leibold EA. Iron Regulates Cytoplasmic Levels of a Novel Iron-responsive Element-binding Protein without Aconitase Activity*. *Journal of Biochem*. 1994;269(39):14252-14260.
 92. Salahudeen AA, Thompson JW, Ruiz JC, et al. An E3 Ligase Possessing an Iron-Responsive Hemerythrin Domain Is a Regulator of Iron Homeostasis. *Science*. 2009;326(5953):722-726. doi:10.1126/science.1176326.
 93. Vashisht AA, Zumbrennen KB, Huang X, et al. Control of Iron Homeostasis by an Iron-Regulated Ubiquitin Ligase. *Science*. 2009;326(5953):718-721. doi:10.1126/science.1176333.
 94. Meyron-Holtz EG, Ghosh MC, Rouault TA. Mammalian Tissue Oxygen Levels Modulate Iron-Regulatory Protein Activities in Vivo. *Science*. 2004;306(5704):2087-2090. doi:10.1126/science.1090701).
 95. Hanson ES, Foot LM, Leibold EA. Hypoxia Post-translationally Activates Iron-regulatory Protein 2*. *Journal of Biochem*. 1999;274(8):5047-5052.
 96. Hanson ES, Rawlins ML, Leibold EA. Oxygen and Iron Regulation of Iron Regulatory Protein 2. *Journal of Biological Chemistry*. 2003;278(41):40337-40342. doi:10.1074/jbc.M302798200.
 97. Chollangi S, Thompson JW, Ruiz JC, Gardner KH, Bruick RK. Hemerythrin-like Domain within F-box and Leucine-rich Repeat Protein 5 (FBXL5) Communicates

- Cellular Iron and Oxygen Availability by Distinct Mechanisms. *Journal of Biological Chemistry*. 2012;287(28):23710-23717. doi:10.1074/jbc.M112.360404.
98. Tang X, Zhou B. Ferritin is the key to dietary iron absorption and tissue iron detoxification in *Drosophila melanogaster*. *FASEB J*. 2013;27(1):288-298. doi:10.1096/fj.12-213595.
99. Rodrigues V, Cheah PY, Ray K, Chia W. malvolio, the *Drosophila* homologue of mouse NRAMP-1 (Bcg), is expressed in macrophages and in the nervous system and is required for normal taste behaviour. *The EMBO Journal*. 1995;14(12):3007-3020.
100. Missirlis F, Kosmidis S, Brody T, et al. Homeostatic mechanisms for iron storage revealed by genetic manipulations and live imaging of *Drosophila* ferritin. *Genetics*. 2007;177(1):89-100. doi:10.1534/genetics.107.075150.
101. Hajdusek O, Sojka D, Kopacek P, et al. Knockdown of proteins involved in iron metabolism limits tick reproduction and development. *Proc Natl Acad Sci USA*. 2009;106(4):1033-1038.
102. Yoshiga T, Georgieva T, Dunkov BC, Harizanova N, Ralchev K, Law JH. *Drosophila melanogaster* transferrin Cloning, deduced protein sequence, expression during the life cycle, gene localization and up-regulation on bacterial infection. *Eur J Biochem*. 1999;260(2):414-420.
103. Lang M, Braun CL, Kanost MR, Gorman MJ. Multicopper oxidase-1 is a ferroxidase essential for iron homeostasis in *Drosophila melanogaster*. *Proc Natl Acad Sci USA*. 2012;109(33):13337-13342. doi:10.1073/pnas.1208703109/-/DCSupplemental.
104. Muckenthaler MU, Gunkel N, Frishman D, Cyrklaff A, Tomanca P, Hentze MW. Iron-regulatory protein-1 (IRP-1) is highly conserved in two invertebrate species. *European journal of biochem*. 1998;254(2):230-237.
105. Rothenberger S, Müllner EW, Kühn LC, Ku LC. The mRNA-binding protein which controls ferritin and transferrin receptor expression is conserved during evolution. *Nucleic Acids Research*. 1990;18(5):1175-1179.
106. Kohler SA, Henderson BR, Kühn LC. Succinate dehydrogenase b mRNA of *Drosophila melanogaster* has a functional iron-responsive element in its 5'-untranslated region. *Journal of Biological Chemistry*. 1995;270(51):30781-30786. doi:10.1074/jbc.270.51.30781.
107. Charlesworth A, Georgieva T, Gospodov I, et al. Isolation and properties of *Drosophila melanogaster* ferritin. *European journal of biochem*. 1997;247(2):470-475.
108. Lind MI, Ekengren S, Melefors O, Söderhäll K. *Drosophila* ferritin mRNA:

- alternative RNA splicing regulates the presence of the iron-responsive element. *FEBS Letters*. 1998;436(3):476-482.
109. Georgieva T, Dunkov BC, Harizanova N, Ralchev K, Law JH. Iron availability dramatically alters the distribution of ferritin subunit messages in *Drosophila melanogaster*. 1999;96(6):2716-2721.
<http://www.pubmedcentral.nih.gov/articlerender.fcgi?artid=15835&tool=pmcentrez&rendertype=abstract>.
110. Lind MI, Missirlis F, Melefors O, et al. Of two cytosolic aconitases expressed in *Drosophila*, only one functions as an iron-regulatory protein. *Journal of Biological Chemistry*. 2006;281(27):18707-18714. doi:10.1074/jbc.M603354200.
111. Kamyshev NG, Iliadi KG, Bragina JV, et al. Novel memory mutants in *Drosophila*: Behavioural characteristics of the mutant nemyP153. *BMC Neurosci*. 2002;3(9):1-10.
112. Lavista-Llanos S, Centanin L, Irisarri M, et al. Control of the hypoxic response in *Drosophila melanogaster* by the basic helix-loop-helix PAS protein similar. *Molecular and Cellular Biology*. 2002;22(19):6842-6853.
doi:10.1128/MCB.22.19.6842-6853.2002.
113. Nichol H, Law JH, Winzerling JJ. Iron metabolism in insects. *annual review of entomology*. 2002;47:535-559.
114. Todorich B, Zhang X, Slagle-Webb B, Seaman WE, Connor JR. Tim-2 is the receptor for H-ferritin on oligodendrocytes. *Journal of Neurochemistry*. 2008;107(6):1495-1505. doi:10.1111/j.1471-4159.2008.05678.x.
115. Missirlis F, Mandilaras K, Pathmanathan T. Iron absorption in *Drosophila melanogaster*. *Nutrients*. 2013;5(5):1622-1647. doi:10.3390/nu5051622.
116. Lill R, Mühlenhoff U. Iron-sulfur protein biogenesis in eukaryotes: components and mechanisms. *Annu Rev Cell Dev Biol*. 2006;22(1):457-486.
doi:10.1146/annurev.cellbio.22.010305.104538.
117. Schilke B, Voisine C, Beinert H, Craig E. Evidence for a conserved system for iron metabolism in the mitochondria of *Saccharomyces cerevisiae*. *Proc Natl Acad Sci USA*. 1999;96(18):10206-10211.
118. Garland SA, Hoff K, Vickery LE, Culotta VC. *Saccharomyces cerevisiae* ISU1 and ISU2: Members of a Well-conserved Gene Family for Iron-Sulfur Cluster Assembly. *J Mol Biol*. 1999;294(4):897-907.
119. Voisine C, Cheng YC, Ohlson M, et al. Jac1, a mitochondrial J-type chaperone, is involved in the biogenesis of Fe S clusters in *Saccharomyces cerevisiae*. *Proc Natl Acad Sci USA*. 2001;98(4):1483-1488.

120. Mühlhoff U, Gerber J, Richhardt N, Lill R. Components involved in assembly and dislocation of iron-sulfur clusters on the scaffold protein Isu1p. *The EMBO Journal*. 2003;22(18):4815-4825. doi:10.1093/emboj/cdg446.
121. Wingert RA, Galloway JL, Barut B, et al. Deficiency of glutaredoxin 5 reveals Fe–S clusters are required for vertebrate haem synthesis. *Nature*. 2005;436(7053):1035-1039. doi:10.1038/nature03887.
122. Hill BG, Dranka BP, Bailey SM, Lancaster JR, Darley-Usmar VM. What part of NO don't you understand? Some answers to the cardinal questions in nitric oxide biology. *J Biol Chem*. 2010;285(26):19699-19704. doi:10.1074/jbc.R110.101618.
123. Crane BR, Arvai AS, Ghosh DK, et al. Structure of Nitric Oxide Synthase Oxygenase Dimer with Pterin and Substrate. *Science*. 1998;279(5359):2121-2126.
124. Alderton WK, Cooper CE, Knowles RG. Nitric oxide synthases: structure, function and inhibition. *Biochem J*. 2001;357(Pt 3):593-615.
125. Simon Daff. NO synthase: Structures and mechanisms. *Nitric Oxide*. 2010;23(1):1-11. doi:10.1016/j.niox.2010.03.001.
126. Cho HJ, Xie Q-W, Calaycay J, et al. Calmodulin Is a Subunit of Nitric Oxide Synthase from Macrophages. *J exp Med*. 1992;176(2):599-604.
127. Stasiv Y, Regulski M, Kuzin B, Tully T, Enikolopov G. The Drosophila Nitric-oxide Synthase Gene (dNOS) Encodes a Family of Proteins That Can Modulate NOS Activity by Acting as Dominant Negative Regulators. *Journal of Biological Chemistry*. 2001;276(45):42241-42251. doi:10.1074/jbc.M105066200.
128. Stasiv Y, Kuzin B, Regulski M, Tully T, Enikolopov G. Regulation of multimers via truncated isoforms: a novel mechanism to control nitric-oxide signaling. *Genes & Development*. 2004;18(15):1812-1823. doi:10.1101/gad.298004.
129. Martínez-Ruiz A, Cadenas S, Lamas S. Nitric oxide signaling: Classical, less classical, and nonclassical mechanisms. *Free Radical Biology and Medicine*. 2011;51(1):17-29. doi:10.1016/j.freeradbiomed.2011.04.010.
130. Feelisch M, Fernandez BO, Bryan NS, et al. Tissue processing of nitrite in hypoxia: an intricate interplay of nitric oxide-generating and -scavenging systems. *Journal of Biological Chemistry*. 2008;283(49):33927-33934. doi:10.1074/jbc.M806654200.
131. Hansen MN, Jensen FB. Nitric oxide metabolites in goldfish under normoxic and hypoxic conditions. *Journal of Experimental Biology*. 2010;213(21):3593-3602. doi:10.1242/jeb.048140.
132. Gladwin MT, Raat NJH, Shiva S, et al. Nitrite as a vascular endocrine nitric oxide reservoir that contributes to hypoxic signaling, cytoprotection, and vasodilation. *AJP: Heart and Circulatory Physiology*. 2006;291(5):H2026-H2035.

doi:10.1152/ajpheart.00407.2006.

133. Lancaster JR. NO and nitrosothiols: spatial confinement and free diffusion. *Am J Physiol Lung Cell Mol Physiol*. 2004;287(3):L465-L466. doi:10.1152/ajplung.00151.2004.
134. Brookes PS, Levonen A-L, Shiva S, Sarti P, Darley-USmar VM. Serial Review: Reactive Nitrogen Species, Tyrosine Nitration and Cell Signaling. *Free Radical Biology and Medicine*. 2002;33(6):755-764.
135. Erusalimsky JD, Moncada S. Nitric oxide and mitochondrial signaling: from physiology to pathophysiology. *Arteriosclerosis, Thrombosis, and Vascular Biology*. 2007;27(12):2524-2531. doi:10.1161/ATVBAHA.107.151167.
136. Galkin A, Higgs A, Moncada S. Nitric oxide and hypoxia. *essays biochem*. 2007;43:29-42.
137. Arnold WP, Mittal CK, Katsuki S, Murad F. Nitric Oxide activates guanylate cyclase and increases guanosine 3':5-cyclic monophosphate levels in various tissue preparations. *Proc Natl Acad Sci USA*. 1977;74(8):3203-3207.
138. Förstermann U, Closs EI, Pollock JS, et al. Nitric Oxide Synthase Isozymes. *Hypertension*. 1994;23(6 PT 2):1121-1131.
139. Reddy D, Lancaster JR, Cornforth DP. Nitrite Inhibition of Clostridium botulinum: Electron Spin Resonance Detection of Iron-Nitric Oxide Complexes. *Science*. 1983;221(4612):769-770.
140. Lancaster JR, Hibbs JB. EPR demonstration of iron-nitrosyl complex formation by cytotoxic activated macrophages. *Proc Natl Acad Sci USA*. 1990;87(3):1223-1227.
141. Pantopoulos K, Hentze MW. Nitric oxide signaling to iron-regulatory protein: Direct control of ferritin mRNA translation and transferrin receptor mRNA stability in transfected fibroblasts. *Proc Natl Acad Sci USA*. 1995;92(5):1267-1271.
142. Weiss G, Goossen B, Doppler W, et al. Translational regulation via iron-responsive elements by the nitric oxide/NO-synthase pathway. *The EMBO Journal*. 1993;12(9):3651-3657.
143. Campillos M, Cases I, Hentze MW, Sanchez M. SIREs: searching for iron-responsive elements. *Nucleic Acids Research*. 2010;38(Web Server issue):W360-W367. doi:10.1093/nar/gkq371.
144. Karunakaran R. A family of promoter probe vectors incorporating autofluorescent and chromogenic reporter proteins for studying gene expression in Gram-negative bacteria. *Microbiology*. 2005;151(10):3249-3256. doi:10.1099/mic.0.28311-0.

145. Wang J-W, Beck ES, McCabe BD. A modular toolset for recombination transgenesis and neurogenetic analysis of *Drosophila*. Roman G, ed. *PLoS ONE*. 2012;7(7):e42102. doi:10.1371/journal.pone.0042102.
146. Sievers F, Wilm A, Dineen D, et al. Fast, scalable generation of high-quality protein multiple sequence alignments using Clustal Omega. *Molecular Systems Biology*. 2011;7:1-6. doi:10.1038/msb.2011.75.
147. Inoue H, Nojima H, Okayama H. High efficiency transformation of *Escherichia coli* with plasmids. *Gene*. 1990;96(1):23-28.
148. FinchTV 1.4.0 (Geospiza, Inc.; Seattle, WA, USA; <http://www.geospiza.com>). 2016.
149. Universal ProbeLibrary Assay Design Center (Roche ; Indianapolis, IN, USA; <http://www.lifescience.roche.com>). 2016.
150. Integrated DNA Technologies, Inc. (IDT; Coralville, Iowa, USA: <http://www.idtdna.com>). 2016.
151. Kuzmich AI, Vvedenskii AV, Kopantzev EP, Vinogradova TV, Kopantzev EP, Vinogradova TV. Quantitative comparison of gene co-expression in a bicistronic vector harboring IRES or coding sequence of porcine teschovirus 2A peptide. *Russ J Bioorg Chem*. 2013;39(4):406-416. doi:10.1134/S1068162013040122.
152. Drapier JC, Hirling H, Wietzerbin J, Kaldy P, Kühn LC. Biosynthesis of nitric oxide activates iron regulatory factor in macrophages. *The EMBO Journal*. 1993;12(9):3643-3649.
153. Wardrop SL, Watts RN, Richardson DR. Nitrogen Monoxide Activates Iron Regulatory Protein 1 RNA-Binding Activity by Two Possible Mechanisms: Effect on the [4Fe-4S] Cluster and Iron Mobilization from Cells †. *Biochemistry*. 2000;39(10):2748-2758. doi:10.1021/bi991099t.
154. Pantopoulos K, Hentze MW. Nitric oxide signaling to iron-regulatory protein: Direct control of ferritin mRNA translation and transferrin receptor mRNA stability in transfected fibroblasts. *Proc Natl Acad Sci USA*. 1995;92(February):1267-1271.
155. Kojima H, Nagano T. Detection and Imaging of Nitric Oxide with Novel Fluorescent Indicators: Diaminofluoresceins. June 1998:1-8.
156. Lacza Z, Horváth EM, Pankotai E, et al. The novel red-fluorescent probe DAR-4M measures reactive nitrogen species rather than NO. *Journal of Pharmacological and Toxicological Methods*. 2005;52(3):335-340. doi:10.1016/j.vascn.2005.06.004.
157. Wildermann B, Bicker G. Developmental Expression of Nitric Oxide/Cyclic GMP Synthesizing Cells in the Nervous System of. *journal of neurobiology*. 1999;38(1):1-15.

158. Hakim TS, Sugimori K, Camporesi EM, Anderson G. Half-life of nitric oxide in aqueous solutions with and without haemoglobin. *physiol Meas*. November 1996;267-277.
159. Archer S. measurement of nitric oxide in biological models. *the faseb journal*. 1993;7(2):349-360.
160. Piper MDW, Blanc E, Leitão-gonçalves R, et al. A holidic medium for *Drosophila melanogaster*. 2014;11(1):1-19. doi:10.1038/nmeth.2731.A.
161. Sang JH. The quantitative nutritional requirements of *drosophila melanogster*. *Journal of Experimental Biology*. 1956;(33):45-72.
162. Llorens JV, Metzendorf C, Missirlis F, Lind MI. Mitochondrial iron supply is required for the developmental pulse of ecdysone biosynthesis that initiates metamorphosis in *Drosophila melanogaster*. *J Biol Inorg Chem*. October 2015:1-10. doi:10.1007/s00775-015-1302-2.
163. Missirlis F, Holmberg S, Georgieva T, Dunkov BC, Rouault TA, Law JH. Characterization of mitochondrial ferritin in *Drosophila*. *Proceedings of the National Academy of Sciences*. 2006;103(15):5893-5898. doi:10.1073/pnas.0601471103.
164. Rabinovich D, Yaniv SP, Alyagor I, Schuldiner O. Nitric Oxide as a Switching Mechanism between Axon Degeneration and Regrowth during Developmental Remodeling. *Cell*. 2016;164(1-2):170-182. doi:10.1016/j.cell.2015.11.047.
165. Yakubovich N, Silva EA, O'Farrell PH. Nitric oxide synthase is not essential for *Drosophila* development. *Current Biology*. 2010;20(4):R141-R142. doi:10.1016/j.cub.2009.12.011.
166. Qiu S, Adema CM, Lane T. A computational study of off-target effects of RNA interference. *Nucleic Acids Research*. 2005;33(6):1834-1847. doi:10.1093/nar/gki324.
167. Meyron-Holtz EG, Ghosh MC, Iwai K, et al. Genetic ablations of iron regulatory proteins 1 and 2 reveal why iron regulatory protein 2 dominates iron homeostasis. *The EMBO Journal*. 2004;23(3):386-395.
168. LaVaute T, Smith S, Cooperman S, et al. Targeted deletion of the gene encoding iron regulatory protein-2 causes misregulation of iron metabolism and neurodegenerative disease in mice. *Nat Genet*. 2001;27(2):209-214.
169. Rogers JT, Randall JD, Cahill CM, et al. An iron-responsive element type II in the 5'-untranslated region of the Alzheimer's amyloid precursor protein transcript. *Journal of Biological Chemistry*. 2002;277(47):45518-45528. doi:10.1074/jbc.M207435200.

170. Chintapalli VR, Wang J, Herzyk P, Dow JAT. FlyAtlas: survey of adult and larval expression. <http://flyatlas.org>. September 2010:1-1.
171. Dhur A, Galan P, Hercberg S. Effects of Different Degrees of Iron Deficiency on Cytochrome P450 Complex and Pentose Phosphate Pathway Dehydrogenases in the Rat. *J Nutr*. 1989;119(1):40-47.
172. Hassett RF, Romeo AM, Kosman DJ. Regulation of High Affinity Iron Uptake in the Yeast *Saccharomyces cerevisiae*. *J Biol Chem*. 1998;273(13):7628-7636.
173. Cowart RE, Singleton FL, Hind JS. A comparison of Bathophenanthrolinedisulfonic Acid and Ferrozine as Chelators of Iron(II) in Reduction Reactions. *analytical Biochemistry*. 1993;211:151-155.
174. Darnell G, Richardson DR. The Potential of Iron Chelators of the Pyridoxal Isonicotinoyl Hydrazone Class as Effective Antiproliferative Agents III: The Effect of the Ligands on Molecular Targets Involved in Proliferation. *american society of Hematology*. 1999;94(2):781-792.
175. McLachlan DRC, Dalton AJ, Kruck TPA, et al. Intramuscular desferrioxamine in patients with Alzheimer's disease. *lancet*. 1991;337(8753):1304-1308.
176. Pahl PMB, Horwitz LD. Cell Permeable Iron Chelators as Potential Cancer Chemotherapeutic Agents. *Cancer Investigation*. 2009;23(8):683-691. doi:10.1080/07357900500359976.
177. Liu ZD, HIDER RC. Design of clinically useful iron(III)-selective chelators. *Med Res Rev*. 2001;22(1):26-64. doi:10.1002/med.1027.
178. Smith SR, Ghosh MC, Ollivierre-Wilson H, Hang Tong W, Rouault TA. Complete loss of iron regulatory proteins 1 and 2 prevents viability of murine zygotes beyond the blastocyst stage of embryonic development. *Blood Cells, Molecules, and Diseases*. 2006;36(2):283-287. doi:10.1016/j.bcmd.2005.12.006.
179. CONTESTABILE A. Regulation of transcription factors by nitric oxide in neurons and in neural-derived tumor cells. *Progress in Neurobiology*. 2008;84(4):317-328. doi:10.1016/j.pneurobio.2008.01.002.
180. Delanoue R, Slaidina M, Léopold P. The Steroid Hormone Ecdysone Controls Systemic Growth by Repressing dMyc Function in *Drosophila* Fat Cells. *Developmental Cell*. 2010;18(6):1012-1021. doi:10.1016/j.devcel.2010.05.007.
181. Kumar S, Bandyopadhyay U. Free heme toxicity and its detoxification systems in human. *Toxicology Letters*. 2005;157(3):175-188. doi:10.1016/j.toxlet.2005.03.004.
182. Morishita T, Tsutsui M, Shimokawa H, et al. Nephrogenic diabetes insipidus in mice lacking all nitric oxide synthase isoforms. *Proc Natl Acad Sci USA*. 2005;102(30):10616-10621.

183. Regulski M, Tully T. Molecular and biochemical characterization of dNOS: A *Drosophila* Ca²⁺/calmodulin-dependent nitric oxide synthase. *Proc Natl Acad Sci USA*. 1995;92(20):9072-9076.
184. Poyton RO, Castello PR, Ball KA, Woo DK, Pan N. Mitochondria and Hypoxic Signaling. *Annals of the New York Academy of Sciences*. 2009;1177(1):48-56. doi:10.1111/j.1749-6632.2009.05046.x.
185. Regulski M, Stasiv Y, Tully T, Enikolopov G. Essential function of nitric oxide synthase in *Drosophila*. *Current Biology*. 2004;14(20):R881-R882. doi:10.1016/j.cub.2004.09.068.
186. Di Cara F, King-Jones K. The Circadian Clock Is a Key Driver of Steroid Hormone Production in *Drosophila*. *Current Biology*. 2016;0(0):1-10. doi:10.1016/j.cub.2016.07.004.
187. Xue Z, Wu M, Wen K, et al. CRISPR/Cas9 Mediates Efficient Conditional Mutagenesis in *Drosophila*. *G Bethesda*. 2014;4(11):2167-2173. doi:10.1534/g3.114.014159/-/DC1.
188. Frickenhaus M, Wagner M, Mallik M, Catinozzi M, Storkebaum E. Highly efficient cell-type-specific gene inactivation reveals a key function for the *Drosophila* FUS homolog cabeza in neurons. *Sci Rep*. 2015;5:9107-9110. doi:10.1038/srep09107.
189. Broderick KE, Feala J, McCulloch A, et al. The nitric oxide scavenger cobinamide profoundly improves survival in a *Drosophila melanogaster* model of bacterial sepsis. *FASEB J*. 2006;20(11):1865-1873. doi:10.1096/fj.06-5780com.
190. Heneka MT, Loschmann P-A, Osswald H. Polymerized Hemoglobin Restores Cardiovascular and Kidney Function in Endotoxin-induced Shock in the Rat. *J Clin Invest*. 1997;99(1):47-54.
191. Kim HW, Greenburg AG. Nitric Oxide Scavenging, Alone or with nitric oxide synthesis inhibition, modulates vascular hyporeactivity in rats with intraperitoneal sepsis. *SHOCK*. 2002;17(5):423-426.
192. Kentish SJ, O'Donnell TA, Wittert GA, Page AJ. Diet-dependent modulation of gastro-oesophageal vagal afferent mechanosensitivity by endogenous nitric oxide. *J Physiol*. 2014;592(15):3287-3301. doi:10.1113/jphysiol.2014.272674.
193. InterPro: Protein sequence analysis & classification (European Bioinformatics Institute ; Cambridge, UK <http://www.ebi.ac.uk/interpro/>). 2016.
194. Muller U. CA²⁺/Calmodulin-dependent Nitric Oxide Synthase in *Apis mellifera* and *Drosophila melangoaster*. *European journal of Neurosci*. 1994;6(8):1362-1370.
195. Muller U, Bicker G. Calcium-activated Release of Nitric Oxide and Cellular Distribution of Nitric Oxide-Synthesizing Neurons in the Nervous System of the

- Locust. *journal of neurosci.* 1994;14(12):7521-7528.
196. Gruntenko NE, Wen D, Karpova EK, et al. Altered juvenile hormone metabolism, reproduction and stress response in *Drosophila* adults with genetic ablation of the corpus allatum cells. *Insect Biochemistry and Molecular Biology*. 2010;40(12):891-897. doi:10.1016/j.ibmb.2010.09.001.
197. Bomtorin AD, Mackert A, Rosa GCC, et al. Juvenile Hormone Biosynthesis Gene Expression in the corpora allata of Honey Bee (*Apis mellifera* L.) Female Castes. Korb J, ed. *PLoS ONE*. 2014;9(1):e86923–12. doi:10.1371/journal.pone.0086923.
198. Cho H-H, Cahill CM, Vanderburg CR, et al. Selective translational control of the Alzheimer amyloid precursor protein transcript by iron regulatory protein-1. *J Biol Chem*. 2010;285(41):31217-31232. doi:10.1074/jbc.M110.149161.
199. Heiman M, Kulicke R, Fenster RJ, Greengard P, Heintz N. Cell type-specific mRNA purification by translating ribosome affinity purification (TRAP). *Nat Protoc*. 2014;9(6):1282-1291. doi:10.1038/nprot.2014.085.
200. Thomas A, Lee P-J, Dalton JE, et al. A Versatile Method for Cell-Specific Profiling of Translated mRNAs in *Drosophila*. Roman G, ed. *PLoS ONE*. 2012;7(7):e40276-e40278. doi:10.1371/journal.pone.0040276.
201. Pelletier J, Sonenberg N. Internal initiation of translation of eukaryotic mRNA directed by a sequence derived from poliovirus RNA. *Nature*. 1988;334(6180):320-325. doi:10.1038/334320a0.
202. Martínez-Salas E, Piñeiro D, Fernández N. Alternative Mechanisms to Initiate Translation in Eukaryotic mRNAs. *Comparative and Functional Genomics*. 2012;2012(6180):391546–12. doi:10.1155/2012/391546.
203. Macejak DG, Sarnow P. Internal initiation of translation mediated by the 5' leader of a cellular mRNA. *Nature*. 1991;353(6339):90-94. doi:10.1038/353090a0.
204. Chappell SA, LeQuesne JP, Paulin FE, et al. A mutation in the c-myc-IRES leads to enhanced internal ribosome entry in multiple myeloma: a novel mechanism of oncogene de-regulation. *Oncogene*. 2000;19(38):4437-4440. doi:10.1038/sj.onc.1203791.
205. Haile DJ, Harford JB, Beinert H, et al. Cellular regulation of the iron-responsive element binding protein: disassembly of the cubane iron-sulfur cluster results in high-affinity RNA binding. 1992;89(24):11735-11739. <http://www.pubmedcentral.nih.gov/articlerender.fcgi?artid=50631&tool=pmcentrez&rendertype=abstract>.
206. Cherny RA, Atwood CS, Xilinas ME, et al. Treatment with a Copper-Zinc Chelator Markedly and Rapidly Inhibits. *neuron*. 2001;30(3):665-676.

207. Vodovotz Y, Lucia MS, Flanders KC, et al. Inducible Nitric Oxide Synthase in Tangle-bearing Neurons of Patients with Alzheimer's Disease. *J exp Med.* 1996;184(4):1425-1433.